TOMAS BATA UNIVERSITY IN ZLIN
FACULTY OF TECHNOLOGY
Polymer Centre

Jakub Sedlák

MULTISCALE HIERARCHICAL ZnO-BASED COMPOSITE SYSTEMS

Víceměřítkové hierarchické kompozitní systémy na bázi ZnO

Doctoral Thesis

Programme:	P 2808 Chemistry and Materials Technology 2808V006
Course:	Technology of Macromolecular Compounds
Supervisor:	doc. Ing. et Ing. Ivo Kuřitka, Ph.D. et Ph.D.
Year:	2014

Doctoral study programme:	P2808 Chemistry and Materials Technology 2808V006 Technology of Macromolecular Compounds
Supervisor:	Assoc. Prof. Ing. et Ing. Ivo Kuřitka Ph.D. et Ph. D.

CONTENT

ACKNOWLEDGEMENTS

I would like to especially thank my supervisor Assoc. Prof. Ing. et Ing. Ivo Kuřitka, Ph.D. et. Ph.D. for his inspiration, patience, guidance and endless ingenuity,

all of the members, colleagues and friends from Polymer Centre, Centre of Polymer Systems and other departments of the University Institute and Faculty of Technology of Tomas Bata University in Zlin for their help and partnership,

to Prof. Petr Sáha, CSc., Assoc. Prof. Dr. Vladimír Pavlínek and Assoc. Prof. Tomáš Sedláček, Ph.D. for creating an outstanding academic and social environment at the Centre of Polymer Systems.

Dr. Filip Mika from Institute of Scientific Instruments of the Academy of Sciences of the Czech Republic, p.r.i. (public research institution) is acknowledged for help with acquisition of the micrographs in Papers IV and V.

Thanks to all my friends for their great company in Olomouc and Zlin,

to Irena and many others not explicitly mentioned here who make life good and interesting.

And last but not least, thanks to my family for their endless care, support and love.

ABSTRACT

The presented doctoral thesis, submitted in the form of a commented, thematically ordered collection of original scientific articles supported by theoretical background, is focused on the preparation of multiscale hierarchical ZnO-based composite systems. Several preparation techniques, including bottom-up as well as top-down methods were employed throughout the work aiming the synthesis of various nanocrystalline ZnO powders that demonstrated the application potential in diverse fields.

In the first study, antibacterial ZnO filler was synthesized by solvothermal microwave assisted process to obtain nanostructured hierarchical raspberry-like sub-micro particles. Their application potential was successfully confirmed with the preparation of an antibacterial composite made by mixing the prepared ZnO particles with medical-grage, softened poly(vinyl chloride) matrix, and with a final evaluation of the surface antibacterial properties.

Methods leading to diverse ZnO morphologies were explored in a preliminary screening study that showed extreme versatility of the two-step synthesis (mechanochemical preparation of a precursor followed by microwave solvothermal synthesis). A follow up study was focused on desirable surface properties of ZnO nanostructured powders as ZnO is often utilized in oil or fat dispersions; the overall surface properties must be suitable for the intended application. Thus, the third study addressed to the preparation of surface-modified nanocrystalline ZnO particles with various lipophilicities and specific surface areas that were produced by a combination of mechanochemical preparation of precursor and subsequent solvo-thermal microwave-enhanced synthesis and coating *in-situ*.

The last two investigations included in this thesis are associated with the synthesis of nanostructured porous ZnO powders by thermal annealing of zinc oxalate dihydrate and zinc peroxide precursor. The structural and morphological parameters of prepared mesoporous ZnO micro-beads and nanocrystalline assembled ZnO spheres were investigated. In addition, the application potential of the prepared ZnO powders was successfully demonstrated by testing the photocatalytic performance by UV degradation of methyl violet 2B. The formation mechanism of mesoporous ZnO micro-beads during annealing of zinc oxalate was identified and basic parameters of the sintering process and crystallite growth were described.

Key words: ZnO, nanocrystallites, surface modification, composite, microwave-assisted synthesis, thermal decomposition

ABSTRAKT

Předkládaná disertační práce ve formě komentovaného tematicky uspořádaného souboru původních článků s doprovodným teoretickým komentářem je zaměřena na přípravu víceměřítkových hierarchických kompozitních systému na bázi ZnO. V práci je aplikováno několik postupů přípravy zahrnujících jak botom-up, tak i top-down, metody vedoucí k různým formám nanokrystalického ZnO, jehož aplikační potenciál byl úspěšně demonstrován v různých oblastech.

První studie pojednává o přípravě antibakteriálních hierarchických nanostrukturovaných ZnO sub-mikronových částic s morfologií připomínající maliny pomocí mikrovlnami asistované solvotermální syntézy. Hodnocení povrchové antibakteriální aktivity materiálu, který byl připraven zamícháním malého množství tohoto ZnO plniva do taveniny medicínského měkčeného polyvinylchloridu, prokázalo vynikající antibakteriální účinnost připraveného kompozitu.

Metody vedoucí k různým morfologiím ZnO byly zkoumány v předběžné orientační studii, která prokázala mimořádnou všestrannost dvoustupňové syntézy (mechanochemická příprava prekurzoru následovaná mikrovlnnou solvotermální syntézou). Následující studie proto již byla zaměřena na ovlivnění povrchových vlastností nanostrukturovaných ZnO částic, které jsou často používány ve formě přísady do olejových nebo tukových disperzí. Třetí studie je proto zaměřena na přípravu povrchově modifikovaných nanostrukturovaných částic ZnO s různě velkým specifickým měrným povrchem a různou lipofilicitou. Tyto materiály byly taktéž připraveny kombinací mechanochemické přípravy prekurzoru následované mikrovlnnou solvotermální syntézou ZnO s *in-situ* povrchovou modifikací.

Poslední dvě studie zahrnuté do disertační práce pojednávají o přípravě nanostrukturovaných porézních ZnO částic pomocí termického rozkladu z prekurzorů šťavelanu zinečnatého dihydrátu a peroxidu zinečnatého. Hlavní pozornost je zde věnována popisu změn strukturních a morfologických parametrů připravených mezoporézních nanostrukturovaných micročástic v závislosti na různé žíhací teplotě prekurzorů. Dále byl identifikován mechanismus růstu nanostrukturovaných mesoporézních ZnO mikročástic připravených termickým rozkladem šťavelanu zinečnatého dihydrátu a byly popsány základní parametry procesu slinování a růstu krystalů. Připravené částice byly následně úspěšně využity při testech fotokatalytické UV degradace metylové violeti 2B.

Klíčová slova: ZnO, nanokrystaly, povrchová modifikace, kompozit, mikrovlnami asistovaná syntéza, termický rozklad.

LIST OF FIGURES

LIST OF TABLES

LIST OF SYMBOLS AND ACRONYMS

(OD)	Zero dimensional structure
(1D)	One dimensional structure
(2D)	Two dimensional structure
(3D)	Three dimensional structure
QDs	Quantum dots
NPs	Nanoparticles
$\tan \delta$	Loss tangent
ε’’	Dielectric loss
ε’	Dielectric constant
ZnO	Zinc Oxide
UV	Ultraviolet
ROS	Reactive oxygen species
UVA	Specific ultraviolet range
UVB	Specific ultraviolet range
LED	Light emitting diode
OLED	Organic light emitting diode
DCSc	Dye sensitized solar cells
PVA	Poly(vinyl alcohol)
PEG	Poly(ethylene glycol)
DEG	Diethylene gylocol
MV	Methyl violet 2B
LD	Lipophilic degree

LIST OF ARTICLES AND AUTHORS' CONTRIBUTIONS

I. SEDLAK, J. (50 %); BAZANT, P.; KLOFAC, J.; PASTOREK, M.; KURITKA, I. Antibacterial Composite Based on Nanostructured ZnO Mesoscale Particles and Poly(vinyl chloride) Matrix. *Materials and Technology, ISSN: 1580-2949 – accepted, scheduled to be published in the issue 2/2015.*

II. SEDLAK, J. (50 %); BAZANT, P.; KOZAKOVA, Z.; MACHOVSKY, M.; PASTOREK, M.; KUŘITKA, I. Nanostructured Zinc Oxide Microparticles with Various Morphologies. *In NANOCON 2011 Conference Proceedings*, pp. 305-309, 2011. ISBN: 978-80-87294-23-9.

III. SEDLAK, J. (50 %); KURITKA, I; MACHOVSKY, M.; SULY, P.; BAZANT, P.; SEDLACEK T. Zinc oxide nanoparticles with surface modified by degradation of capping polymers in situ during microwave synthesis. *Submitted to Advanced Powder Technology.*

IV. SEDLAK, J. (50 %); KURITKA, I; MACHOVSKY, M.; BAZANT, P.; JANOTA, P.; DVORACKOVA, M. ZnO micro-beads with mesoporous architecture prepared by annealing at different temperatures and their photocatalytic activity. *Submitted to Materials Characterization.*

V. MACHOVSKY, M.; SEDLAK, J. (40 %); JANOTA, P.; URBANEK, P.; HAJEK, M.; DVORACKOVA, M.; KURITKA, I. Photocatalytic properties of nanocrystalline assembled ZnO spheres. Manuscript in preparation.

1 INTRODUCTION

Hierarchically ordered structures hold their own position within nanotechnology as they represent special types of nanostructures, which are built up from lower dimensional units such as rods, wires or plates, by controlled crystallization and aggregation. These 3-dimensional materials can offer advantages arising from high surface area, as the building blocks are often at the level of nanoscale. On the other hand, primary nanocrystals can self-assemble to complex structures such as hierarchical flowers or spheres ranging from mesoscale up to microscale, driven by the reduction of overall system energy. Therefore, multiscale hierarchical nanostructured materials are interesting because of both (i) the properties gained at the nanoscale and (ii) composite processability gained at the meso to micro scale.

Zinc Oxide is a particularly interesting material that can be obtained in various size scales and morphologies, and thus, has a variety of final properties. Microwave-assisted solvothermal chemistry became a popular method for the production of various inorganic powders; time reduction as well as high yields are the main benefits of the microwave synthesis process.

2 NANOMATERIALS

The simplest definition of nanomaterials is given by their size. Indeed, any material can be categorized as a nanomaterial if the sizes of its' individual building blocks are smaller than 100 nm in at least one dimension. Another more specific definition states, that nanomaterials have properties which depend inherently on their size, and such properties can be significantly different when compared to the properties of micro or bulk materials. In principle, there are two main approaches leading to production of nanomaterials called “bottom-up” and “top-down” techniques. The bottom-up approach is preferred in nanotechnology, whereas the top-down approach is used just in minority cases and its dominant application lies in conventional technologies [1].

From the point of dimensionality, one can distinguish among (i) zero-dimensional (0D) structures such as quantum dots or nanoparticles, (ii) one-dimensional (1D) structures including nanowires, nanotubes and nanorods or (iii) two-dimensional (2D) structures such as thin films [2]. Processes leading to three-dimensional (3D) hierarchical ordered structures are still not perfectly understood and therefore attract much attention from the research community [3-5].

2.1 Bottom-Up versus Top-Down approach

As mentioned above, bottom-up and top-down techniques represent different ways of preparation of nanostructures. The typical example of a top-down method for making nanoparticles is milling, in contrast to the synthesis of a colloidal dispersion by the bottom-up method. Both of these approaches play important roles in modern industry as well as nanotechnology. Obviously, there are some advantages and disadvantages of both approaches. The biggest issue related to with top-down methods such as lithography or milling is the presence of structural defects and surface impurities. This would have a significant influence on physical properties and surface chemistry of nanomaterials, since the surface to volume ratio in nanostructures and nanomaterials is very large and therefore a crucial parameter [1,2].

The bottom-up process is related to building up materials from atoms, molecules or clusters. An example of such a process can be found in polymer chemistry, where it is well known that polymers are synthesized by connecting smaller individual parts called monomers by the polymerization process. Similarly, in the crystal growth process, atoms, ions, and molecules assemble into the crystal structure one after another, upon contacting the growth surface. With nanomaterials there is very little opportunity for the top down approach because almost all the tools we have are too large to manipulate such small objects. Botom-up processes also promise fabrication of nanostructures with fewer defects, and more homogenous chemical composition as compared to the top-down process and are therefore generally more favorable [2].

2.2 Properties of nanomaterials

Unique properties of nanostructured materials depend mostly on their surface characteristics, because unlike bulk materials, the number of surface atoms is not negligible. The surface to volume ratio of atoms is the important parameter which is directly related to the size of particles in the matter. For example, if considering a cube of iron of 1cm^3, the percentage of surface atoms would be only 10^{-5} %. If we divide this cube into smaller cubes with an edge of 10 nm, the percentage of surface atoms will increase to 10 %. In the case of an iron cube of 1 nm^3 each atom will be a surface atom [2]. This huge increase of surface to volume atoms should demonstrate why we expect great changes in physical and chemical properties of nanostructured materials when compared to their bulk counter-parts. Similarly, the specific surface area and surface energy are also strongly size dependent parameters which are important when considering nanometer range, often resulting in thermodynamic instability or metastability. Therefore, such an unstable system often tends to reduction of large surface energy by the agglomeration, sintering or so called "Ostwald ripening" [2].

A good example where nanotechnology can significantly change properties of materials is the UV absorption shift of TiO_2 particles by the change of nanocrystals size. Generally for TiO_2, UV absorption maxima can be adjusted within the range of 200 to 550 nm by varying particle size. When decreasing the size of TiO_2 particles, significant blue shift is observed; red shift is observed with an increase in size. The use of ultrafine UV absorbing TiO_2 particles would lead to a nanocomposite which is perfectly transparent in the visible region [1].

3 ZINC OXIDE STRUCTURE AND PROPERTIES

Zinc oxide has been in use since 2000 B.C. as a part of medicinal ointments for boils and carbuncles treatment. More recently, well-known applications of ZnO are in ceramics, paints and coatings, cosmetics; the most important use of ZnO over the last century remains associated with the rubber (polymer) industry [6]. As a member of the II-VI binary compound semiconductors group, zinc oxide crystallizes in a cubic zinc blende, cubic rock salt or hexagonal wurtzite, whereas the only thermodynamically stable phase under ambient conditions is that of wurtzite symmetry [7].

Zinc oxides' leading characteristics are a wide band gap at 3.37 eV and a large exciton binding energy of 60 meV at room temperature [8]. These properties make a ZnO a promising semiconductor candidate with possible applications in light emitting diodes [9], dye-sensitized solar cells [10] and transparent electrodes [11]. Also, gas-sensing properties of nanostructured ZnO were successfully discovered [12,13]. Another interesting property of ZnO is the photocatalytic degradation of organic pollutants present in wastewater [14,15]. Zinc oxide has become a serious point of interest since Sawai et al. in 1995 first reported antibacterial activity of a ZnO powder slurry [16]. In addition, ZnO exhibits good biocompatibility and therefore seems to be a very promising material for future applications in bioimaging and drug delivery [17]. If nano zinc oxide is utilized as filler in polymers, polymer nanocomposites with enhanced properties can be obtained [18,19]. This matter will be discussed in more detail in the chapter dealing with polymer nanocomposites.

In the past decade, many different strategies have been employed to synthesize ZnO nanomaterials rich in morphologies. These has been varied from (i) zero dimensional quantum dots QDs, (ii) one dimensional nanowires/nanorods, (iii) two dimensional structures such as thin films or (IV) superstructures with complex 3D hierarchical morphology [20-22]. Amongst three general processes applicable for nanoparticle production, including solid-state, gas-phase and liquid-phase, the latter seems to be of biggest importance especially for metal oxide particles such as zinc oxide. Liquid phase processes generally enable better control over structural, compositional and morphological features of the final nanomaterials by using lower cost equipment [23]. Solid-sate processes such as milling involve structural defects, and are predominantly used for the production of micro-sized powders. Gas-phase processes are successfully employed for the low-cost production of large quantities of nanopowders but utilize much more expensive equipment [24].

So called “chimie douce” or wet chemical processes proceed under relatively low temperatures and have become an important group. They include several sub-processes which can be classified into five major categories: (i) sol-gel processing, (ii) the precipitation method, (iii) water-oil emulsion (reverse micelle), (iv) the polyol method and (v) hydrothermal synthesis [24]. Several proposals for the synthesis of ZnO nanomaterials have been suggested, such as spray pyrolysis of a ZnO precursor on a polymer substrate [21], mechanochemical synthesis of nanocrystaline ZnO [25], hydrothermal synthesis of various morphologies of nanostructured ZnO [4], a precipitation method [26], thermal decomposition of a ZnO precursor [27], a sol-gel process [28], a solvothermal method [5], polyol-mediated [29] and microwave-assisted synthesis [30-32].

3.1 Fabrication of hierarchical nanostructures

Generally, one can choose between two main strategies for the fabrication of hierarchical nanostructures. The first method comprises of nanoparticle synthesis and its’ assembly into super-particulate complex structure in one step [33] while the other method of synthesis and arrangement into 1-, 2-, or 3- dimensional structures proceeds in two successive steps [34]. Considering the first method, in many instances nature is providing good examples of hierarchical complex structures obtained at mild conditions via controlled crystallization and aggregation [35].

Formation of mesocrystals (“mesoscopically structured crystals”) as the special kind of colloidal crystals involves crystallization and aggregation in a one step process. In contrast frequently used two-step processes include nanocrystals synthesis and their subsequent assembly with the help of physical methods, such as solvent evaporation or application of magnetic or electric fields. Indeed, in most cases the preparation of two or three dimensional super-structures starts by drop coating of colloidal nanoparticles solution onto solid substrate followed by evaporation of the solvent [23].

Crystal coarsening has been traditionally described by the Ostwald ripening process, which is characterized by the growth of large particles at the expense of smaller ones, leading to a more thermodynamically stable system via the reduction of surface energy. This process requires sufficiently high molecular solubility in the continuous medium as well as high interface energy of the crystal [36,37]. As an alternative, the oriented attachment process may take place if the surface energy and solubility of the material is lower [23]. Oriented attachment involves spontaneous self-organization of adjacent particles in that way so they share common crystallographic orientation, followed by connection of these particles at the planar interface [36]. Oriented attachment belongs to the group of nonclassical crystallization driven by the reduction of the large surface energy of nanoparticles, through elimination of high energy facets or possible interaction of dipoles carried by the nanoparticles. But the detailed mechanisms are still not clear [36,38,39].

Examples of quasi one, two, and three dimensional structures obtained through the oriented attachment process in organic solvents are not exceptional. On the contrary, presence of aqueous media often results in formation of one-dimensional oxidic structures which are difficult to obtain in organic solvents. Just a few studies on 1D structures in organic solvents have been reported [23]. Among previously mentioned methods for the fabrication of ZnO nanomaterials, processes utilizing microwave energy has taken a big portion of scientists' effort in the last decade [40-42] and therefore will be discussed in more detail in following chapter.

3.2 Microwave synthesis

Microwave energy has been successfully applied in various areas of modern synthetic chemistry during the past decade. New techniques for the production of organic as well as inorganic materials were developed hand in hand with extensive progress in the availability of broad range experimental apparatuses. On one hand, a simple modified domestic microwave oven equipped with an infrared temperature sensor and reflux cooling system can be utilized. On the other hand, the use of a professional closed-vessel microwave reactor designed for precise pressure and temperature control with the possibility of stirring and cooling of the system would lead to great improvement of the reproducibility. Practically all microwave-assisted syntheses are performed in equipment operating at 2.45 GHz which corresponds to a wavelength of 12.25 cm and photon energy of 0.0016 eV. Microwave energy is thus too small to induce chemical reactions by direct absorption of electromagnetic energy, in contrast to ultraviolet and visible radiation used in photo-chemistry [43].

Generally, microwave dielectric heating is a matter of interaction of microwaves with specific materials such as solvents or precursors.

The crucial material parameter here is the ability to absorb and convert microwave energy into heat. Two main mechanisms of microwave heating consist of dipolar polarization and ionic conduction. Any non-ionizied substance able to generate heat when exposed to microwaves must possess a dipole moment. When such molecules are irradiated by MW, their dipoles try to realign according to the high frequency oscillating electric field, resulting in the loss of energy in the form of heat through molecular friction and dielectric loss. The other heating mechanism called ionic conduction is manifested when working with mobile charged particles, usually ions. Charged ions oscillate back and forth under the agitation of the microwave field, so that they collide with adjacent molecules or atoms and create heat due to the kinetic motion. A good example of such behavior can be observed when heating distilled or tap water: at the same conditions the latter will be heated faster due to the presence of ions [40,43]. Ionic conduction is particularly important if working with ionic liquids, which interact very efficiently with microwaves and are rapidly heated at rates of around 10 °C/s without a significant increase of pressure. When considering strongly conducting or semiconducting materials such as metals (e.g. Au, Pt) a related heating mechanism which can induce flow of electrons on the surface can take a place. Surface electron flow can heat the material by ohmic-resistance heating mechanisms [40,41]. In general, heating of particular material under microwaves is dependent on the dielectric properties of the material. The capability of such a material to transform microwave energy into heat at a specific frequency and temperature is defined by loss tangent tan δ according to equation 1.

$$\tan\delta = \frac{\varepsilon''}{\varepsilon'} \qquad \text{(Eq. 1)}$$

Here ε'' is the dielectric loss describing the conversion of electromagnetic radiation into heat, and ε' is the dielectric constant representing the polarizability of molecules in the electric field. Solvents can be categorized as low (tan δ < 0.1), medium (tan δ 0.1-0.5) and high (tan δ > 0.5) microwave-absorbing. In more detail, there are other parameters which can sometimes influence the heating rate, other than that given by tangent loss, such as heat of vaporization, specific heat capacity or the penetration depth of microwave irradiation into the sample [41]. Microwave heating can be classified as "volumetric" heating since there is a simultaneous raise of temperature within the whole volume. This is in contrast to conventional heating where the reaction mixture is heated first from the wall of the vessel. In the literature, one can find a description of so-called “microwave effects” which might be responsible for as of yet incompletely understood microwave-matter interaction, and could explain why the outcomes of the syntheses in microwaves are different from those performed by conventional heating at the same temperature. The category of specific microwave effects includes the superheating effect at atmospheric pressure, selective heating of strongly absorbing material in a medium with lower polarity, and the presence of an inverse temperature gradient due to the elimination of the wall effect. Presence of so-called “non-thermal” microwave effects is still controversial topic within the scientific community. Non thermal effects have been postulated for a proposed direct interaction of an electric field with specific molecules in the reaction mixture which is not connected to a macroscopic temperature effect [40].

In past years, various microwave wet chemistry reactions have been successfully utilized for the preparation of morphology-rich ZnO nanostructures as well as other metal and metal oxide particles [42]. Among them, two main groups can be generalized as hydrothermal and solvothermal processes. Hydrothermal synthesis belongs to a so-called “green chemistry” approach employing water as the solvent for reactants. Since water is a polar substance, it has good potential to absorb microwave energy and transfer it into heat by both dipolar polarization and ionic conduction mechanisms. Typical dielectric characteristics of water compared to other solvents can be found in Table 1. One can see that loss tangents of polar organic solvents are much higher than that of non-polar organic solvent or water which implies better microwaves absorption, thus speeding-up of reaction.

Table 1 Dielectric properties of various microwave solvents [41]

Solvent	Dielectric constant (ε’)	Dielectric loss (ε’’)	Loss tangent (δ)
Water	80.4	9.89	0.123
Ethanol	24.3	22.90	0.941
Ethylene glycol	37.7	50.90	1.350
Hexane	1.9	0.038	0.020

Water-mediated synthesis protocols often lead to the formation of one-dimensional structures such as nanorods or nanowires [44,45]. Rarely, they lead to three-dimensional self-assembled hierarchical flower-like structures which are interesting mainly due to their promising technological potential for electronic devices, sensors, or photocatalysis [30,46,47]. On the other hand, a main drawback of hydrothermal process is the insolubility of most of the organic precursors, resulting in heterogeneous reaction mixtures [40]. Moreover, energy demand for preparation of distilled water is not negligible. Therefore, plenty of reactions are performed under aqueous-free solvothermal conditions by using organic solvents [29,48-50].

Generally, two different ways including surfactant-controlled or solvent-directed solvothermal reactions can be followed. The main drawbacks of surfactant directed methods lie in the higher amount of organic impurities as well as lower accessibility of the nanoparticles surface due to the adsorption of surfactants. This has a subsequent negative influence on sensing and catalytic applications. On the other hand, solvent directed procedures are generally simpler, starting only from metal oxide precursors and routine organic solvent, and leading to higher purity products. Furthermore, organic solvent can play both roles involving reactant and particle growth modifier [23,42]. Indeed, it acts on one hand as a donor of oxygen for metal oxide creation and on the other hand as a capping agent that binds to the surface of particles. Thus, it modifies the particle growth and finally affects the morphology and assembly. Formation of spherically shaped particles or complex architectures is frequently observed within the solvothermal reactions compared to one-dimensional structures commonly seen under hydrothermal conditions. Presence of a certain amount of water in solvent-directed reactions also plays an important role, especially in polyol-mediated reactions starting from metal acetate reactants. The small amount of water is usually added into the system through the use of hydrated precursors or solvents which generally modify hydration and condensation of metal precursors, resulting in different crystal growth [23,29,48].

4 NANOCOMPOSITES

Nanocomposites are composite materials with at least one phase exhibiting the special properties of nanomaterials. Supposedly, the oldest type of nanocomposite is that with more or less spherical nanoparticles present in gold-ruby-glass vase, consisting of a glass matrix with gold nanoparticles produced by the Assyrians in the 17th century BC. Generally, three most important types of nano-composites differ in the dimensionality of the second phase, which can be formed either by (0D) isolated nanoparticles, (1D) nanotubes, nanorods and nanowires, or by (2D) stacks of layers [1]. Continuous development and availability of nanomaterials promise new and enhanced nanocomposites that can find use in a wide range of application such as electronics, pharmaceutical, medicine and material science. One area of particular interest is the development of polymer nanocomposites. These are usually formed from a combination of inorganic nanomaterials and organic polymer matrix, hence exhibiting properties that are representative of both components [51].

4.1 Polymer nanocomposites

Polymer nanocomposites are polymer matrix composites which contain materials having at least one dimension below 100 nm. The small size offers some level of controllable performance that is different from the expectations developed in the macroworld. Indeed, there must be some advantage in achieving the nanoscale whether it is for mechanical reinforcement or the enhancement of another desirable property. The polymer-nanomaterial interface is the key determinant of nanocomposite properties. To imagine the importance of polymer-nanocomposite interface some simple calculations are helpful. If we consider 1μm cube, the surface area equals 6 μm^2, which is 6 x 10^6 nm^2 if expressed in nanometers. If the micron cube were to fracture up to 1 nm length cubes, then the total surface area of one of these cubes generated will be 6 nm^2 and the total number of cubes generated would be 10^9. Therefore, the total surface are of the generated cubes equals 6 x 10^9 mm^2 representing an increase of the total surface area by a factor of 10^3. With such as huge increase of interfacial area it is reasonable to expect some difficulties in mixing. For example, if polymers are compounded with nanoclay precursors, the increase of interfacial area (polymer-platelet) can result in a viscosity increase of an order of magnitude [51].

There are generally three ways of preparation for nano-composites: (i) melt compounding (ii) film casting and (iii) in-situ polymerization [52]. In melt compounding, the objective is to achieve distributive mixing ideally leading to homogenous distribution of an additive in a polymer matrix. The objective is to surround each individual particle with the coating of polymer matrix, which is not always possible due to the different surface energies of the polymer matrix and particles, leading to their aggregation or agglomeration [51,52]. To overcome this problem, surface functionalization of particles prior to compounding usually takes place [52]. Melt processing has been studied by many authors regarding thermoplastic resin nanocomposites. The influence of ZnO nanoparticles on composite photo-degradation [53,18], mechanical [18,19,53,54], thermal [53,54], barrier [19] and antibacterial properties [18,54] has been investigated. Dielectric properties of polyvinyl alcohol-zinc oxide nanocomposite films prepared by solvent casting [55], as well as mechanical and antibacterial properties of polyurethane based coatings reinforced by ZnO nanoparticles prepared by an in-situ copolymerization process [57] have been also studied.

4.2 Applications of ZnO in nanocomposites

In past years, zinc oxide nanostructures have been successfully applied in the form of various nanocomposites, reaching different functions according to the intended application as specified in following paragraphs.

4.2.1 Antibacterial or UV blocking polymer-ZnO nanocomposites

The influence of ZnO nanoparticulate fillers on antibacterial effects of various polymer nanocomposites against both gram-positive and gram-negative bacteria, represented mostly by *Staphylococcus aureus* and *Escherichia coli*, respectively, have been proven by many authors. ZnO NPs were added to polymers such as polyurethanes [56,57], polypropylene [54], high density polyethylene [18] or poly(vinyl chloride) [58], where all authors observed reduction of bacterial species as compared to the initial untreated polymer samples. To date, there exist several proposals of the mechanism of antibacterial action of ZnO such as formation of reactive oxygen species ROS [58], zinc ions Zn^{2+} [54] or hydrogen peroxide H_2O_2 generated from the surface of ZnO [18,56,57]. As it stands, to the best of my knowledge, the exact role of antibacterial action of ZnO nanoparticles is not clear. Moreover ZnO NPs UV absorption has been advantageously used for the preparation of UV resistant nano ZnO/glass fibre/epoxy composite in the whole UVA and UVB range [59]. Another research group prepared ZnO NPs by the wet chemical process, followed by their coating on bleached cotton fabric. UV blocking properties of cotton fabric treated by ZnO NPs showed 75 % absorption of UV light as compared to 20 % absorption for untreated samples [60].

4.2.2 ZnO for photocatalysis and gas sensors

Good accessibility of the metal oxide nanoparticle surface prepared by surfactant free methods seems to be profitable for both photocatalytic and gas sensing properties, since several studies confirmed that the presence of surfactants lowered photocatalytic activity of metal oxide nano powders [23]. ZnO hollow spheroids were successfully used for the complete photocatalytic degradation of aqueous solution of rhodamine B (as the model organic dye used for textiles colouring) under UV light within 300 minutes. Neither in the presence of ZnO spheroids and absence of UV light nor with UV illumination and without the ZnO, did any photocatalytic degradation of rhodamine B took place [61]. Similarly, another group of authors synthesized nanorods assembled flowers which demonstrated 91 % and 80 % degradation of methylene blue and rhodamine B dye, respectively, within 140 minutes [62]. In addition, the effect of morphology of ZnO particles prepared by microwave assisted solvothermal synthesis on photodegradation of methyl orange was evaluated among six different samples. The best result represented by 98 % degradation of methyl orange within 40 min was manifested by hierarchically structured spheres; the authors' explanation was related to the highest specific surface area [63].

Several groups have focused on the preparation of metal oxide semiconductor gas sensors in the form of thin films. These operate upon the change of the resistance of metal oxide nanoparticles due to the adsorption of reducing gases [64]. In a similar way, ZnO based sensors designed for nitrogen dioxide [12], ammonia [13] and ethanol [65] were successfully fabricated.

4.2.3 ZnO for light emitting diodes and solar cells

Since ZnO semiconducting NPs possess a wide band gap of about 3.37 eV and a large exciton binding energy at of 60 eV at room temperature, their electronic and luminescent properties have been extensively studied in connection with the potential applications in light emitting devices (LEDs). Within this field, most of the attention has been devoted to low dimensional structures such as ZnO quantum dots, nanorods or nanowires [66]. Moreover, organic light emitting diodes (OLEDs) utilize a nanocomposite layer composed of a semiconductive polymer and luminescent ZnO nanoparticles [9]. Continuous improvement of dye sensitized solar cells (DSCs) represents one option for harvesting energy from the light. For this purpose, DSCs based on ZnO hierarchical nanostructures manifested maximum conversion efficiency up to 5.4 % [10].

5 AIMS OF WORK

The main aim of the present dissertation work arose from literature review as preparation of ZnO nanostructured materials with hierarchical structure and demonstration of its application potential. It can be subdivided into following goals:

- Preparation of the nanostructured material by chosen synthesis methods with respect to desired structure and morphology of the ZnO product.
- Characterization of morphology, structure, optical, surface and other properties of the prepared powdered materials.
- Testing of a functional property selected with respect to the possible application and demonstration of the potential usefulness of prepared materials.
- Preparation of a composite system by mixing of selected ZnO fillers with a chosen polymer matrix.
- Evaluation of the obtained composite properties, in terms of mechanical and antibacterial properties.

6 METHODOLOGY

6.1 Materials

Oxalic acid dihydrate, $C_2H_2O_4 \cdot 2H_2O$, zinc acetate dihydrate, $Zn(CH_3COO)_2 \cdot 2H_2O$, anhydrous sodium carbonate Na_2CO_3, 25-29 % aqueous ammonia, hydrogen peroxide, ethylene glycol and diethylene glycol were all supplied by Penta (Czech Republic). Polyethylene glycol 400, poly(vinyl alcohol) Mowiol 8-88, and medical grade poly(vinyl chloride) were supplied by Fluka (Germany), Sigma Aldrich (Switzerland), and Modenplast (Italy), respectively. Distilled and demineralised water as well as ethanol were used as needed within individual experiments.

6.2 Zinc oxides syntheses

Paper I: Powdered zinc oxide with hierarchical morphology on mesoscale (hierarchical raspberry-like particles) was synthesized by fast and simple microwave enhanced solvothermal reaction. The microwave synthesis of hierarchical raspberry-like powdered ZnO was done in the microwave open vessel system MWG1K-10 (Radan, The Czech Republic, 800W, 2.45 GHz), which is based on modification of a domestic microwave oven by drilling a hole in the ceiling for external cooler and equipped by external source of microwave energy that allows to control the duty cycle. The reaction mixture was heated in a quasi-continuous mode at maximum heating power.

Paper II: ZnO micro and nanoparticulate materials were synthesized in two step process, including mechanochemical preparation of precursor (vibration mill) followed by microwave assisted solvothermal synthesis. Microwave assisted synthesis of surface modified ZnO particles was performed in modified domestic microwave oven (CRW-TECH, frequency 2.45 GHz, maximum power 1150 W, (unknown land of origin) equipped with an external condenser. All mixtures were heated at maximum heating power.

Paper III: ZnO nanoparticles surface modified by degradation of polymer capping agents were synthesized in two step process, including mechanochemical preparation of precursor (vibration mill) followed by microwave assisted solvothermal synthesis with *in-situ* coating. Microwave assisted synthesis of surface modified ZnO particles was performed in modified domestic microwave oven (CRW-TECH, frequency 2.45 GHz, maximum power 1150 W, (unknown land of origin) equipped with an external condenser. All mixtures were heated at maximum heating power.

Paper IV: Preparation of porous ZnO microbeads and nanocrystalline assembled ZnO spheres was accomplished by the use of a muffle furnace (LMH 07/12, LAC, Czech Republic). The ZnO porous polyhedral microbeads were synthesised by two-stage process consisting of a precipitation of organic precursor and its subsequent thermal decomposition by annealing at different temperatures.

Paper V: The nanocrystalline assembled ZnO (raspberry) spheres were obtained by two-stage procedure consisting of recrystallization of dissolved commercial ZnO powder (used in rubber industry) obtaining zinc peroxide precursor and its subsequent thermal decomposition by annealing at different temperatures.

Detailed description of synthetic procedures for individual ZnO based materials can be found in attached articles (**Papers I-V**).

6.3 Composite preparation

The melt mixing process was chosen for the preparation of multiscale polymer composite system based on the hierarchical raspberry-like ZnO filler and medical grade plasticized PVC matrix loaded in the concentration range from 0.5 to 3wt. %. Compounding of ZnO filler to polymer matrix was done by batch mixer machine (Brabender Plasti-Corder, Germany) equipped by a 50 cm^3 mixing chamber (Brabender W50 EHT, Germany).

Compounds were hot pressed into sheets with 1 mm thickness aiming the purpose for standardized testing of composite mechanical properties and surface antibacterial activity.

Detailed description regarding compounding of ZnO to polymer matrix can be found in corresponding article (Paper I).

6.4 Characterization

Nowadays, many methods are available for structural and morphological examination of powdered inorganic materials as well for specific characterization of polymer composites. The utilized methods therefore include techniques regarding the aims of the work and their list is presented below.

Powder X-ray diffraction (XRD) analysis was utilized for phase characterization of prepared precursors and synthesized ZnO based particles by the X-ray diffractometer X´Pert PRO (PANalytical, The Netherlands) with Cu Kα radiation of λ = 0.1540598 nm. The size of ZnO nanocrystallites was considered to be nearly identical with the size of diffracting area d_{diffr} which is easily accessible via Scherrer's formula using $\Delta(2\theta)$ which is full-width at half-maximum (FWHM) of XRD patterns. The particle shape and other factors were neglected to simplify the procedure and the calculation followed the well-known formula [67]:

$$d_{diffr} = \frac{0.9\,\lambda}{\beta\ \cos\theta} \qquad \text{(Eq. 2)}$$

Where the constant 0.9 is the shape factor, λ is the wavelength of the X-ray source, β is the FWMH in radians. The actual value of β was obtained by deconvolution of instrumental broadening effects using Warren correction method. The θ is the Bragg angle, i.e. the half of the 2θ position of the selected diffraction line.

Thermogravimetric analysis (TGA) was performed on the thermogravimeter TA Q 500 (TA Instruments, United States) in order to elucidate the thermal decomposition behaviour of precursors as well as to find out the information concerning the purity of prepared powders.

Scanning electron microscopy (SEM) was carried out to observe the morphology of prepared powdered materials and for the characterization of fillers dispersion and distribution at the cross-section of prepared polymer composites by the scanning electron microscope Tescan Vega LMU (Tescan, Czech Republic).

Diffuse reflectance infrared Fourier transform spectroscopy (DRIFT) was utilized for structural characterization of powdered materials with the aid of FTIR spectrometer Nicolet 6700 (Thermo Scientific, United States)

The ultra violet visible absorption spectroscopy (UV-vis) was used for optoelectronic characterization of prepares powdered materials by UV-vis spectrometer AvaSpec 2048-2 (Avantes, The Netherlands) with the light source type AvaLight-DHS-DUV. Integrating sphere ($BaSO_4$ coated) and white tile $BaSO_4$ reflectance standard were used for relative diffuse reflectance (DR-UV-vis) spectrometry. Moreover, the UV-vis spectrometer (UV-Vis Varian Cary 300, Varian Inc., United States) was used for transmission measurements of the MV solutions to evaluate the photocatalyst efficiency within the wavelengths in the range from 300 to 800 nm.

The Brunauer-Emmet-Teller plot (BET) was used for characterization of specific surface area of prepared ZnO powders via the analysis of nitrogen adsorption/desorption isotherms at 77 K recorded by Belsorp-mini II (BEL Japan, Inc., Japan). The grain size is expressed as the mean diameter d_{BET} according to [68]:

$$d_{BET} = \frac{6}{\rho_S \cdot A_{BET}} \quad \text{(Eq. 3)}$$

Where the ρ_s is a density of adsorbent material.

Mechanical properties (Young's modulus, elongation at break and tensile strength) of composites were evaluated by tensile tests performed at the Testometric universal testing machine M350-5CP (Labor machine, Ltd., Czech Republic) according to ISO 527-1,3 standard.

The photoluminescence (PL) spectra were measured at the room temperature by using Fluorescence spectrometer FLS 920 (Edinburgh Instruments, United Kingdom) with a monochromatized Xe lamp (150 W) as the excitation source. Samples for PL measurements were prepared by spin casting onto glass/ITO substrates using spin coater Laurell WS-650-MZ-23NPP (Laurell Technologies Corporation,United States) without futher treatment.

6.5 Testing of antibacterial activity

The evaluation of surface antibacterial activity of the composites against bacteria adherence and growth was performed according to the ISO 22196: 2007 (formerly known as JIS Z-2801) standard. Gram-positive bacteria were represented by *Staphylococcus aureus* ATCC 6538P and Gram-negative by *Escherichia coli* ATCC 8739 both obtained from The Czech Collection of Microorganisms (The Czech Republic). The size of test specimens was 50 mm x 50 mm x 1 mm. The HERAcell 150i incubator (Thermo Scientific, USA) was used for cultivation. The antibacterial activity *R* was calculated using equation 4:

$$R = (U_t - U_0) - (A_t - U_0) = U_t - A_t \quad \text{(Eq. 4)}$$

Where *R* is the antibacterial activity; U_0 is the average of the common logarithm of the number of viable bacteria, in cells/cm^2, recovered from the untreated test specimens immediately after inoculation; U_t is the average of the logarithm of the number of viable bacteria, in cells/cm^2, recovered from the untreated test specimens immediately after 48 hours; A_t is the average of the logarithm of the number of viable bacteria, in cells/cm^2, recovered from the treated test specimens immediately after 48 hours. The number of colonies was counted after 24 hours and controlled after 48 hours for eventual presents of slowly growing colonies for both untreated and treated test specimens which improves the original standard protocol. All tests were repeated in triplicate.

6.6 Testing of photocatalytic activity

The photocatalytic activity of ZnO porous powders was evaluated by measuring photocatalytic degradation of Methyl Violet 2B in distilled water under the constant illumination of 100W focused UV-lamp (Super-Light C 10 A-SH, Helling Gmbh., Germany) with the strongest emission at 365 nm. The temperature of the reaction was maintained at aprox. 25 °C by thermostatic circulation through the double-wall glass baker.

In a typical experiment, 20 mg of the ZnO porous powdered sample was added into the double-wall glass baker containing 50 ml of methyl violet 2B solution having concentration of 3.5 mg/l. Before the degradation starts, the suspension was stirred in the dark for 30 minutes to assure an adsorption/desorption equilibrium of used dye at the surface of ZnO particles. During the degradation, 12 solutions of about 1mL were withdrawn from the reaction suspension within the time range from 0 to 120 minutes and filtered through a syringe filter to completely remove the ZnO catalyst from the solution. Time dependent degradation was monitored by measurement of absorption of Methyl violet solutions at 580 nm by UV-vis spectroscopy. The photocatalysts efficiency was estimated as a ratio between actual and initial concentration of the dye plotted against time of UV irradiation. The initial concentration of the dye in the solution was set in that way so that the degradation test proceeds within 120 min. All obtained curves obey first (or pseudofirst) order reaction kinetics [69]. The rate constant was obtained from fitting the first order model into the data.

6.7 Testing of lipophilic degree

The lipophilic degree (LD) of nanoparticles is usually characterized by examination of dispersibility of defined amount of nanoparticles in water with the addition of organic solvent (methanol). Hence, the LD is expressed actually in vol % units. The original method [70,71] is relatively material demanding as each test of single liquid concentration consumes 0.5 g of sample. Therefore, we adopted the LD concept but modified the procedure in accordance with the framework of theoretical and practical analysis of wetting and dewetting of powders [72]. A series of stock water-methanol mixtures was prepared ranging from pure distilled water up to pure methanol graded in 5 vol % steps. The lipophilic degree was estimated as the concentration of the water-methanol mixture which readily wetted the tested powder. In more detail, the procedure was as follows: A small amount of powder (approx. 0.5 g) was spread into a uniformly thick layer on a glass substrate and tested by droplets of 5 μL of testing liquids. The measurement was several times repeated for each sample in ascending as well as in descending order of used concentrations to find precisely the transition between wetting and dewetting behaviour.

7 SUMMARY OF RESULTS

On the basis of literature research presented above, the possible applications of ZnO nanostructured particles covers numerous areas including antibacterial agents and photocatalyst. Therefore, the synthesis strategies of ZnO were directed towards both of these applications by the combination of top-down (microwave synthesis) and bottom-up (milling, thermal annealing) methods.

In the first article (**Paper I**), solvothermal microwave-assisted synthesis was chosen with the aim of preparing an active ZnO filler with a hierarchical structure from solution of zinc acetate dihydrate as a common zinc source in diethylene glycol.

The phase structure of synthesized ZnO filler presented on the diffractogram in Figure 1a) confirmed the hexagonal ZnO wurtzite structure. Moreover, the evident broadness of diffraction lines implied that synthesized particles are in nano-scale dimensions. This observation was also supported by findings from optical characterization by diffuse reflectance UV-vis spectroscopy presented in Figure 1b). Here, the position of the absoprtion maxima peak below 380 nm towards to nano-sized partilcles as well because of its slight blue-shift from typical bulk ZnO [73].

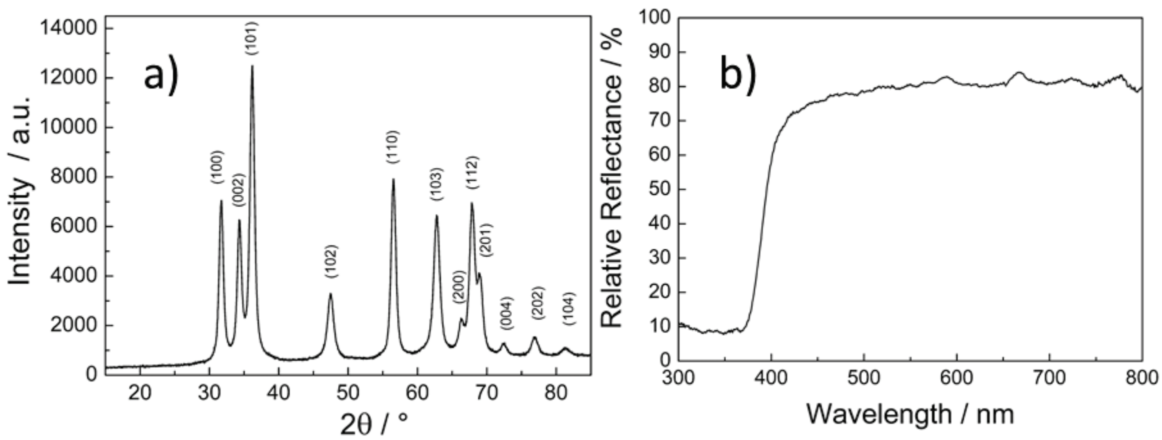

Figure 1 a) XRD diffractogram and b) UV-vis diffuse reflectance spectrum of prepared ZnO filler

Moreover, the morphology of prepared ZnO manifested by the SEM and TEM image in Figure 2 revealed that obtained filler consists of globular raspberry-like particle aggregates with diameter ranging from 200 nm up to 1 μm, while these aggregates are assembeled from much smaller nanocrystalls as can be clearly seen from TEM image.

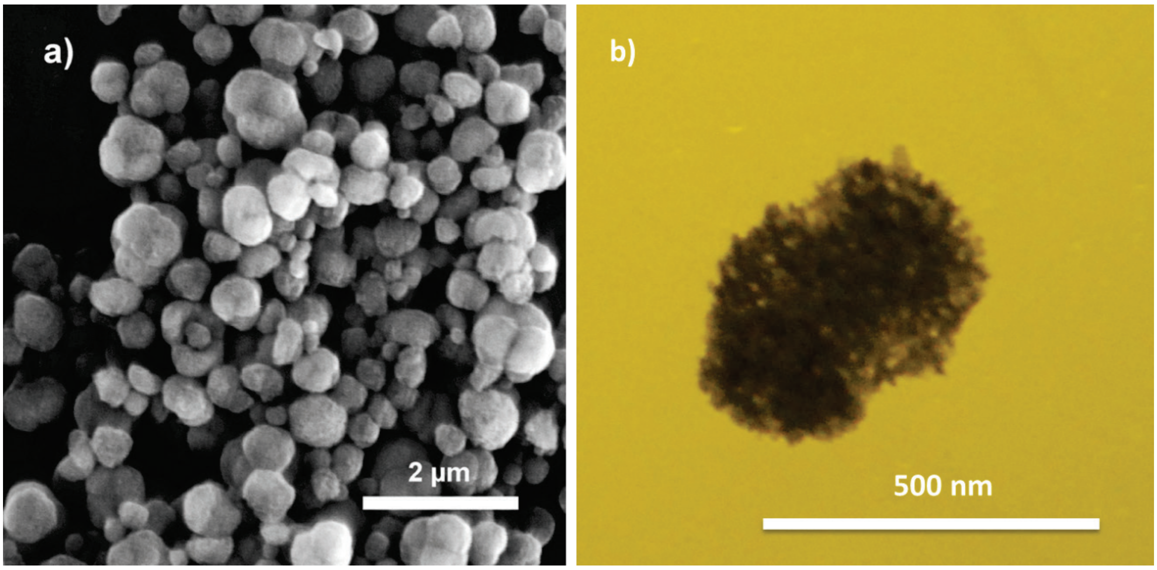

Figure 2 a) SEM image and b) TEM image of raspberry-like ZnO hierarchical filler (note: TEM image belongs to unpublished data)

The as prepared filler was afterwards compounded with medical grade PVC by the melt-mixing process aiming the preparatin of low-content loaded antibacterial polymer composite. The filler dispersion in prepared composites was achieved at the aggregate level and its good distribution in PVC matrix is manifested by the SEM images in Figure 3 representing the sample with 2 wt% ZnO loading. There are no visible agglomerates of the globular aggregates within the polymer matrix. On the other hand, the aggregates were not disaggregated by the mixing procedure.

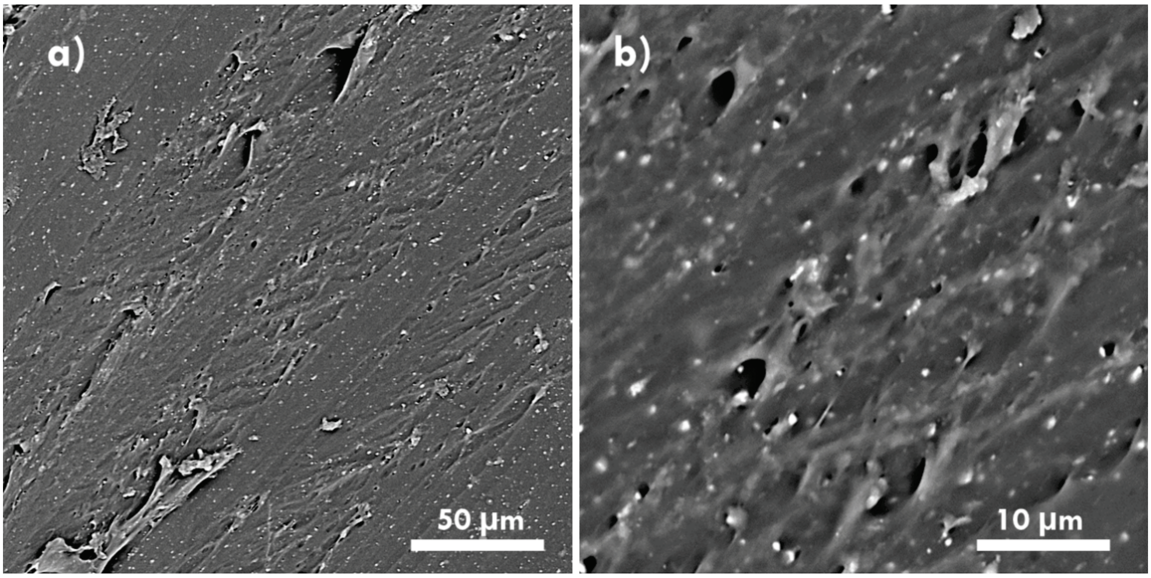

Figure 3 a) low and b) high magnification SEM image of crossection of the prepared composite material filled with 2 wt% of ZnO.

The influence of ZnO filler on the mechanical properties of prepared composites including Young's modulus, elongation at break and tensile strength was found to be negligible. The incorporation of ZnO filler up to 3 wt% neither did not deteriorate nor improve the properties of the neat medical grade plasticized PVC matrix, which is designed by its producer to be an optimal flexible material for medical devices such as urinary catheters or blood bags.

In order to evaluate the antibacterial activity of whole PVC/ZnO composite, the standard testing method based on ISO 22196: 2007 providing quantitative evaluation of the surface antibacterial activity was utilized. The summary of antibacterial activity of prepared composites is shown in Table 2.

Table 2 Summary of the surface antibacterial activity evaluation results obtained for prepared PVC/ZnO composites

Concentration of ZnO filler (wt %)	The treated specimens after 48 h E. coli N (cfu cm^{-2})	The treated specimens after 48 h S. aureus N (cfu cm^{-2})	Antibacterial activity (log CFU) E. coli $R = U_t - A_t$	Antibacterial activity (log CFU) S. aureus $R = U_t - A_t$
0	4.0×10^6	7.5×10^4	$U_t = 6.6$	$U_t = 4.9$
0.5	1.5×10^5	8.0×10^4	1.4	0
1	1.7×10^5	1.0×10^0	1.4	4.9
2	< 1	2.2×10^0	> 6.6	4.5
3	< 1	1.3×10^0	> 6.6	4.8

Obtained R values representing antibacterial activity of composites against both bacteria are high enough for composites filled by 2 and 3 wt%. The R value should not be lower than 2 for materials that can be classified as possessing an antibacterial surface suitable for less demanding applications for plastics in hygiene, household or public interiors. However, medical devices are more demanding on the antibacterial performance of materials. R-values of 5 or even 6 are expected for currently used high-end commercial materials, especially those with organic additives intended to be used for indwelling medical devices [74]. The surface antibacterial activities of composites containing 2 or 3 wt% of the filler against *E. coli* meet these strongest requirements while the activity against *S. aureus* is not so high. On the other hand, *S. aureus* is a very resistant bacterium which is difficult to suppress. From this point of view, the performance of our prepared composites seems to be sufficiently high. Additionally, as the bacteria gain antibiotic resistance, the organic molecular additives in antimicrobial polymer systems may be found to be inefficient or ineffective and the inorganic nanofillers will serve as the last line of defense.

*****

A two-step process was introduced in **Paper II**. First, a precursor was mechanochemically prepared from zinc acetate dihydrate and sodium carbonate in presence of DEG. Then, the second step was MW assisted solvothermal synthesis. The precursor was dispersed in a solvent and exposed to microwaves. This study had a screening character. Therefore, different solvents were used (water and EG) and various synthesis times (20 or 40 min). Figure 4 (left graph panel) shows XRD pattern of the precursor. Compared with the ICDD cards (reference code: 00-003-0787), diffraction peaks fit well with that of $Zn_4CO_3(OH)_6{\cdot}H_2O$ (zinc carbonate hydroxide hydrate). Figure 4 (right graph panel) shows UV-vis DR spectrum of the precursor, which confirms that no ZnO absorbing near 400 nm is present.

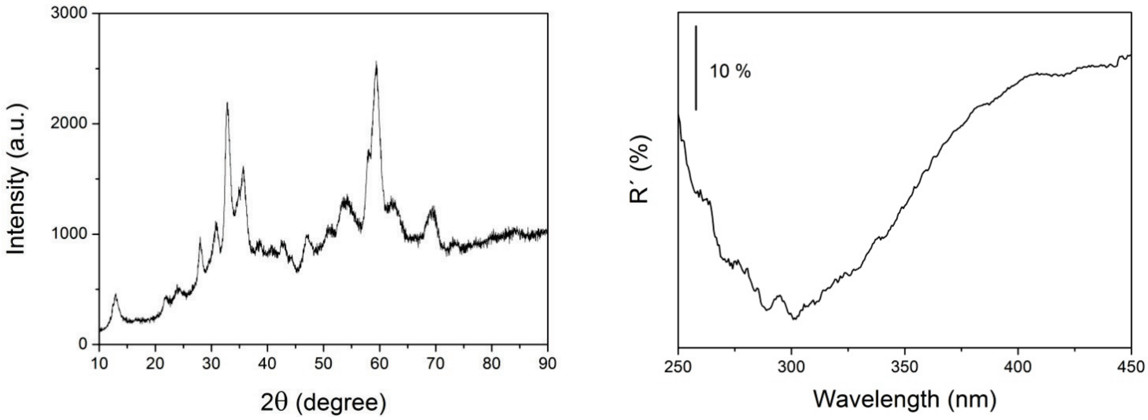

Figure 4 (a) XRD pattern of the precursor and (b) UV-vis DR spectrum of the precursor.

Figure 5 (a) shows the SEM image of the precursor that does not reveal any specific shape, just irregular pointed particles of submicrometric size. Figure 5 (b) shows the SEM image of the product made with PEG addition and demineralised water used as solvent irradiated by MW for 20 minutes. The product is needle-like in shape. Needles are approximately from 4 to 6 μm length and less than 1 μm width. Residuals of very fine nanofibres resembling snow or dust in the image are most likely the constituents of the growing needles. Figure 5 (c) presents SEM image of another product made with PEG however EG was used as the solvent and MW exposure took 20 minutes. This product was obtained exclusively in form of thin curtain-like platelets with very fine porous structure. With the aid of the last picture Figure 5 (d), the influence of reaction time on final structure of the particles can be demonstrated. The last product was prepared under similar conditions as the previous one with the only difference which is two times longer reaction time (i.e. 40 minutes). The prolongation of reaction time resulted to assembling of platelets into urchin-like microstructures.

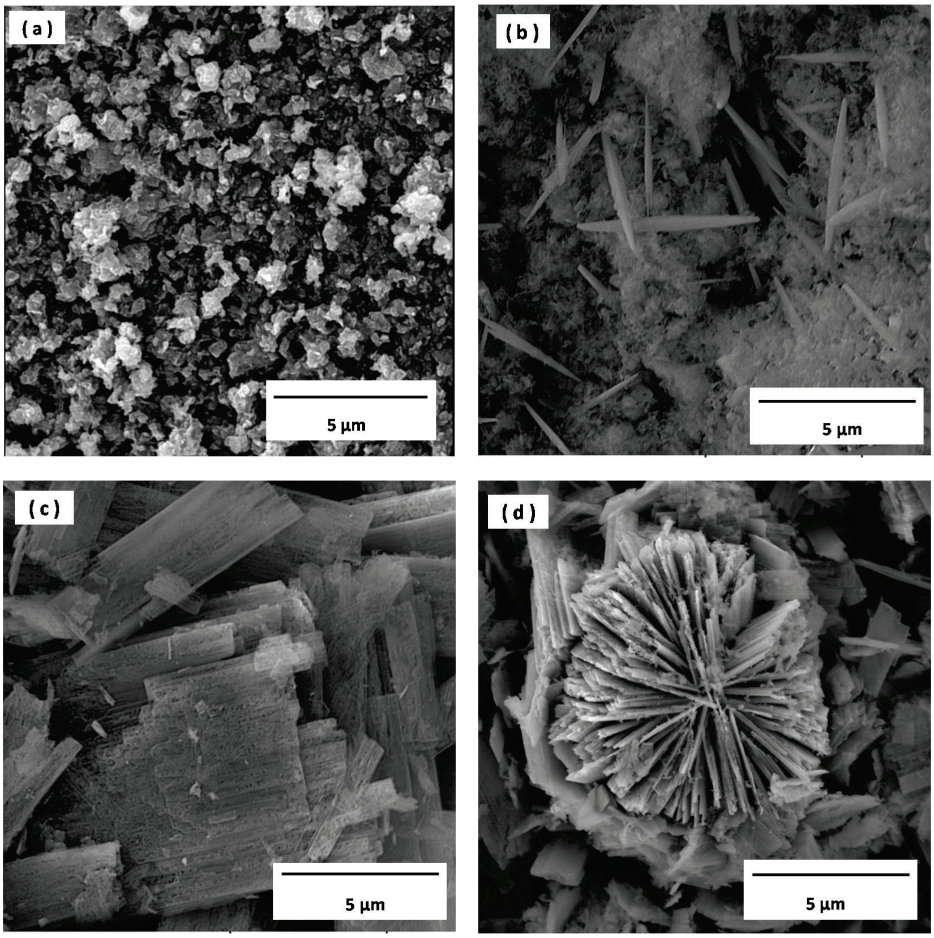

Figure 5 SEM image of the precursor (a) and SEM images of the final products 1, 2, 3, (b), (c), (d) respectively.

According to XRD analysis, the phase composition of products was assigned to hexagonal wurtzite form of ZnO which fitted well to entries for ZnO in ICDD XRD spectra database although some impurities in the form of reactant residuals were found as well.

To summarise: needle, platelete- and urchin- shaped nanostructured ZnO microparticles were successfully prepared by the simple two stage method during this preliminary study. The size of prepared particles ranged from hundreds of nanometers to micrometers. A large variability of possible hierarchically organised structures was discovered with many influencing factors on their origin. Therefore, it was considered to limit the used solvents on the DEG due to its highest boiling temperature among tested liquids and improve the mechanochemical step of the reaction for further and more focused work reported in following paper.

*****

Paper III continues to fulfill the intention to synthesize ZnO based nanoparticles possessing various degree of surface structure, as it was mentioned in theoretical part, that the surface structure determines significantly the overall properties of nanomaterials. Thus ZnO based powdered materials with different specific surface area and lipophilicity were prepared by two-stage process combining both, (i) top-down (milling) and (ii) bottom-up (microwave-assisted solvothermal synthesis) methods. The submicron precursor was prepared mechanochemiclally from common chemicals in the presence of polymer capping agents and subsequently irradiated by microwaves for different time (S1-1.5 min; S2-2 min; S3-2.5 min; S4-3min; S5-4 min; S6-5min). The preparation procedure can be followed from simplified scheme in Figure 6.

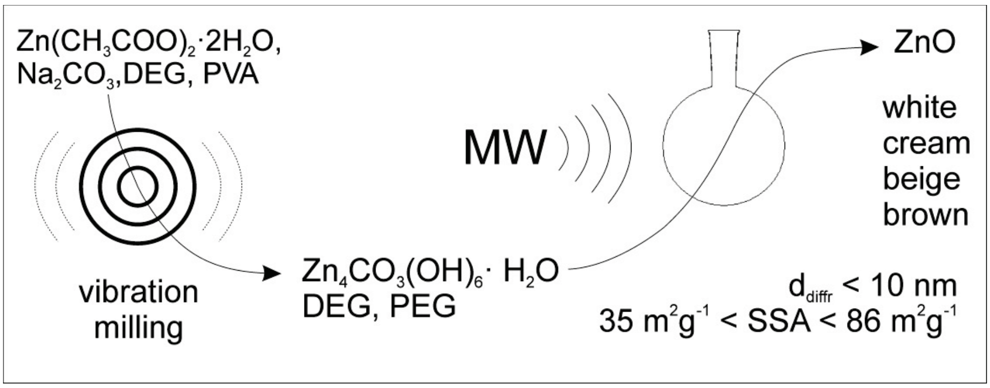

Figure 6 Simplified scheme of the two-stage proccess for preparation of surface modified ZnO based nanoparticles

The phase conversion of submicron inorganic precursor (zinc carbonate hydroxide hydrate) to the final ZnO nanoparticles (hexagonal ZnO wurtzite structure) during the varying MW reaction time was confirmed by the comparison of obtained XRD diffractograms with ICDD XRD spectra database. ZnO development at the expense of zinc carbonate hydroxide hydrate is shown in Figure 7 as the dependency of normalised intensities of selected diffraction lines from obtained diffractograms on the time of MW reaction.

As can be seen from Figure 7, the results testified for complete conversion of precursor within 2.5 minutes, whereas at the same time, the conversion of zinc oxide was at the half way only and reached nearly maximum between 4 and 5 minutes of the MW reaction. Therefore we focused on another diffraction line which certainly does not belong to the ZnO diffraction pattern but can be found in the precursor's diffractogram. The residual intensity of this line in the sample S6 testified for incomplete yet nearly full conversion of the intermediate to the ZnO product.

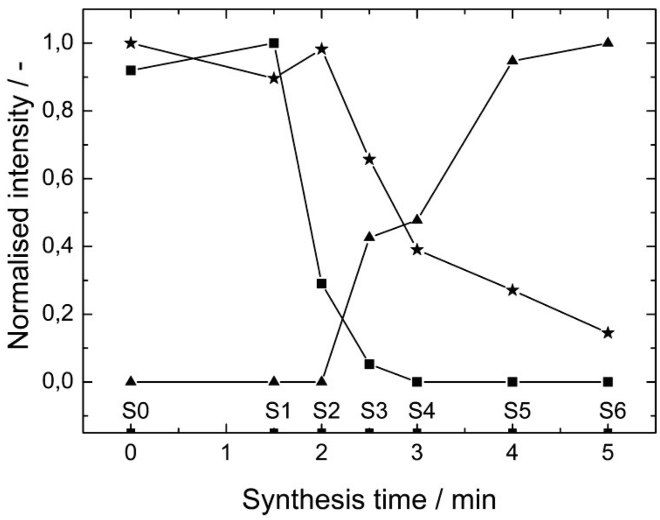

Figure 7 Normalised intensities of selected diffraction lines plotted versus reaction time. Used symbols are associated with diffractogram peaks at 2θ angles as follows: full squares for diffraction line of the precursor 28.07°, full triangles for diffraction line of ZnO at 56.5° and stars for diffraction line of the precursor intermediate product at 59.6°.

The progress of ZnO structure as well as organic film coating manifested by DR-UV-vis spectrometry can be seen in Figure 8 a). The spectra of precursor S0 and sample S1 do not possess almost any absorption between 350 and 400 nm which confirms absence of ZnO. Development of ZnO structure is clearly observable for samples S3, S4, S5 and S6 by the presence of strong absorption maxima below 380 nm. This value is blue-shifted from typical bulk ZnO maximum [73] confirming thus the nano-dimensionality of prepared materials.

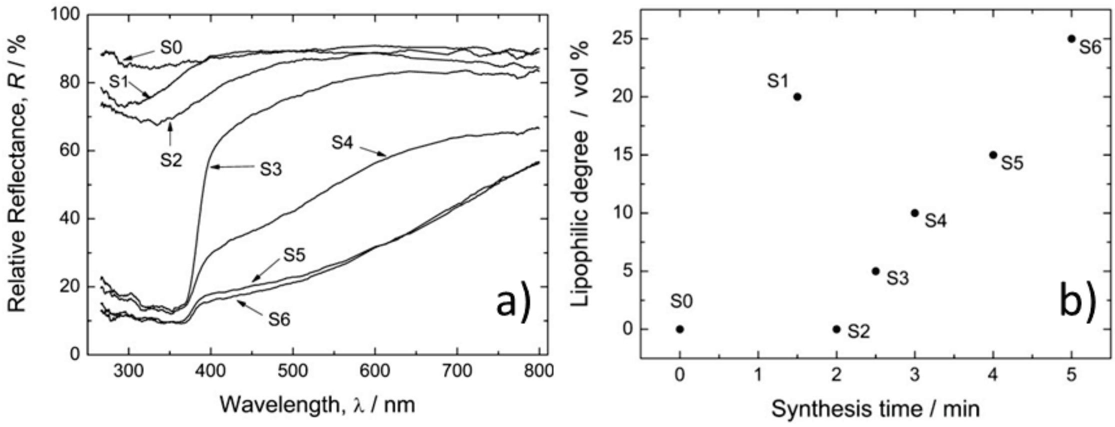

Figure 8 a) DR-UV-vis spectra of the precursor S0 and products S1-S6 and b) the dependence of their LD on the synthesis.

Evolution of organic film coating can be observed by broad tails of absorption curves ranging far to the red region. The main change can be seen between samples S3, S4 and S5. The sample S4 represents evidently the transition step for the reaction. Observed trends are in agreement with the naked eye observation of colour of prepared powders that changed from white (S0, S1) via cream (S2), beige (S3), light brown (S4), brown (S5) to dark brown (S6), respectively. The spectral and colour change can be associated with the MW heating thermal degradation of used polymers present in the reaction mixture. The observed changes correspond to development of conjugated double bond structures, so called oligo or polyenes.

The surface properties, namely specific surface area and lipopilicity, of prepared nano-particulate material were obtained to vary with the synthesis time. The graph in Figure 8 b) shows lipophilicity results. The precursor behaves hydrophilically while the S1 sample has LD of 20 vol %. The material S2 is again hydrophilic and then the LD increases nearly linearly with synthesis time progress up to 25 vol % for sample S6. It seems that the initial role of added polymers is rather complicated and obtained results can be attributed to both (i) structural changes and (ii) development of polyene double bonds caused by polymer thermal degradation. Once the progressive polymer degradation in DR-UV-vis spectra was observed, it was possible to expect increase in lipophilicity of prepared particles. Moreover, the formation of ZnO which is normally (in dark) hydrophobic may contribute to the LD increase too. Similar interpretation could be used for changes of specific surface area of prepared powder materials, so that the key factors responsible for SSA ranging from 35 to 86 m^2/g are both (i) structural changes and (ii) the progress of polymer coating degradation.

*****

The work summarised in the last two articles (**Paper IV and V**) focuses on the preparation of nanocrystalline ZnO powders by simple procedure based on the thermal decomposition of two different precursors followed by testing of their photocatalytic performance.

In Paper IV, precursor of zinc oxalate dihydrate was prepared by precipitation of solutions of zinc acetate and oxalic acid. SEM images of the precursor and annealed porous nanocrystalline ZnO micro-beads are shown in Figure 9.

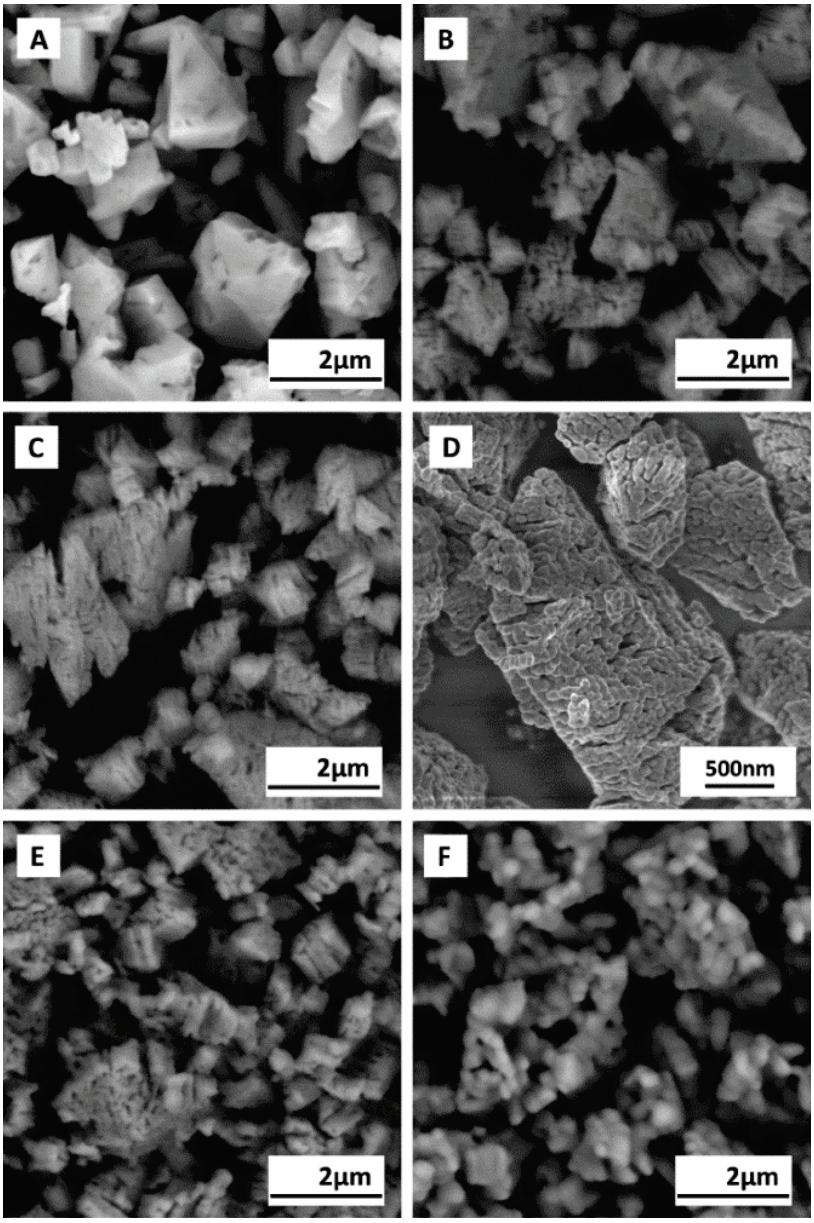

Figure 9 SEM images of precursor ($ZnC_2O_4.2H_2O$) and products prepared by annealing of the precursor at different temperatures, A: precursor; B: 400 °C; C,D: 500 °C; E: 700 °C; F: 900 °C.

The results obtained from SEM observation are in good agreement with structural and morphological parameters obtained from XRD and BET analyses from which some of them are displayed in Table. It is evident, that the diameter of nanocrystallites (d_{diffr}) estimated according to equation 2 grows with increasing temperature of annealing. By assumption, that the grains have spherical shape and uniform size, the average particle size can be obtained according to equation 3 as the Grain size (d_{BET}). Obtained values confirm reasonable coarsening of particles due to sintering with increasing annealing temperature. In next, BET analysis was also used for estimation of the mean pore diameter that decreased slowly by increase of annealing temperature from 4.7 to 4.0 nm and prepared materials can be therefore classified as mesoporous. In addition, the specific Crystallite surface area (A_{diffr}) can be easily calculated from the size of crystallites and the material density of ZnO (5.6 g/cm^3).

Table 3 Summary of XRD and BET analyses of annealed $ZnC_2O_4.2H_2O$ samples and rate constant obtained for the photocatalysis test.

	Annealing temperature	400 °C	500 °C	700 °C	900 °C
XRD	Crystallite size, d_{diffr} [nm]	21.0	47.1	67.8	79.3
	Crystallite surface area, A_{diffr} [m^{2}g^{-1}]	51.0	22.7	15.8	13.5
BET	BET surface area, A_{BET} [m^{2}g^{-1}]	29.9	10.2	3.4	1.7
	BET mean pore diameter, $d_{p\ BET}$ [nm]	4.7	4.4	4.2	4.0
	Grain size, d_{BET} [nm]	35.8	105.0	315.1	630.3
UV cat.	Rate constant, k [s^{-1}]	0.0438 ± 0.0018	0.066 ± 0.002	0.0412 ± 0.0015	0.0391 ± 0.0019

Volume of crystallites (V_{diffr}) can be calculated with the same easiness and obtained values are shown in Figure 10. The dependence of V_{diffr} on temperature is perfectly linear. This result is not that surprising as it looks if a simple fact taken into account that the growth of one crystallite proceeds at the expense of other crystallites and the total volume change is zero. The ball diagram inserted into the graph shows, how many crystallites of each size are needed to create one nearest bigger crystallite. The intercept of the linear dependence with the abscissa is the minimum possible temperature at which the crystallite size would be theoretically zero. This initial minimum temperature is 663.7 K (390.5 °C) which is identical with the temperature of the maximum decomposition rate of the precursor.

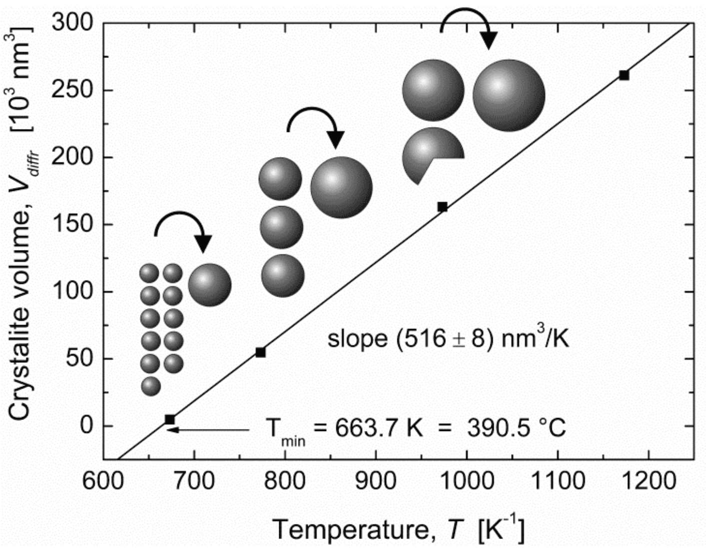

Figure 10 Calculated crystallite volume of ZnO samples annealed from $ZnC_2O_4.2H_2O$ at different temperature.

The results obtained from X-ray diffraction line broadening analysis can be compared with the results obtained from gas sorption BET analysis. The first and usually the most sought after information from BET analysis is the Specific surface area (A_{BET}). On the first sight, the A_{BET} is smaller than the specific crystallite surface area. The X-ray diffraction characteristics are correctly obtained for coherently diffracting areas, i.e. to the size of nanocrystallites (nanocrytalline domains) while gas sorption analysis examines the actual surface of the porous body accessible to N_2 molecules, which means, that it characterises the surface of grains.

According to simple geometrical assumptions, the ratio between grain and crystallite volumes can be calculated which characterises how many crystallites are agglomerated into one grain. Obtained results are shown in Figure 11. The value increases from cca 5 for 400 °C up to cca 500 for 900 °C. The observed linear logarithmic dependence on thermodynamic temperature can be extrapolated to the initial temperature and compared with the crystallite volume dependence. It seems that the first crystallites appear already in a grain assembly with the mean number of crystallites about 4.5 per grain. On the other hand, the hypothetical 1:1 ratio is expectable at 232 °C which is deep below the decomposition temperature of the precursor and evidently cannot be correct, thus this extrapolation supports the hypothesis of initial agglomeration.

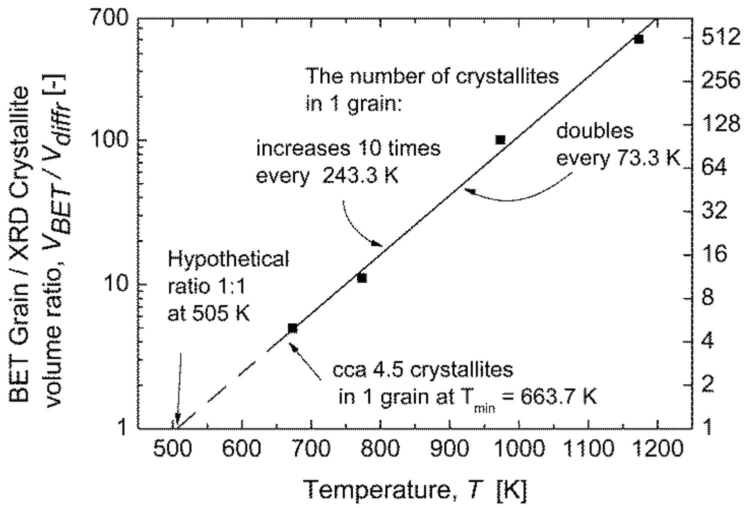

Figure 11 Plot of BET Grain / XRD Crystallite volume ratio vs temperature for ZnO annealed from $ZnC_2O_4.2H_2O$.

The analysis of obtained data can be much more refined and various characteristics of the annealing process can be evaluated. A basic crystal growth model can be used where linear relationship between the rate of grain growth and the inverse grain size is assumed, which in turn is proportional to the radius of curvature of the grain [75,76]. The activation energy of the grain sintering process 72 kJ/mol was calculated, while the nanocrystallite growth was found to be governed by the crystalline boundary mobility and linearly dependent on reciprocal thermodynamic temperature. Hence, the value of 6.4 x 10^{-16} cm^2s^{-1} was obtained from the slope of this dependence and it can be considered as the mean self-diffusion coefficient (*Ds*) estimation for temperature range 670-1150 K which is in excellent agreement with the values from the comprehensive reference of Erhart and Albe [77]. Moreover, even the self-diffusion coefficient obeys Arrhenius law with the activation energy corresponding to the migration barrier. This energy was obtained as 31 kJ/mol which is equivalent to 0.32 eV. This value is much smaller than values of migration barriers reported for oxygen or zinc vacancy diffusion mechanisms thus the zinc interstitials are considered to be responsible for the observed crystallite growth [78]. Our estimated value is somewhat smaller than 0.55 eV that was found by Thomas [79]. However, according to more elaborated recent analysis and theoretical calculation of Erhart and Albe [77], there are several different mechanisms of Zn interstitials diffusion possible and among them the energetic barrier of 0.32 eV can be associated with the interstitial *in plane mechanism* and with the *interstitialcy out of plane* mechanism of Zn diffusion in the ZnO lattice.

The photodegradation of methyl violet 2B (MV) solution in the presence of ZnO photocatalyst was monitored by UV-vis spectroscopy. Figure 12 a) exemplifies obtained UV-vis spectra for the system containing ZnO annealed at 500 °C.

Here, the dye degradation is manifested by the decrease of the absorption maxima at 580 nm. Figure 12 b) shows the photodegradation curves of the dye for all ZnO samples prepared at various annealing temperatures. The ratio between actual and initial concentration is plotted against time of UV irradiation. As can be seen, complete degradation of the dye is accomplished within the 120 minutes and all curves obey first (or pseudofirst) order reaction kinetics. The rate constant was obtained from fitting the first order model into the data. The highest degradation rate constant (consult Table 3) was found for sample annealed at 500 °C.

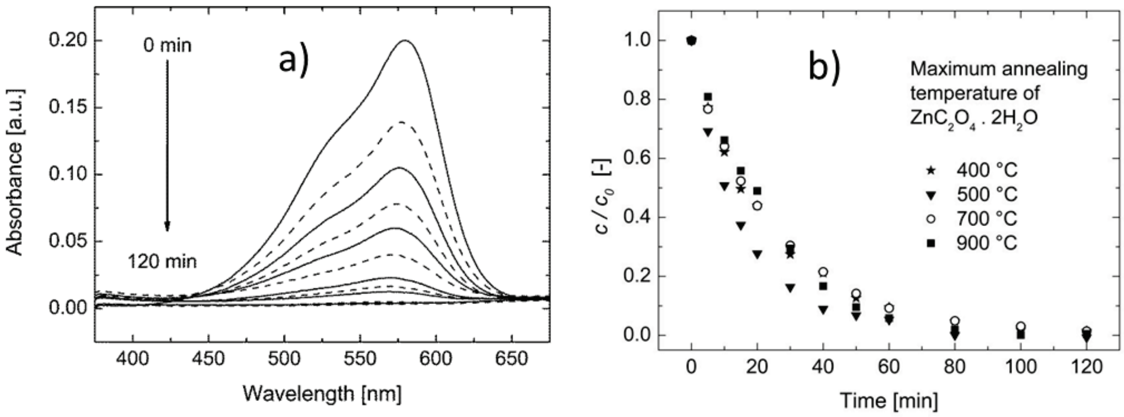

Figure 12 UV-vis spectra of of methyl violet in the presence of ZnO annealed at 500 °C and b) photocatalytic degradation curves of methyl violet as a function of time for ZnO mcicro-beads annealed from $ZnC_2O_4.2H_2O$ at different temperatures, as illustrated in the graph.

In the last article (**Paper V**) nanocrystalline assembled ZnO spheres were obtained via thermal annealing of zinc peroxide precursor at five different temperatures. Here, zinc peroxide was prepared by recrystallization of dissolved commercial ZnO powder in the presence of aqueous ammonia and hydroxide peroxide. The morphology of prepared powders studied by SEM revealed spherically shaped particles as depicted in Figure 13. The high resolution SEM image of the precursor (image b) shows its relatively rough surface that became finer for samples annealed at 200 °C (image c) due to the release of the oxygen caused by thermal annealing. Another significant change corresponding to growth of crystallite size can be clearly observed for sample annealed at

500 °C (image e). Moreover, the hierarchically structured morphology of nanocrystalline assembled ZnO spheres is clearly visible. Within the higher annealing temperatures the sintering process take a place as can be seen from coalescence of individual grains from low magnification image of sample annealed at 900 °C. These results are in good agreement with structural parameters, i.e. XRD and BET analyses that are summarised in the Table 4.

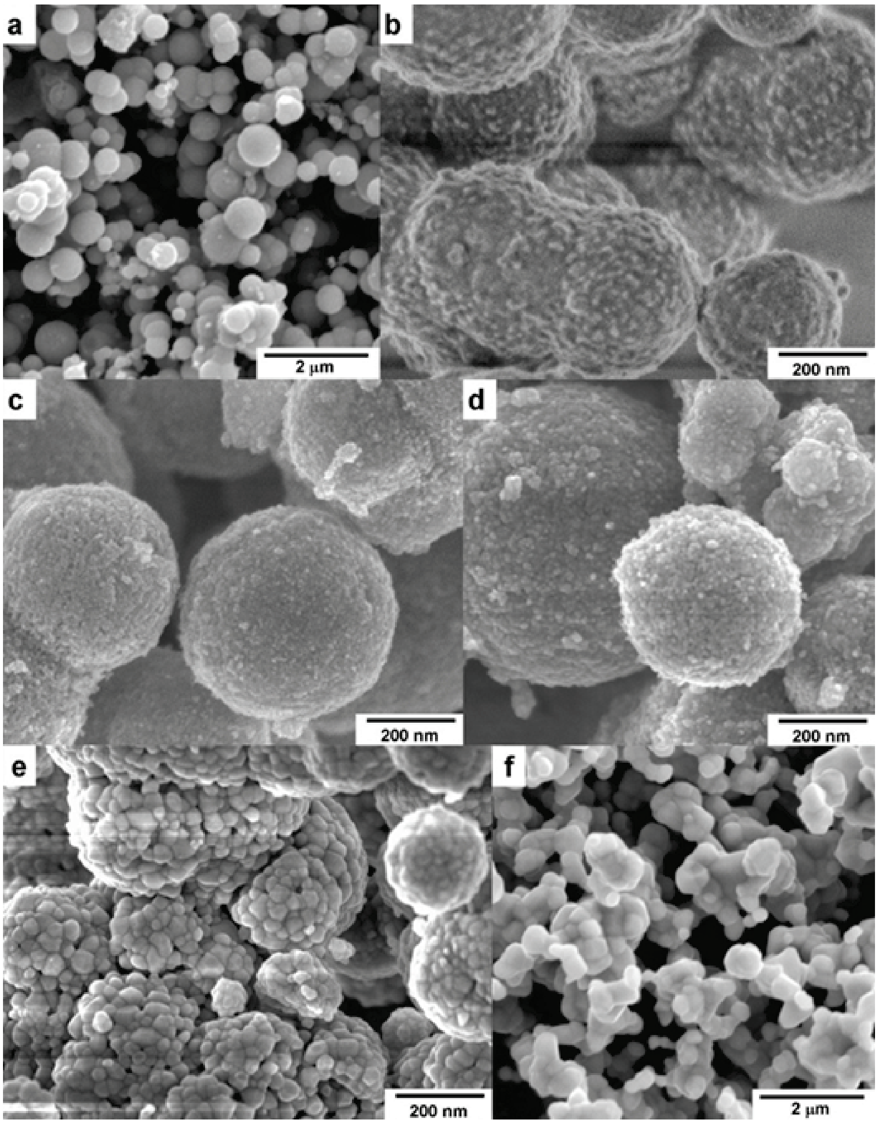

Figure 13 SEM images of precursor (ZnO_2) and products prepared by annealing of the precursor at different temperatures, a,b: precursor; c: 200 °C; d: 300 °C; e: 500 °C; f: 900 °C.

ZnO photocatalytic performance against methyl violet 2B (MV) was monitored by UV-vis spectroscopy. Figure 14 a) shows obtained UV-vis spectra for the system containing ZnO annealed at 900 °C.

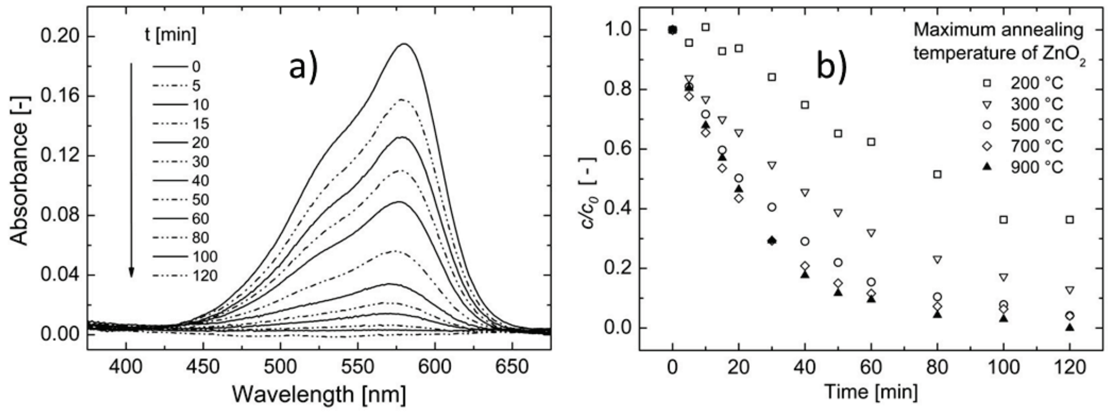

Figure 14 a) UV-vis spectra of of methyl violet in the presence of ZnO annealed at 900 °C and b) photocatalytic degradation curves of methyl violet as a function of time for ZnO_2 annealed at different temperatures, as illustrated in the graph.

Figure 14 b) shows the photodegradation curves of the dye for all nanocrystalinne assembled ZnO spheres. The ratio between actual and initial concentration is plotted against time of UV irradiation. The complete degradation of the dye is accomplished within the 120 minutes and all curves obey first (or pseudofirst) order reaction kinetics. The rate constants were obtained from fitting the first order model into the data. The highest degradation rate constant corresponds to sample annealed at 700 °C.

Table 4 Summary of selected XRD and BET analyses of annealed ZnO_2 samples. The last row contains rate constant obtained for the photocatalysis reaction.

	Annealing temperature	200 °C	300 °C	500 °C	700 °C	900 °C
XRD	Crystallite size, d_{diffr} [nm]	6.5	10.0	37.1	55.9	66.7
BET	BET surface area, A_{BET} [m^2g^{-1}]	41.2	37.0	6.3	1.7	1.2
	Grain size, d_{BET} [nm]	26.0	29.0	170.1	630.3	892.9
UV cat.	Rate constant, k [s^{-1}]	0.005 ± 0.003	0.0210 ± 0.0017	0.0335 ± 0.0015	0.0443 ± 0.0011	0.0400 ± 0.0015

8 CLOSING REMARKS

8.1 Conclusions and contribution to science and technology

The dissertation thesis contributes to the general knowledge as well as technology according to the goals as follows:

- Two extremely fast microwave-assisted solvothermal procedures in open vessel system were introduced;
    - Synthesis protocol described in Paper I yields product in reasonable amount and desired function within a few minutes;
    - Mechanochemical synthesis of precursor followed by microwave enhanced synthesis was introduced in Paper II and showed extreme versatility of achievable product morphologies. It was further used in a more focused Paper III for preparation of *in-situ* surface modified ZnO by degradation of capping polymers within one step with relatively easily controllable lipophilicity degree;

- The possibility of preparation of larger (micrometric) objects by thermal decomposition of crystalline precursors was revived (Paper IV and V) and it was demonstrated that various mesoporous nanostructured crystalline microbeads can be obtained by manipulation with the annealing temperature;

- While the synthesis of zinc oxalate dihydrate (Paper IV) is a common technique, an original delicate synthesis protocol was elaborated for preparation of zinc peroxide (in Paper V), moreover, the process of zinc peroxide annealing to obtain zinc oxide nanostructured particles was developed and described (Paper V);

- All (Paper I, II, IV and V) prepared ZnO based powder materials have nanocrystalline building blocks and create higher structure on mesoscale while the overall size of particles lies from sub-micro to micro scale, however the morphology of the surface modified particles was not directly revealed (Paper III) due to low resolution of the available SEM;

- The formation mechanism of nanostructured mesoporous ZnO microbeads prepared by thermal annealing of zinc oxalate dihydrate was identified; basic parameters of the sintering process and crystallite growth were described including activation energies and self-diffusion coefficient value. Some of possible zinc interstitials diffusion mechanisms were identified as responsible for the crystallite growth (Paper IV);

- Application potential of hierarchical and mesoporous ZnO nanocrystalline powders was demonstrated by case studies focused on (Paper I) preparation of antibacterial polymer system using medical grade PVC matrix with excellent antibacterial activity against *E. coli* and *S. aureus*, (Paper II) lipophilicity evaluation which testifies for the applicability of the surface modified materials in oil and fat dispersions, and (Paper III and IV) testing of the photocatalytic performance by UV degradation of methyl violet 2B.

Adoption and further development of the microwave enhanced solvothermal synthesis of hierarchical ZnO and coated ZnO *in situ* during MW reaction will contribute to the environmental protection thanks to the enormous decrease of the reaction times from hours to minutes. Next, it will contribute to the development of high performance functional materials as demonstrated by development of antibacterial polymer system and photocatalysts.

8.2 Future prospective

Prepared hierarchical ZnO can be used in material design in the field of medical plastics as well as for antibacterial polymer based materials utilized in household or public interiors, cars and other applications.

Mesoporous ZnO powders demonstrated ability to be used as photocatalysts, e.g. in the field of water purification.

The surface modification of ZnO material which results into controllable lipophilicity could be used for preparation of materials suitable for cosmetics or additives in various polymer compounds.

REFERENCES

[1] *Nanomaterials*, Dieter Vollath. Wiley, 2008, ISBN 978-3-527-31531-4.

[2] *Nanostructures & Nanomaterials*, Guoyhong Cao. Imperial College Press, 2004, ISBN: 1-86094-480-9.

[3] ZHU, P.L.; ZHANG, J.W.; WU, Z.S.; ZHANG, Z.J. Microwave-assisted synthesis of various ZnO hierarchical nanostructures: Effects of heating parameters of microwave oven. *Crystal Growth & Design*, 2008. Vol. 8, No. 9, p. 3148-3153.

[4] SHANG, T.M.; SUN, J.H.; ZHOU, Q.F.; GUAN, M.Y. Controlled synthesis of various morphologies of nanostructured zinc oxide: flower, nanoplate, and urchin. *Crystal Research and Technology*, 2007, Vol. 42, No. 10, p. 1002-1006.

[5] GU, P.F.; WANG, X.D.; LI, T.; YU, H.Y.; MENG, H.M. Solvothermal synthesis and growth mechanism of asymmetric ZnO hierarchical structures in diethylene glycol with ammonia solution. *Crystal Research and Technology*, 2013, Vol. 48, No. 11, p. 989-995.

[6] MOEZZI, A.; MCDONAGH, A.M.; CORTIE, M.B. Zinc oxide particles: Synthesis, properties and applications. *Chemical Engineering Journal*, 2012. Vol. 185, p. 1-22.

[7] *Zinc Oxide, Fundamentals, Materials and Device Technology*, Hadis Morkoç and Ümit Özgür. Wiley, 2009, ISBN: 978-3-527-40813-9.

[8] JIANG, H.; HU, J.Q.; GU, F.; LI, C.Z. Large-scaled, uniform, monodispersed ZnO colloidal microspheres. *Journal of Physical Chemistry C*, 2008. Vol. 112, No. 32, p. 12138-12141.

[9] GUO, H.G.; ZHOU, J.Z.; LIN, Z.G. ZnO nanorod light-emitting diodes fabricated by electrochemical approaches. *Electrochemistry Communications*, 2008. Vol. 10, No. 1, p. 146-150.

[10] ZHANG, Q.F.; DANDENEAU, C.S.; ZHOU, X.Y.; CAO, G.Z. ZnO Nanostructures for Dye-Sensitized Solar Cells. *Advanced Materials*, 2009. Vol. 21, No. 41, p. 4087-4108.

[11] MELENDREZ, M.F.; HANKS, K.; LEONARD-DEEPAK, F.; SOLIS-POMAR, F.; MARTINEZ-GUERRA, E.; PEREZ-TIJERINA, E.; JOSE-YACAMAN, M. Growth of aligned ZnO nanorods on transparent electrodes by hybrid methods. *Journal of Material Science*, 2012. Vol. 47, No. 4, p. 2025-2032.

[12] CHEN, M.; WANG, Z.H.; HAN, D.M. GU, F.B.; GUO, G.S. High-sensitivity NO2 gas sensors based on flower-like and tube-like ZnO nanomaterials. *Sensors and Actuators B-Chemical*, 2011. Vol. 157, No. 2, p. 565-574.

[13] MANI, G.K.; RAYAPPAN, J.B.B. A highly selective room temperature ammonia sensor using spray deposited zinc oxide thin film. *Sensors and Actuators B-ChemicaL*, 2013. Vol. 183, p. 459-466.

[14] LI, X.Y.; WANG, J.A.; YANG, J.H.; LANG, J.H.; LU, S.Q.; WEI, M.B.; MENG, X.W.; KOU, C.L.; LI, X.F. Comparison of photocatalytic activity of ZnO rod arrays with various diameter sizes and orientation. *Journal of Alloys and Compounds*, 2013. Vol. 580, p. 205-210.

[15] AKIN, M.B.; ONER, M. Photodegradation of methylene blue with sphere-like ZnO particles prepared via aqueous solution. *Ceramics International*, 2013. Vol 39, No. 8, p. 9759-9762.

[16] SAWAI, J.; IGARASHI, H.; HASHIMOTO, A.; KOKUGAN, T.; SHIMIZU, M. Evaluation of Growth-inhibitory Effect of Ceramics Powder Slurry on Bacteria by Conductance method. *Journal of Chemical Engineering of Japan*, 1995. Vol. 28, No. 3, p. 288-293.

[17] XIONG, H.M. ZnO Nanoparticles Applied to Bioimaging and Drug Delivery. *Advanced Materials*, 2013. Vol. 25, No. 37, p. 5329-5335.

[18] LI, S.C.; LI, Y.N. Mechanical and Antibacterial Properties of Modified Nano-ZnO/High-Density Polyethylene Composite Films with a Low Doped Content of Nano-ZnO. *Journal of Applied Polymer Science*, 2010. Vol. 116, No. 5, p. 2965-2969.

[19] LEPOT, N.; VAN BAEL, M.K.; VANDEN RUL, H.; D'HAEN, J.; PEETERS, R.; FRANCO, D.; MULLENS, J. Influence of incorporation of ZnO nanoparticles and biaxial orientation on mechanical and oxygen barrier properties of polypropylene films for food packaging applications. *Journal of Applied Polymer Science*, 2011. Vol. 120, No. 3, p. 1616-1623.

[20] ZHANG, J.J.; GAO, G.; LIU, F.Q. Preparation of zinc oxide nanocrystals with high stability in the aqueous phase. *Journal of Applied Polymer Science*, 2013. Vol. 128, No. 3, p. 2162-2166.

[21] KRIISA, M.; KARBER, E.; KRUNKS, M.; MIKLI, V.; UNT, T.; KUKK, M.; MERE, A. Growth and properties of ZnO films on polymeric substrate by spray pyrolysis method. *Thin Solid Films*, 2014. Vol. 555, p. 87-92.

[22] JANG, E.S.; WON, J.H.; KIM, Y.W.; CHENG, Z.; CHOY, J.H. Synthesis of porous and nonporous ZnO nanobelt, multipod, and hierarchical nanostructure from Zn-HDS. *Journal of Solid State Chemistry*, 2010. Vol. 183, No. 8, p. 1835-1840.

[23] *Metal Oxides Nanoparticles in Organic Solvents: Synthesis, Formation, Assembly and Application*, Markus Niederberger and Nicola Pinna. Springer, 2009, ISBN: 978-1-84882-670-0.

[24] *Nanomaterials Handbook*, Edited by Yury Gogotsi. Chapter: Perspectives on the Science and Technology of Nanoparticle Synthesis, Ganesh Skandan and Amit Singhal. CRC Press Taylor & Francis Group, 2006, ISBN: 978-0-8493-2308-9.

[25] AO, W.Q.; LI, J.Q.; YANG, H.M.; ZENG, X.R.; MA, X.C. Mechanochemical synthesis of zinc oxide nanocrystalline. *Powder Technology*, 2006. Vol. 168, No. 3, p. 148-151.

[26] MUSIC, S.; SARIC, A.; POPOVIC, S. Dependence of the microstructural properties of ZnO particles on their synthesis. *Journal of Alloys and Compounds*, 2008. Vol. 448, No. 1-2, p. 277-283.

[27] YANG, Y.; LI, X.F.; CHEN, J.B.; CHEN, H.L.; BAO, X.M. ZnO nanoparticles prepared by thermal decomposition of beta-cyclodextrin coated zinc acetate. *Chemical Physics Letters*, 2003. Vol. 373, No. 1-2, p. 22-27.

[28] FARHADI-KHOUZANI, M.; FERESHTEH, Z.; LOGHMAN-ESTARKI, M.R.; RAZAVI, R.S. Different morphologies of ZnO nanostructures via polymeric complex sol-gel method: synthesis and characterization. *Journal of Sol-Gel Science and Technology*, 2012. Vol. 64, No. 1, p. 193-199.

[29] CHIENG, B.W.; LOO, Y.Y. Synthesis of ZnO nanoparticles by modified polyol method. *Materials Letters*, 2012. Vol. 73, p. 78-82.

[30] PHURUANGRAT, A.; THONGTEM, T.; THONGTEM, S. Microwave-assisted synthesis of ZnO nanostructure flowers. *Material Letters*, 2009. Vol. 63, No. 13-14, p. 1224-1226.

[31] LIU, J.S.; CAO, J.M.; LI, Z.Q.; JI, G.B.; ZHENG, M.B. A simple microwave-assisted decomposing route for synthesis of ZnO nanorods in the presence of PEG400. *Material Letters*, 2007. Vol. 61, No. 22, p. 4409-4411.

[32] MACHOVSKY, M.; KURITKA, I.; SEDLAK, J.; PASTOREK, M. Hexagonal ZnO porous plates prepared from microwave synthesized layered zinc hydroxide sulphate via thermal decomposition. *Materials Research Bulletin*, 2013. Vol. 48, No. 10, p. 4002-4007.

[33] JIA, B.X.; JIA, W.N.; WANG, J.; QU, F.Y.; WU, X. Growth of Thin Sheet Assembled Hierarchical ZnO Nanostructures. *Journal of Nanomaterials*, 2012. Article number 796815.

[34] ZHOU, H.J.; TIAN, Z.R. Recent advances in multistep solution nanosynthesis of nanostructured three-dimensional complexes of semiconductive materials. *Progress in Natural Science: Materials International*, 2013. Vol. 23, No. 3, p. 273-285.

[35] SANCHEZ, C.; ARRIBART, H.; GUILLE, M.M.G. Biomimetism and bioinspiration as tools for the design of innovative materials and systems. *Nature Materials*, 2005. Vol. 4, No. 4, p. 277-288.

[36] *Mesocrystals and Nonclassical Crystallization*, Helmut Cölfen and Markus Antonietti. Wiley, 2008, ISBN: 978-0-470-02981-7.

[37] HU, P.; ZHANG, X.; HAN, N.; XIANG, W.C.; CAO, Y.B.; YUAN, F.L. Solution-Controlled Self-Assembly of ZnO Nanorods into Hollow Microspheres. *Crystal Growth & Design*, 2011. Vol. 11, No. 5, p. 1520-1526.

[38] DISTASO, M.; MACKOVIC, M.; SPIECKER, E.; PEUKERT, W. Early Stages of Oriented Attachment: Formation of Twin ZnO Nanorods under Microwave Irradiation. *Chemistry – A European Journal*, 2012. Vol. 18, No. 42, p. 13265-13268.

[39] HAPIUK, D.; MASENELLI, B.; MASENELLI-VARLOT, K.; TAINOFF, D.; BOISRON, O.; ALBIN, C.; MELINON, P. Oriented Attachment of ZnO Nanocrystals. *Journal of Physical Chemistry C*, 2013. Vol. 117, No. 19, p. 10220-10227.

[40] *Aqueous Microwave Assisted Chemistry: Synthesis and Catalysis*, Edited by Vivek Polshettiwar and Rajender S. Varma. Chapter: Fundamentals of Aqueous Microwave Chemistry, Vivek Polshettiwar and Rajender S. Varma. Royal Society of Chemistry, 2010, ISBN: 978-1-84973-038-9.

[41] *Microwave Heating as a tool for Sustainable Chemistry*, Edited by Nicholas E. Leadbeater. Chapter: Microwave Heating as a tool for Sustainable Chemistry: An Introduction, Nicholas E. Leadbeater and Jason R. Schmink. CRC Press, Taylor & Francis Group 2011, ISBN: 978-1-4398-1269-3.

[42] BAGHBANZADEH, M.; CARBONE, L.; COZZOLI, P.D.; KAPPE, C.O. Microwave-Assisted Synthesis of Colloidal Inorganic Nanocrystals. *Angewandte Chemie International Edition*, 2011. Vol. 50, No. 48, p. 11312-11359.

[43] *Practical Microwave Synthesis for Organic Chemists: Strategies, Instruments, and Protocols*, C. Oliver Kappe, Doris Dallinger and S. Shaun Murphree. Wiley, 2009, ISBN: 978-3-527-32097-4.

[44] RAI, P.; SONG, H.M.; KIM, Y.S.; SONG, M.K.; OH, P.R.; YOON, J.M.; YU, Y.T. Microwave assisted hydrothermal synthesis of single crystalline ZnO nanorods for gas sensor application. *Material Letters*, 2012. Vol. 68, p. 90-93.

[45] SHIM, J.B.; CHANG, H.; KIM, S.O. Rapid Hydrothermal Synthesis of Zinc Oxide Nanowires by Annealing Methods on Seed Layer. *Journal of Nanomaterials*, 2011. Article Number: 582764.

[46] HUANG, J.F.; XIA, C.K.; CAO, L.Y.; ZENG, X.R. Facile microwave hydrothermal synthesis of zinc oxide one-dimensional nanostructure with three-dimensional morphology. *Materials Science and Engineering: B Advanced Functional Solid-State Materials*, 2008. Vol. 150, No. 3, p. 187-193.

[47] ZHU, Z.F.; YANG, D.; LIU, H. Microwave-assisted hydrothermal synthesis of ZnO rod-assembled microspheres and their photocatalytic performances. *Advanced Powder Technology*, 2011. Vol. 22, No. 4, p. 493-497.

[48] SAITO, N.; HANEDA, H.; Hierarchical structures of ZnO spherical particles synthesized solvothermally. *Science and Technology of Advanced Materials*, 2011. Vol. 12, No. 6. Article Number: 064707.

[49] HAMMARBERG, E.; PRODI-SCHWAB, A.; FELDMANN, C. Microwave-assisted polyol synthesis of aluminium- and indium-doped ZnO nanocrystals. *Journal of Colloid and Interface Science*, 2009. Vol. 334, No. 1, p. 29-36.

[50] De La GARZA, M.; LOPEZ, I.; AVINA, F.; GOMEZ, I. Microwave-assisted solvothermal synthesis of porous zinc oxide nanostructures. *Journal of Ovonic Research*, 2013. Vol. 9, No. 4, p. 89-94.

[51] *Polymer Nanocomposites Handbook*, Edited by Rakesh K. Gupta, Elliot Kennel and Kwang-Jea Kim. Chapter: The Incorporation of Nanomaterials into Polymer Media, Henry C. Ashton. CRC Press Taylor & Francis Group, 2010, ISBN: 978-0-8493-9777-6.

[52] ALTHUES, H.; HENLE, J.; KASKEL, S. Functional inorganic nanofillers for transparent polymers. *Chemical Society reviews*, 2007. Vol. 36, No. 9, p. 1454-1465.

[53] ZHAO, H.X.; LI, R.K.Y. A study on the photo-degradation of zinc oxide (ZnO) filled polypropylene nanocomposites. *Polymer*, 2006. Vol. 47, No. 9, p. 3207-3217.

[54] ALTAN, M.; YILDIRIM, H. Effects of compatibilizers on mechanical and antibacterial properties of injection molded nano-ZnO filled polypropylene. *Journal of Composite Materials*, 2012. Vol. 46, No. 25, p. 3189-3199.

[55] ROY, A.S.; GUPTA, S.; SINDHU, S.; PARVEEN, A.; RAMAMURTHY, P.C. Dielectric properties of novel PVA/ZnO hybrid nanocomposite films. *Composites Part B Engineering*, 2013. No. 47, p. 314-319.

[56] MA, X.Y.; ZHANG, W.D. Effects of flower-like ZnO nanowhiskers on the mechanical, thermal and antibacterial properties of waterborne polyurethane. *Polymer Degradation and Stability*, 2009. Vol. 94, No. 7, p. 1103-1109.

[57] LI, J.H.; HONG, R.Y.; LI, M.Y.; LI, H.Z.; ZHENG, Y.; DING, J. Effects of ZnO nanoparticles on the mechanical and antibacterial properties of polyurethane coatings. *Progress in Organics Coatings*, 2009. Vol. 64, No. 4, p. 504-509.

[58] GEILICH, B.M.; WEBSTER, T.J. Reduced adhesion of Staphylococcus aureus to ZnO/PVC nanocomposites. *International Journal of Nanomedicine*, 2013. Vol. 8, p. 1177-1184.

[59] WONG, T.T.; LAU, K.T.; TAM, W.Y.; LENG, J.S.; ETCHES, J.A. UV resistibility of a nano-ZnO/glass fibre reinforced epoxy composite. *Materials & Design*, 2014. Vol. 56, p. 254-257.

[60] YADAV, A.; PRASAD, V.; KATHE, A.A.; RAJ, S.; YADAV, D.; SUNDARAMOORTHY, C.; VIGNESHWARAN N. Functional finishing in cotton fabrics using zinc oxide nanoparticles. *Buletin of Materials Science*, 2006. Vol. 29, No. 6, p. 641-645.

[61] SINHA, A.K.; BASU, M.; PRADHAN, M.; SARKAR, S.; PAL, T. Fabrication of Large-Scale Hierarchical ZnO Hollow Spheroids for Hydrophobicity and Photocatalysis. *Chemistry A European Journal*, 2010. Vol. 16, No. 26, p. 7865-7874.

[62] RAHMAN, Q.I.; AHMAD, M.; MISRA, S.K.; LOHANI, M.B. Hexagonal ZnO nanorods assembled flowers for photocatalytic dye degradation: Growth, structural and optical properties. *Superlattices and Microstructures*, 2013. Vol. 64, p. 495-506.

[63] ZHANG, L.; ZHU, Y.J. ZnO micro- and nano-structures: microwave-assisted solvothermal synthesis, morphology control and photocatalytic properties. *Applied Physics A – Materials Science & Processing*, 2009. Vol. 97, No. 4, p. 847-852.

[64] LEE, J.H.; Gas sensors using hierarchical and hollow oxide nanostructures: Overview. *Sensors and Actuators B – Chemical*, 2009. Vol. 140, No. 1, p. 319-336.

[65] ZHANG, Y.Y.; FU, W.Y.; SUI, Y.M.; YANG, H.B.; CAO, J.; LI, M.H.; LI, Y.X.; ZHOU, X.M.; LENG, Y.; ZAHO, W.Y.; CHEN, H.I.; ZHANG, L.N.; JING, Q.A.; ZHAO, H.I. Twinned tabour-like ZnO: Surfactant-, template-free synthesis and gas sensing behaviors. *Applied Suraface Science*, 2011. Vol. 257, No. 13, p. 5784-5788.

[66] WILLANDER, M.; NUR, O.; SADAF, J.R.; QADIR, M.I.; ZAMAN, S.; ZAINELABDIN, A.; BANO, N.; HUSSAIN, I. Luminescence from zinc oxide nanostructures and polymers and their hybrid devices. *Materials*, 2010. Vol. 3, No. 4, p. 2643-2667.

[67] *X-ray diffraction*. Warren, B. E., Dover ed.; Dover Publications: New York, 1990, ISBN: 978-0-4866-6317-3.

[68] *Adsorption by powders and porous solids: principles, methodology, and applications*. ROUQUEROL, F.; ROUQUEROL , J.; SING, K. S. W., 2nd ed. Academic Press: San Diego, 1999, ISBN: 978-0-12-598920-6.

[69] KAUR, J.; BANSAL, S.; SINGHAL, S. Photocatalytic degradation of methyl orange using ZnO nanopowders synthesized via thermal decomposition of oxalate precursor method, *Physica B-Condensed Matter*, 2013, Vol. 416, p. 33-38.

[70] HONG, R.Y.; PAN, T.T.; QIAN, J.Z.; LI, H.Z. Synthesis and surface modification of ZnO nanoparticles, *Chemical Engineering Journal*, 2006. Vol. 119, No. 2-3, p. 71 - 81.

[71] HONG, R.; LI, H.H.; WANG, H.; LI, Z.H. Comparison of schemes for preparing magnetic Fe_3O_4 nanoparticles. *China Particuology*, 2007. Vol. 5, No. 1-2, p. 186 - 191.

[72] CHANDER, S.; HOGG, R.; FUERSTENAU, D.W. Characterization of the wetting and dewetting behavior of powders. *Kona*, 2007. Vol. 25, p. 56 - 75.

[73] HU, Z.S; OSKAM, G.; PENN, R.L.; PESIKA, N.; SEARON, P.C. The influence of anion on the coarsening kinetics of ZnO nanoparticles. *Journal of Physical Chemistry B*, 2003. Vol. 107, No. 14, p. 3124-3130.

[74] JONES, A. Killer Plastics: Antimicrobial Additives for Polymers. *Plastics Engineering*, 2008. Vol. 64, No. 8, p. 36-40.

[75] BECK, P. A.; KREMER, J. C.; DEMER, L. J.; HOLZWORTH, M. L., Grain growth in high-purity aluminum and in an aluminummagnesium alloy. *Transactions of the American Institute of Mining and Metallurgical Engineers,* 1948. Vol. 175, p. 372-400.

[76] BURKE, J. E., Some factors affecting the rate of grain growth in metals. *Transactions of the American Institute of Mining and Metallurgical Engineers,* 1949. Vol. 180, p. 73-91.

[77] ERHART, P.; ALBE, K., Diffusion of zinc vacancies and interstitials in zinc oxide. *Applied Physics Letters*, 2006. Vol. 88, Article No. 201918.

[78] JANOTTI, A.; VAN DE WALLE, C. G., Fundamentals of zinc oxide as a semiconductor. *Reports on Progress in Physics,* 2009. Vol. 72, Article No. 126501.

[79] THOMAS, D. G., Interstitial zinc in zinc oxide. *Journal of Physics and Chemistry of Solids*, 1957, Vol. 3, p. 229-237.

CURRICULUM VITAE

Name:	Jakub Sedlák
Date of birth:	1984, November 03
Place of birth:	Ostrava, Czech Republic
Permanent address:	Sosnová 85, 793 14, Czech Republic
Nationality:	Czech
Affiliation:	Polymer Centre, Faculty of Technology, Tomas Bata University in Zlin, Namesti T. G. Masaryka 275, 762 72 Zlin, Czech Republic
Phone:	(+420)-57-603-8128
E-mail:	j1sedlak@ft.utb.cz

Education:	2010 – to date
	Faculty of Technology, Tomas Bata University in Zlin, Czech Republic, Ph.D. studies at the Polymer Centre in Chemistry and Materials Technology, Technology of Macromolecular compounds
	August 2008-January 2009
	Institute of Technology, Linköping University, Sweden, ERASMUS/SOCRATES exchange studies related to nanotechnology and polymers
	2008-2010
	Faculty of Technology, Tomas Bata University in Zlin, Czech Republic, Master's degree Ing. (MSc.) in Chemistry and Materials Technology, Polymer Engineering

2005-2008

Faculty of Technology, Tomas Bata University in Zlin, Czech Republic, Bachelor's degree Bc. (BSc.) in Chemistry and Materials Technology

Projects:

CZ.1.05/2.1.00/03.0111 Centre of Polymer Systems – Research Project Staff

IGA/FT/2014/008 Polymer systems with potential applications in medicine - member of research team

IGA/FT/2013/026 Antibacterial polymer systems – project leader

IGA/FT/2012/042 Composite materials with controlled release of active species - project leader

IGA/5/FT/11/D Microwave synthesis of fillers and preparation of composite materials with antibacterial activity – member of research team

LIST OF PAPERS

Journal articles

1. SEDLAK, J.; BAZANT, P.; KLOFAC, J.; PASTOREK, M.; KURITKA, I. Antibacterial Composite Based on Nanostructured ZnO Mesoscale Particles and Poly(vinyl chloride) Matrix. *Materials and Technology*, ISSN: 1580-2949 – accepted, scheduled to be published in the issue 2/2015.

2. SEDLAK, J.; KURITKA, I; MACHOVSKY, M.; SULY, P.; BAZANT, P.; SEDLACEK T. Zinc oxide nanoparticles with surface modified by degradation of capping polymers in situ during microwave synthesis. Submitted to *Advanced Powder Technology*.

3. SEDLAK, J.; KURITKA, I; MACHOVSKY, M.; BAZANT, P.; JANOTA, P.; DVORACKOVA, M. ZnO micro-beads with mesoporous architecture prepared by annealing at different temperatures and their photocatalytic activity. Submitted to *Materials Characterization.*

4. MACHOVSKY, M.; SEDLAK, J.; JANOTA, P.; URBANEK, P.; HAJEK, M.; DVORACKOVA, M.; KURITKA, I. Photocatalytic properties of nanocrystalline assembled ZnO spheres. Manuscript in preparation.

5. MACHOVSKY, M.; KURITKA, I.; SEDLAK, J.; PASTOREK, M. Hexagonal ZnO porous plates prepared from microwave synthesized layered zinc hydroxide sulphate via thermal decomposition. Materials Research Bulletin, 2013. Vol. 48, No. 10, p. 4002-4007.

6. KLOFAC, J.; KURITKA, I.; BAZANT, P.; JEDLICKOVA, K.; SEDLAK, J. Model Antimicrobial Polymer System Based on Poly(vinyl chloride) and Crystal Violet. *Materials and Technology*, 2014. Vol. 48, p. 33-39.

7. BAZANT, P.; MUNSTER, L.; MACHOVSKY, M.; SEDLAK, J.; PASTOREK, M.; KOZAKOVA, Z.; KURITKA, I. Wood flour modified by hierarchical Ag/ZnO as potential filler for wood-plastic composites with enhanced surface antibacterial performance. Submitted to *Industrial Crops and Products*.

Conference proceedings

1. SEDLAK, J.; BAZANT, P.; KOZAKOVA, Z.; MACHOVSKY, M.; PASTOREK, M.; KUŘITKA, I. Nanostructured Zinc Oxide Microparticles with Various Morphologies. *In NANOCON 2011 Conference Proceedings*, 2011. ISBN: 978-80-87294-23-9.

2. SEDLAK, J.; PASTOREK, M.; KURITKA, I. Preparation of Surface Modified Zinc Oxide Microparticles. *In Plastko 2012 Conference proceedings*, 2012. ISBN 978-80-7454-137-7.

3. KLOFAC, J.; MUNSTER, L.; BAZANT, P.; SEDLAK, J.; KURITKA, I. Preparation of Flower-like ZnO Microparticles by Microwave Assisted Synthesis. *In NANOCON 2012 Conference proceedings*, 2012. ISBN 978-80-87294-32-1.

4. MUNSTER, L.; KLOFAC, J.; SEDLAK, J.; BAZANT, P.; MACHOVSKY, M.; KURITKA, I. Microwave Assisted Modification of Bio-template by Ag-ZnO Sub-microparticles. *In NANOCON 2012 Conference proceedings*, 2012. ISBN 978-80-87294-32-1.

APPENDIX – PAPERS INCLUDED TO THE THESIS

Paper I.

SEDLAK, J. (50 %); BAZANT, P.; KLOFAC, J.; PASTOREK, M.; KURITKA, I. Antibacterial Composite Based on Nanostructured ZnO Mesoscale Particles and Poly(vinyl chloride) Matrix. *Materials and Technology, ISSN: 1580-2949 – accepted, scheduled to be published in the issue 2/2015.*

Antibacterial Composite Based on Nanostructured ZnO Mesoscale Particles and Poly(vinyl chloride) Matrix

Jakub Sedlák[1,2], Pavel Bažant[1,2], Jiří Klofáč[1,2], Miroslav Pastorek[1,3], Ivo Kuřitka[1,2]

[1]*Centre of Polymer Systems, University Institute, Tomas Bata University in Zlin, Nad Ovcirnou 3685, 760 01 Zlin, Czech Republic*

[2]*Polymer Centre, Faculty of Technology, Tomas Bata University in Zlin, Namesti T.G. Masaryka 275, 762 72 Zlin, Czech Republic*

[3]*Department of Polymer Engineering, Faculty of Technology, Tomas Bata University in Zlin, Namesti T.G. Masaryka 275, 762 72 Zlin, Czech Republic*

E-mail: j1sedlak@ft.utb.cz

Tel: +420 576 031 222; Fax: +420 576 031 444

The microwave assisted solvothermal synthesis of inorganic ZnO nanoparticles is a facile method yielding broad variety of active fillers with specific properties. The synthesis of hierarchical nanostructured zinc oxide mesoscale particles was carried out under continuous microwave irradiation from soluble zinc acetate as the precursor in diethylene glycol solvent. Prepared ZnO particles were characterized by X-ray diffractometry, scanning electron microscopy and UV-VIS spectrometry. A composite was obtained by mixing of these particles with the softened medical grade poly(vinyl chloride) as a model polymer matrix to develop an antibacterial polymer system with possible application for plastic medical devices. Testing of antibacterial activity of the composite confirmed excellent performance against *Escherichia coli* (gram-negative) and sufficient activity against *Staphylococcus aureus* (gram-positive) bacteria according to ISO 22196: 2007. In addition, no adverse effects of the filler on mechanical properties of the composite were observed in comparison with the neat PVC

resin. Therefore, prepared composites can be considered as suitable candidates for application in plastic medical devices and other industries.

Keywords: antibacterial, PVC, composite, ZnO, nanoparticles

1 INTRODUCTION

Nosocomial infections have become serious problem of today's hospital environment. The prevalence of medical devices related infections (MDIs) rapidly grows among hospital-acquired infections and high health risks are especially associated with the devices which are in close contact with the inner parts of patient's body.[1] As the polymers are the most frequently used material in medical devices, the prevention against bacteria adhesion and growth on their surface is an absolute imperative.[2] There are two principally different strategies how to resolve this problem. First approach uses organic antimicrobial additives to plastics. They are very efficient however their mechanism of action requires diffusion out of the plastic surface and they can be classified as migratory additives. In contrast to that, the second approach uses inorganic additives with very low solubility which ensures sufficient surface antibacterial activity and minimum leakage of the active species into the patients body.[3] Therefore, utilization of inorganic antibacterial nanopowders by compounding them with the commercial polymer resins seems to be the simplest way leading to enhanced antibacterial activity of polymer composite system.

In recent years, a great effort has been spent by the community of researchers for the synthesis and utilization of nanomaterials in the field of medical materials.[4] Zinc oxide is one of the promising candidates from the group of metal oxides (e.g. CaO, MgO, TiO_2, Cu_2O) that can be obtained with various properties depending on nanoparticles size and shape as the crucial parameters.[5] ZnO is biocompatible material possessing antimicrobial properties against the gram-negative as well as gram-positive bacteria. The mechanisms of antibacterial action are still not perfectly understood but there are several proposals for explanation of the microbial inhibition such as the generation of reactive oxygen species (ROS) such as hydroxyl radicals and singlet oxygen or the release of Zn^{2+} cations.[6,7]

Up to now, a large variety of physical and chemical methods were developed for ZnO nanoparticles preparation such as thermal decomposition, hydrothermal, solvothermal or microwave assisted synthesis. The lastly mentioned microwave energy exclusively reduces the reaction time as well as the energetic demands of the process.[8-12]

Here we report on a fast and simple solvothermal microwave assisted synthesis of hierarchical nanostructured mesoscale ZnO aggregates, their compounding into medical grade plasticized PVC as a model polymer matrix suitable for utilization in medical devices and evaluation of the surface antimicrobial and mechanical properties of final composites.

2 EXPERIMENTAL

2.1. Materials

All chemical reagents used in the experiment were of analytical grade and used as received without further purification. Zinc acetate dihydrate, p.a., (purity 99 %, Penta, The Czech Republic), Diethylene glycol, p.a., (purity 99 %, Penta, The Czech Republic). Azeotropic denatured ethanol (The Czech Republic) was used for washing the product. Medical grade softened PVC resin RB-3 (Modenplast Medical, Italy) was used as a polymer matrix.

2.2 Synthesis of ZnO antibacterial filler

At first 2.195 g of $Zn(CH_3COO)_2 \cdot 2H_2O$ was completely dissolved in 100 ml of diethylene glycol at the temperature about 100 °C within 30 minutes agitation on magnetic stirrer. Obtained solution was transferred to the 250 ml boiling flask and irradiated under reflux for 5 minutes by microwaves. The product was cooled down naturally after turning off the microwave oven. Powder was collected by centrifugation, washed with ethanol and air-dried up to the constant weight. The microwave reaction was performed in a microwave open vessel system MWG1K-10 (Radan, The Czech Republic, 800W, 2.45 GHz), which is based on modification of a domestic microwave oven by drilling a hole in the ceiling for external cooler and equipped by external source of microwave energy that allows to control the duty cycle. The reaction mixture was heated in a quasi-continuous mode at maximum heating power.

2.3. Compounding the ZnO filler with PVC matrix

The PVC-filler compounds were prepared by the melt-mixing process with the use of Brabender Plasti-Corder machine (Brabender, Germany) equipped by a 50 cm^3 mixing chamber and mixing elements working in contra-rotating mode. In this way, four mixtures differing from each other by the load of the filler in the polymer matrix were compounded with the composition as follows: 0.5; 1; 2; and 3 wt%. Compounding process consisted of three continual phases. The first started by feeding the mixing chamber by PVC pelletes and synthesized filler in the form of fine powder at 20 rpm for two minutes. In the next step, when the feeding of the chamber was finished, the engine speed was continuously increased from 20 up to 50 rpm within one minute. The last part of mixing was done at 50 rpm for 5 minutes. The mixing process was monitored with the aid of measuring the torque of the drive engine. Processing time of 8 minutes was enough to obtain a constant torque value for all samples. No resin discoloration or other signs of the polymer deterioration connected with the use of ZnO filler were observed under used mixing conditions. Prepared compounds were compress-molded to square-shaped sheets with dimensions 50 mm x 50 mm x 1 mm at 180 °C for 2.5 minutes. Blank samples without filler were prepared in the same way as the filled ones.

2.4 Characterization

Synthesized powder was characterized by X-ray powder diffraction (XRD) using the X´Pert PRO (PANalytical, The Netherlands) with Cu Kα radiation source (λ = 1.540598 Å). Micrographs of prepared powder and cross-section surfaces of composites were taken by the scanning electron microscope Vega II (Tescan, The Czech Republic) and UV-VIS absorption spectra were collected by the Avaspec UV-VIS spectrometer (Avantes, The Netherlands) with the source type AvaLight-DHS-DUV and integrating sphere ($BaSO_4$ coated) was used for diffuse reflectance measurement. Mechanical properties of composites were evaluated by tensile tests performed at Testometric universal testing machine M350-5CP (LABOR machine Ltd., The Czech Republic) according to ISO 37: 2005 standard with testing specimen type 2. The speed of the moving clamps was 250 mm/min. All sample measurements were 6 times replicated.

2.5. Antibacterial testing

The evaluation of surface antibacterial activity of the composites against bacteria adherence and growth was performed according to the ISO 22196: 2007 (formerly known as JIS Z-2801) standard. Gram-positive bacteria were represented by *Staphylococcus aureus* ATCC 6538P and Gram-negative by *Escherichia coli* ATCC

8739 both obtained from The Czech Collection of Microorganisms (The Czech Republic). The size of test specimens was 50 mm x 50 mm x 1 mm. The HERAcell 150i incubator (Thermo Scientific, USA) was used for cultivation. The antibacterial activity R was calculated using Equation (1)

$$R = (U_t - U_0) - (A_t - U_0) = U_t - A_t \qquad (1)$$

Where R is the antibacterial activity; U_0 is the average of the common logarithm of the number of viable bacteria, in cells/cm^2, recovered from the untreated test specimens immediately after inoculation; U_t is the average of the logarithm of the number of viable bacteria, in cells/cm^2, recovered from the untreated test specimens immediately after 48 hours; A_t is the average of the logarithm of the number of viable bacteria, in cells/cm^2, recovered from the treated test specimens immediately after 48 hours. The number of colonies was counted after 24 hours and controlled after 48 hours for eventual presents of slowly growing colonies for both untreated and treated test specimens which improves the original standard protocol. All tests were repeated in triplicate.

3 RESULTS AND DISCUSSION

The crystalline phase structure of synthesized filler is manifested on the diffractogram in Figure 1. By comparison with JCDD PDF-2 entry 01-079-0207, diffraction peaks were labelled as (100), (002), (101), (102), (110), (103), (200), (112), (201), (004), (202) and (104) and assigned to the hexagonal ZnO wurtzite structure. Moreover, the evident broadness of diffraction lines implies that synthesized particles are in nano-scale dimensions.

Figure 2 shows diffuse reflectance UV-VIS (DR-UV-VIS) spectrum of prepared ZnO nanocrystals which possess a strong absorption with the maximum below 380 nm. This peak is slightly blue shifted from typical position of bulk ZnO[12] which points towards the nano-sized particles similarly as the XRD analysis. Morphology of prepared filler is presented in the SEM image in Fig. 3a). As can be seen the material consists of globular-like particle aggregates with diameter ranging from 200 nm up to 1 μm. According to the XRD analysis and DR-UV-VIS measurement it can be concluded that these aggregates are assembled from much smaller nanocrystals.

The filler dispersion in prepared composites was achieved at the aggregate level and their good distribution in PVC matrix is manifested as shown in the SEM image in Fig. 3b) on the sample with 2 wt% of the filler. There are no visible agglomerates of the globular aggregates within the polymer matrix. On the other hand, the aggregates were not disaggregated by the mixing procedure.

Mechanical properties of prepared composites were characterized by the use of tensile tests and Young's modulus, elongation at break and tensile strength were chosen as the three representative quantities for evaluation of the filler content effects on the composite performance. As summarized in Table 1, no significant changes of mechanical properties were observed across all samples. Thus, it can be concluded that (i) incorporation of inorganic ZnO filler up to 3 wt% did not change the properties of the neat medical grade plasticized PVC matrix which is already designed by its producer to be an optimal flexible material for medical devices such as urinal catheters or blood bags and that (ii) the filler has no adverse influence on the application potential of the prepared antibacterial composite.

The quantitative evaluation of the surface antibacterial activity of as prepared ZnO/PVC composites is summarized in Table 2. The obtained *R* values representing antibacterial activity of composites against both bacteria are high enough for composites filled by 2 and 3 wt%. The *R* value should not be lower than 2 for materials that can be classified as possessing an antibacterial surface suitable for instance for hygienic applications or less demanding applications. However, medical devices are more demanding on the antibacterial performance of used materials. R-values of 5 or even 6 are expected for nowadays used high-end commercial materials especially those with organic additives intended to be used in indwelling medical devices.[13] The surface antibacterial activity of composites containing 2 or 3 wt% of the filler against *E. coli* meet these strongest requirements while the activity against *S. aureus* is not so high. Similar antibacterial performance was obtained recently for antibacterial systems containing hybrid Ag/ZnO filler employing nanosilver in addition to nanostructured ZnO.[14] On the other hand, *S. aureus* is a very vital and resistant bacterium which is difficult to suppress and inhibit the bacterial growth. Concurrent studies reported reductions from the control samples about 70 up to 95 % for much higher nano ZnO loadings in PVC matrices which means that *R* values less than 2 were claimed as success by their authors.[1] However, other strains were used throughout these studies and the surface activity estimation methods were similar but not identical with ISO 22196: 2007 as well. From this point of view, and with the full awareness of the peculiar comparability among different published results, the performance of our prepared composites seems to be sufficiently high. Next, as the bacteria gain on antibiotic resistance, the organic molecular additives in antimicrobial polymer systems may be found to be inefficient or ineffective and the inorganic nanofillers will serve as the last line of defense.

4 CONCLUSIONS

The present study describes microwave assisted synthetic route leading to the development of hierarchical nanostructured ZnO mesoscale filler. The synthesized powder was clearly identified to have ZnO hexagonal wurtzite structure and globular morphology of aggregated nanocrystals. The composite materials compounded by medical grade softened PVC with as-prepared filler showed excellent antibacterial activity values against *E. coli* and satisfactory antibacterial activity values against *S. aureus*. Moreover obtained composites kept the suitable mechanical properties of the neat PVC resin which were deteriorated neither by the processing nor by the effects of the nanofiller. These facts suggests that the prepared nanostructured mesoscale ZnO/PVC composite has application potential in medicine as the material for medical devices being in the direct contact with the human body besides many other possible utilizations.

ACKNOWLEDGMENT

The authors wish to thank the internal grant of TBU in Zlin No. IGA/FT/2013/026 funded from the resources of specific university research for financial support.

This article was written with the support of the Operational Program “Research and Development for Innovations” co-funded by the European Regional Development Fund (ERDF) and the national budget of the Czech Republic, within the Centre of Polymer Systems project (reg. number: CZ.1.05/2.1.00/03.0111).

This article was written with the support of the Operational Program “Education for Competitiveness” co-funded by the European Social Fund (ESF) and the national budget of the Czech Republic, within the “Advanced Theoretical and Experimental Studies of Polymer Systems” project (reg. number: CZ.1.07/2.3.00/20.0104).

REFERENCES

1. X. Y. Ma, W. D. Zhang, Polymer Degradation and Stability, 94(2009)1103-1109

2. Y. Yang, H. Chen, B. Zhao, et all, Journal of Crystal Growth, 263(2004)447-453
3. A. Jones, Plastics Engineering, 64(2008)34-40
4. B. M. Geilich, T. J. Webster, International Journal of Nanomedicine, 8(2013)1177-1184
5. J. Sawai, Journal of Microbiological Methods, 54(2003)177-182
6. N. Padmavathy, R. Vijayaraghavan, Science and Technology of Advanced Materials, 9(2008)035004 (7pp)
7. K. H. Tam, A. B. Djurisic, C. M. N. Chan, et all, Thin Solid Films, 516(2008)6167-6174
8. H. Lu, S. Wang, L. Zhao, et all, Journal of Materials Chemistry, 21(2011)4228-4234
9. P. Tonto, O. Mekasuwandumrong, S. Phatanasri, et all, Ceramics International, 34(2008)57-62
10. J. Zhu, J. Zhang, H. Zhou, et all, Trans. Nonferrous Met. Soc. China, 19(2009)1578-1582
11. A. Phuruangrat, T. Thongtem, S. Thongtem, Materials Letters, 63(2009)1224-1226
12. N. S. Pesika, K. J. Stebe, P. C. Searson, J. Phys. Chem. B, 107(2003)10412-10415
13. P. Bazant, I. Kuritka, O. Hudecek, M. Machovsky, M. Mrlik, T. Sedlacek, Polymer Composites, 35(2014)1, 19-26

Figure captions

Figure 1 X-Ray diffractogram of prepared ZnO filler

Figure 2 UV-VIS diffuse reflectance spectrum of prepared ZnO filler. Relative reflectance is plotted versus wavelength.

Figure 3 SEM images of a) prepared ZnO filler and b) crossection of the prepared composite material with 2 wt% of ZnO filler.

Table 1 Summary of selected mechanical properties of prepared composites and their standard deviations

Concentration of ZnO filler (wt%)	Young's Modulus (MPa)	Elongation at Break (%)	Tensile Strength (MPa)
0	9.9 ± 0.2	501 ± 17	19.1 ± 0.9
0.5	9.8 ± 0.2	494 ± 30	19.0 ± 1.1
1	10.3 ± 0.3	500 ± 20	19.4 ± 0.8
2	10.1 ± 0.3	497 ± 9	19.4 ± 0.8
3	9.2 ± 1.0	520 ± 20	18.4 ± 0.4

Table 2 Summary of the surface antibacterial activity evaluation results obtained for prepared composites

Concentration of ZnO filler (wt%)	The treated specimens after 48 h E. coli N (cfu cm^{-2})	The treated specimens after 48 h S. aureus N (cfu cm^{-2})	Antibacterial activity (log CFU) E. coli, $R = U_t - A_t$	Antibacterial activity (log CFU) S. aureus, $R = U_t - A_t$
0	4.0×10^6	7.5×10^4	$U_t = 6.6$	$U_t = 4.9$
0.5	1.5×10^5	8.0×10^4	1.4	0
1	1.7×10^5	1.0×10^0	1.4	4.9
2	< 1	2.2×10^0	> 6.6	4.5
3	< 1	1.3×10^0	> 6.6	4.8

Figure 1

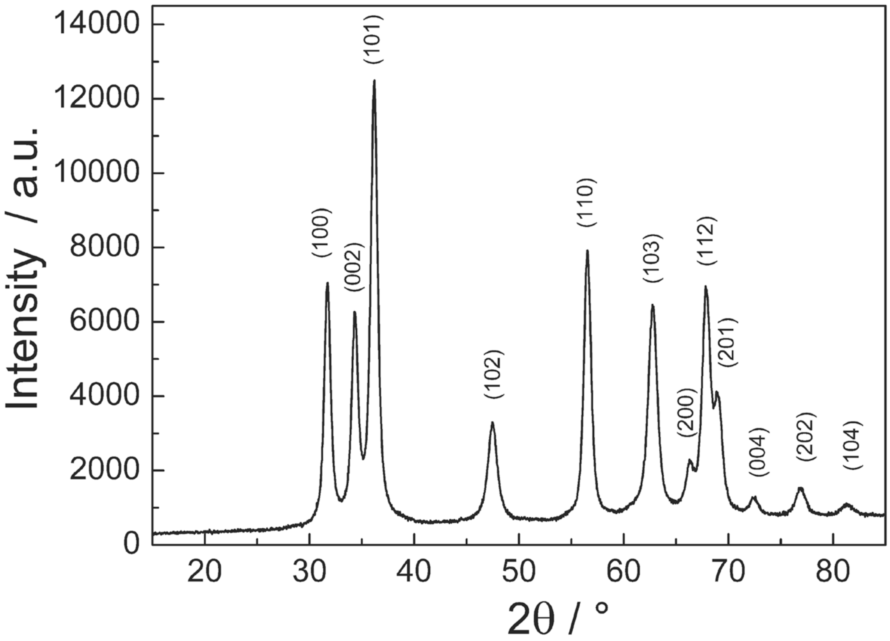

14000
12000
10000
8000
6000
4000
2000
0
Intensity / a.u.
20
30
40
50
60
70
80
2θ / °
(100)
(002)
(101)
(102)
(110)
(103)
(200)
(112)
(201)
(004)
(202)
(104)

Figure 2

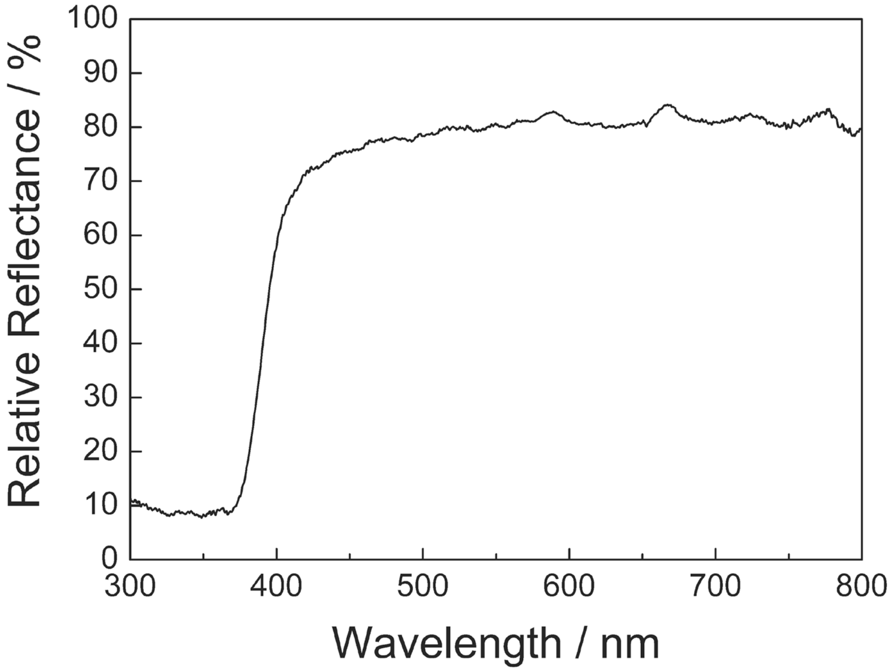

Relative Reflectance / %
100
90
80
70
60
50
40
30
20
10
0
300
400
500
600
700
800
Wavelength / nm

Figure 3

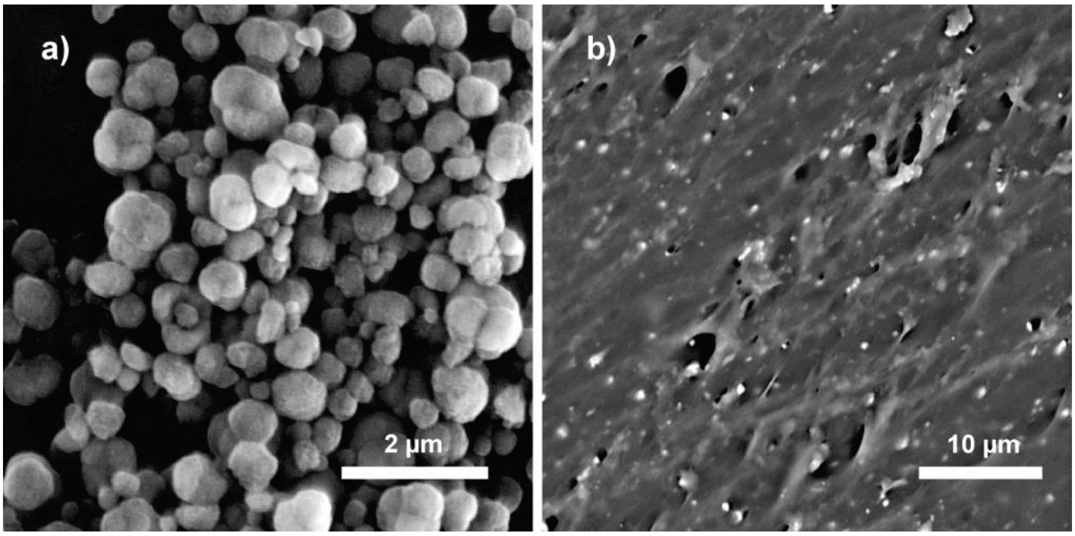

Paper II.

SEDLAK, J. (50 %); BAZANT, P.; KOZAKOVA, Z.; MACHOVSKY, M.; PASTOREK, M.; KUŘITKA, I. Nanostructured Zinc Oxide Microparticles with Various Morphologies. *In NANOCON 2011 Conference Proceedings*, pp. 305-309, 2011. ISBN: 978-80-87294-23-9.

NANOSTRUCTURED ZINC OXIDE MICROPARTICLES WITH VARIOUS MORPHOLOGIES

Jakub SEDLÁK [a], Pavel BAŽANT [a], Zuzana KOŽÁKOVA [a], Michal MACHOVSKÝ [a], Miroslav PASTOREK [b], Ivo KUŘITKA [a]

[a] *CENTRE OF POLYMER SYSTEMS, Faculty of Technology, Tomas Bata University in Zlín, Nám. T. G. Masaryka 5555, 760 01 Zlín, Czech Republic*

[b] *DEPARTMENT OF POLYMER ENGINEERING, Faculty of Technology, Tomas Bata University in Zlin, Nám. T. G. Masaryka 275, 762 72 Zlín, Czech Republic*

Abstract

In this paper we present a simple two stage preparation method of nanostructured zinc oxide microparticles by using microwave-assisted solvothermal synthesis. Zinc acetate dihydrate and sodium carbonate were used as starting materials, ethyleneglycol (EG), diethyleneglycol (DEG) and demineralised water were used as solvents and polyethylene glycol (PEG) was used as a surface stabilising agent. Obtained powders show various morphology which is influenced by the time duration of microwave assisted reaction and particularly by selection of suitable solvent. According to their morphology, prepared particles are categorised as needle-like structure, platelet structures and urchins-like structures and other shapes, which demonstrates a great potential of this synthesis route. Prepared materials were characterized by Scanning Electron Microscopy (SEM), X-ray diffraction (XRD) and Ultraviolet-visible diffusion reflectance spectroscopy (UV-VIS-DRS).

Keywords: microwave synthesis, ZnO, microparticles, nanoparticles

INTRODUCTION

Nanosized ZnO is very attractive II-VI semiconductor material because of its unique properties such as wide band gap (3.37 eV) and large exciton binding energy (60 meV) at room temperature [1]. ZnO nanocrystals have found many applications including solar cells, gas sensors, UV - protection, light emitting diodes etc [2-5]. Up to now, numerous different methods have been developed to synthesize nanocrystaline ZnO powders, e.g. mechanochemical [6], precipitation [7-9], hydrothermal [10-12], thermal decomposition [13,14], sol-gel [15], solvothermal [16] and microwave assisted [17,18]. Microwave radiation is an efficient heating method, which can significantly decrease reaction time and it has been already used for successful preparation of different materials [4,16,17]. Here we adopted and further developed a fast and easy method for preparation of ZnO nanoparticles in two stages. First step is mechanochemical preparation of a precursor in the form of a nanopowder, from which are prepared particles by solvothermal reaction in microwave apparatus with open vessel reflux system in the second preparation step. This method offers short reaction time and saving of energy consumption.

EXPERIMENTAL

All of the chemical reagents used in the experiment were of analytical grade. Zinc acetate dihydrate, p.a, (Purity 99 %, Penta, Czech Republic), Sodium carbonate anhydrous, p.a., (Purity 99 %, Penta, Czech Republic), Ethylene glycol, p.a., (Purity 99 %, Penta, Czech Republic), Polyethylene glycol 400, p.a., (Fluka, Germany). Microwave reaction was performed in a modified domestic microwave oven (CRW-TECH, frequency 2.45 GHz, maximum power 1150 W). Products number 2 and 3 were heated at maximum heating power (1150 W), product number 1 was heated at variable heating powers. Energy consumption was measured during every synthesis. Preparation of precursor started by grinding of 8.8g $Zn(CH_3COO)_2{\cdot}2H_2O$ for 5 min before it was mixed with 16 ml of PEG and then 4.24 g of Na_2CO_3 was added. After 20 min of grinding, the mixture was firstly washed by demineralised water and secondly by alcohol to remove possible by-product or rests of starting chemicals. After that, the mixture was left to dry on the air naturally. In the second step a 0.5 g of a precursor was moved to the boiling flask together with 10 ml of PEG and 80 ml of EG or demineralised water was added. The mixture was sonicated in ultrasound bath for 10 min (Elma S 80, Ultrasonic) to achieve better dispersion of the precursor in the liquid medium. The mixture was then irradiated for 20 or 40 minutes by microwaves. The product was collected by suction filtration, washed with demineralised water followed by alcohol and finally dried in air. Detailed description of preparation of individual products is summarized in a Table1.

Table 1: List or prepared products

Product number	Composition	Microwave synthesis time
1	0,5 g precursor 10 ml PEG 400 80 ml demineralised water	20 min
2	0,5 g precursor 10 ml PEG 400 80 ml EG	20 min
3	0,5 g precursor 10 ml PEG 400 80 ml EG	40 min

The powders were characterized by X-ray powder diffraction (XRD) using PANalytical X´Pert PRO X-ray diffractometer with Cu Kα radiation (λ = 1.540598 Å). Scanning electron microscope Tescan Vega II was used for obtaining micrographs and UV-VIS spectrometer Avaspec Avantes with source type AvaLight-DHS-DUV and integrating sphere ($BaSO_4$ coated) was used for diffuse reflectance (DR) spectrometry in UV-VIS.

RESULTS AND DISCUSSION

Fig. 1 (a) shows XRD pattern of the precursor. Compared with the JCPDS cards (reference code: 00-003-0787), diffraction peaks fits well with that of $Zn_4CO_3(OH)\cdot 6H_2O$ (Zinc Carbonate Hydroxide Hydrate). Fig. 1(b) shows UV-VIS DR spectrum of the precursor, which confirms that no ZnO absorbing near 400 nm is present.

a) b)

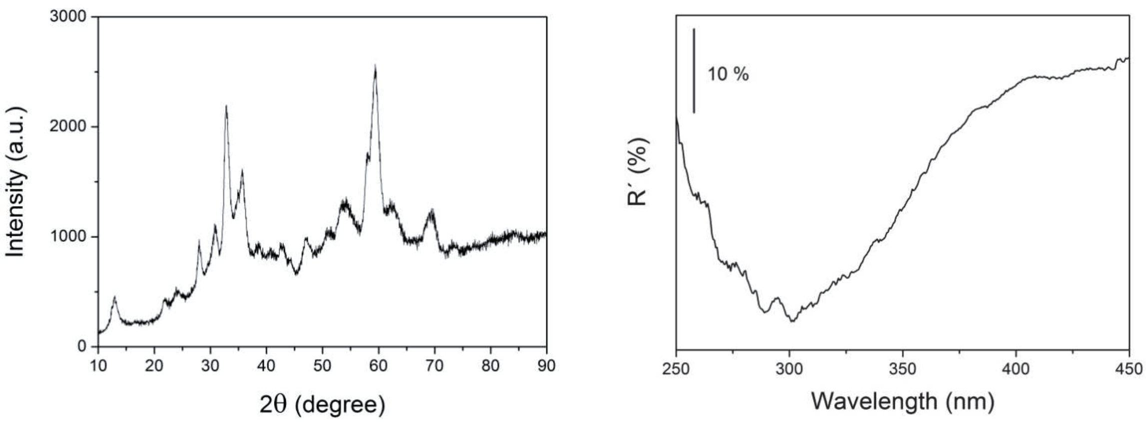

Fig. 1 (a) XRD pattern of the precursor and (b) UV-VIS DR spectrum of the precursor.

Fig. 2 (a) shows the SEM image of the precursor that do not reveal any specific shape, just irregular pointed particles of submicrometric size. Fig. 2(b) shows the SEM image of product 1 made with PEG and demineralised water for 20 minutes. As can be seen, this product is needle-like in shape. Needles are approximately from 4 to 6 μm length and less than 1 μm width. Residuals of very fine nanofibres resembling snow or dust in the image are most likely the constituents of the growing needles Fig. 2(c) presents SEM image of product 2 made with PEG and EG for 20 minutes. Product 2 was obtained exclusively in form of thin curtain-like platelets with very fine nanoporous structure. With the aid of the last picture Fig. 2(d) can be demonstrated the influence of reaction time on final structure of the particles. Product 3 is made as well as product 2 from dispersion with PEG and EG, with the only difference that is longer reaction time i.e. 40 minutes. The assembling of platelets into urchin-like microstructures is supported by longer synthesis time.

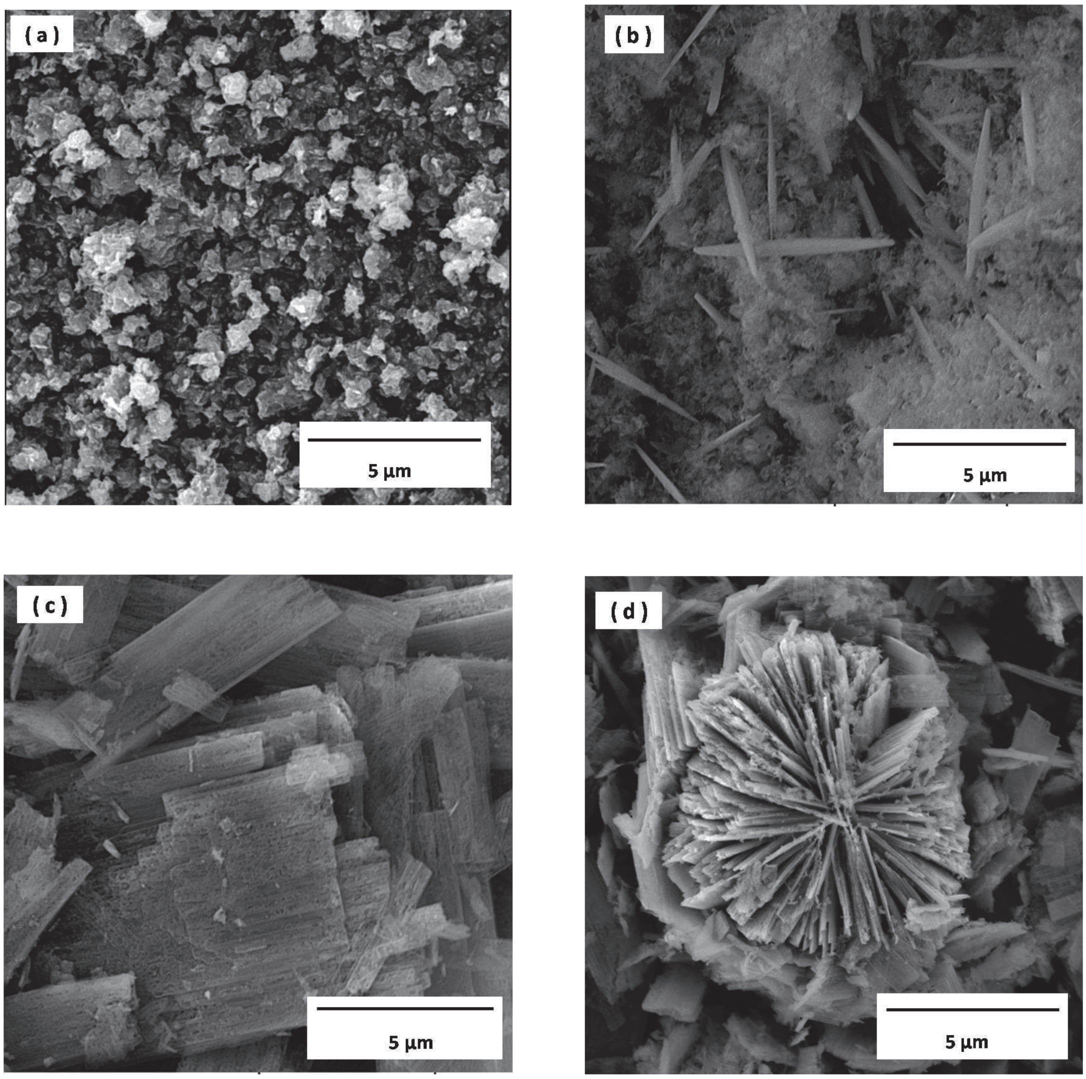

Fig. 2 SEM image of the precursor (a) and SEM images of the final products 1, 2, 3, (b), (c), (d) respectively.

Fig. 3 (a), (b) and (c) shows XRD patterns of final products 1, 2, 3 respectively. Compared with the JCPDS cards, diffraction peaks labelled as (100), (002), (101), (102), (110), (103), (200), (112), (201), (004), (202), (104) and (203) fits well with hexagonal ZnO wurtzite structure (reference code: 01-079-0207) and diffraction peaks labelled with symbol * with that of $Zn(CH_3COO)_2{\cdot}2H_2O$ (reference code: 00-001-0215), which stayed in the final products as a certain impurity. Fig. 3(d) shows UV-VIS optical DR spectra of the final products testifying the presence of ZnO by pronounced decrease of relative reflectance in spectral range below 400 nm.

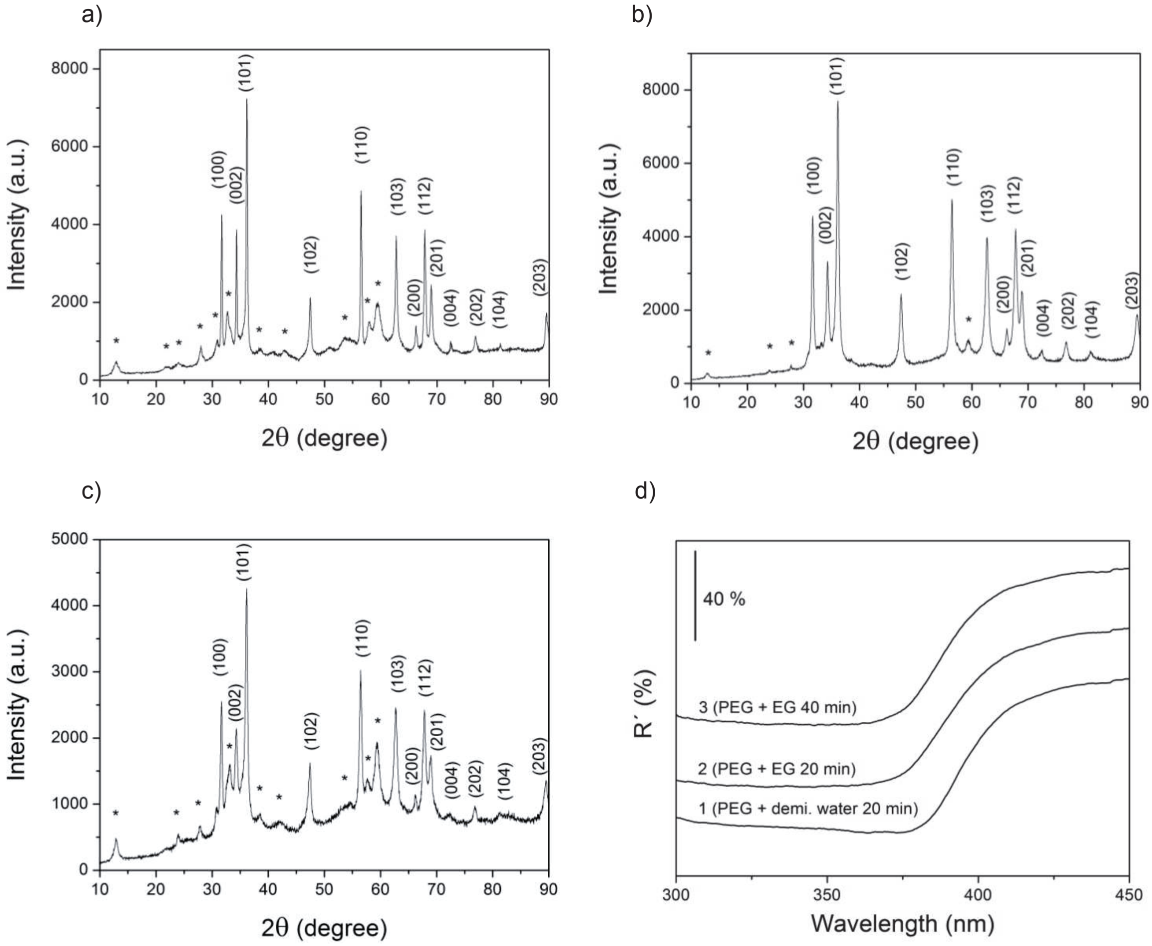

Fig. 3 (a), (b), (c) XRD patterns of final products 1, 2, 3 respectively and (d) UV-VIS optical DR spectra of final products 1, 2, 3

CONCLUSION

In summary, needle, urchin- and platelete-shaped nanostructured ZnO microparticles were successfully prepared by simple two stage method, based on combination of mechanochemical preparation of the precursor and solvothermal microwave-assisted reaction with open reflux system. The size of prepared particles ranges from hundreds of nanometers to micrometers.

ACKNOWLEDGMENTS

This article was written with support of Operational Program Research and Development for Innovations co-funded by the European Regional Development Fund (ERDF) and national budget of Czech Republic, within the framework of project Centre of Polymer Systems (reg. number: CZ.1.05/2.1.00/03.0111).

This work was supported by the internal grant of TBU in Zlín No. IGA/5/FT/11/D funded from the resource of specific university research.

LITERATURE

[1] J. Zhu, J. Zhang. H. Zhou, W. Qin, L. Chai, Y. Hu, Trans. Nonferrous Met. Soc. China 19 (2009) 1578-1582
[2] S. Rani, P. Suri, P.K. Shishodia, R.M. Mehra, Solar Energy Mat. & Solar Cells 92 (2008) 1639-1645
[3] M. Chen, Z. Wang, D. Han, F. Gu, G. Guo, Sensors and Actuators B 157 (2011) 565-574
[4] I.A. Siddiquey, T. Furusawa, M. Sato, N. Suzuki, Mat. Research Bulletin 43 (2008) 3416-3424
[5] H. Guo, J. Zhou, Z. Lin, Electrochemistry Communications 10 (2008) 146-150
[6] W. Ao, J. Li, H. Yang, X. Zeng, X. Ma, Powder Technology 168 (2006) 148-151
[7] A. Aimable, M.T. Buscaglia, V. Buscaglia, P. Bowen, J. European Ceram. Society 30 (2009) 591-598
[8] Ch, Chen, P, Liu, Ch. Lu, Chemical Engineering J. 144 (2008) 509-513
[9] S. Musić, A. Šarić, S. Popović, J. Alloys and Comp. 448 (2008) 277-283
[10] T. Shang, J. Sun, Q. Zhou, M. Guan, Cryst. Res. Technol. 42 (2007) 1002-1006
[11] J. Song, S. Baek, J. Lee, S. Lim, J. Chem. Technol. and Biotechnol. 83 (2008) 345-350
[12] H. Hu, X. Huang, Ch. Deng, X. Chen, Y. Qian, Mat. Chemistry and Physics 106 (2007) 58-62
[13] Y. Yang, H. Chen, B. Zhao, X. Bao, J. Crystal Growth 263 (2004) 447-453
[14] Y. Yang, X. Li, J. Chen, H. Chen, Chemical Physics Letters 373 (2003) 22-27
[15] S. Suwanboon, ScienceAsia 34 (2008) 031-034
[16] P. Tonto, O. Mekasuwandumrong, S. Phatanasri, V. Pavarajarn, P. Praserthdam, Ceram. International 34 (2008) 57-62
[17] J. Liu, J. Cao, Z. Li, G. Ji, M. Zheng, Mat. Letters 61 (2007) 4409-4411
[18] X. Chu, T. Chen, W. Zhang, B. Zheng, H. Shui, Sensors and Actuators B 142 (2009) 49-54

Paper III.

SEDLAK, J. (50 %); KURITKA, I; MACHOVSKY, M.; SULY, P.; BAZANT, P.; SEDLACEK T. Zinc oxide nanoparticles with surface modified by degradation of capping polymers in situ during microwave synthesis. *Submitted to Advanced Powder Technology*.

Zinc oxide nanoparticles with surface modified by degradation of capping polymers *in situ* during microwave synthesis

Jakub Sedlák[1], Ivo Kuřitka*[,1], Michal Machovský[1], Pavol Šuly[1], Pavel Bažant[1], Tomáš Sedláček[1]

[1]Centre of Polymer Systems, University Institute, Tomas Bata University in Zlin, Nad Ovcirnou 3685, 760 01 Zlin, Czech Republic

*E-mail to corresponding author: kuritka@cps.utb.cz, Tel.: +420 576 038 049, Fax: +420 576 031 444;

Emails to other authors: J. Sedlák: j1sedlak@ft.utb.cz; M. Machovský: machovsky@cps.utb.cz; P. Šuly: suly@ft.utb.cz; Pavel Bažant: bazant@uni.utb.cz; T. Sedláček: sedlacek@cps.utb.cz;

Abstract: Surface modified zinc oxide nanoparticles with variable lipophilicity were prepared by the help of microwave-assisted solvothermal synthesis from mechano-chemically prepared precursor. Sodium carbonate and zinc acetate dihydrate were used as starting materials, diethylene glycol was used as a solvent, poly(ethylene glycol) and polyvinyl alcohol were used as surface capping agents. The zinc oxide was obtained during the first three minutes of reaction and its surface was further modified with prolonged time of the reaction due to degradation of polymers used as capping and stabilising agents. Scanning Electron Microscopy was employed for powder morphology evaluation. Inorganic phase structure development was characterized by means of X-Ray Diffraction. Nanostructured composite materials with crystallite size below 10 nm were obtained with specific surface area varying from 35 to 86 m^2g^{-1} according to Brunauer-Emmet-Teller analysis. The progress of degradation of adsorbed polymer moieties was manifested by the powder colour change. Optical properties as well as the structure of materials were further analysed by Diffuse

Reflectance Ultraviolet-visible Spectroscopy and Diffuse Reflectance Infrared Fourier Transform Spectroscopy and correlated with Thermogravimetric observations and Lipophilicity degree analysis.

Keywords:

zinc oxide; nanocomposite; microwave; lipophilicity; surface

Highlights:

- Mechanochemical preparation of precursor from simple chemicals
- Extremely fast microwave assisted solvothermal synthesis of ZnO nanoparticles
- Particles covered by organic shell from adsorbed degraded capping polymers
- Prepared nano-ZnO with variable surface lipophilicity and specific surface area

1. Introduction

Zinc oxide is a versatile semiconductive material with wide direct band gap (3.3 eV), and large exciton binding energy (60 meV) [1], potentially applicable in electronics [2], solar energy conversion [3], light emitting devices [4], gas-sensors [5], etc. Apart from its application in sophisticated devices, ZnO powder is also a relatively cheap chemical available in large amounts and various forms ready for applications as pigments [6], UV-protecting additive [7], antimicrobial and antifungal fillers for polymers [8,9], sun-screens and medical ointments [10,11]. The chemical properties of ZnO are utilised in chemical engineering and material processing. The largest quantity is consumed in rubber industry because ZnO is still unrivalled activator of sulphur vulcanisation [12]. On the other hand, much finer and demanding application of ZnO can be found in photocatalysis [13] and biomedicine [14,15]. Zinc oxide has most likely the most abundant forms among metal oxide materials. The properties of ZnO are strongly dependent on its structure, morphology, aspect ratio, particle size and orientation [16-18]. Moreover, a careful reading of all above mentioned literature sources points towards the importance of surface structure and properties as the crucial factors for almost all applications of ZnO powder materials.

Surface modification of microparticles or nanoparticles is one of the most effective ways of controlling their properties for preparation of new types of smart materials with desired structure [19]. In the past decade, many scientists were focused on improving surface properties of different zinc oxide powder materials [20-22]. Some applications require bare ZnO particles with specific surface defect microstructure [23]. The easiest way how to obtain such particles usually employs calcination at optimum temperature and atmosphere [24]. On the other hand, it is often required to cover the ZnO particle surface by a functional shell and many methods have been proposed for such surface modifications of ZnO. So far, coated ceramic fillers have been successfully prepared [25,26]. Thin SiO_2 coatings are used to avoid photodegradation of polymer matrix when the ZnO powder is used as UV absorber in plastics [27] or in sunscreens [28]. On contrary, organic coatings usually serve as stabilising and dispersing agents that do not passivate the material function and the spectrum of surface functionalization approaches is at least as wide as for inorganic ones [29].

According to our opinion, it is reasonable to couple synthesis of ZnO particles with the coating operation into one reaction step, which can be beneficial in terms of time, material and energy savings, especially if combined with the use of a rapid synthesis method.

Microwave (MW) radiation is an efficient heating method, which can significantly decrease reaction time and its advantages were already demonstrated by preparation of different materials in our previous works [30-33]. Here we adopted [34] and further developed a fast and easy method for preparation of surface modified ZnO nanoparticles with an organic shell layer in two stages. Mechanochemical preparation of a precursor from simple chemicals in the first step is followed by a MW assisted solvothermal reaction step in an open vessel reflux system used with advantage under atmospheric pressure. The MW enhanced reaction takes a few minutes only. The surface coating is developed at the expense of progressive degradation of capping and stabilizing polymers in the high boiling temperature solvent reaction mixture. The coating properties are simply dependent on the MW exposure time.

2. Materials and Methods

2.1 Synthesis methodology

Sodium carbonate anhydrous, p.a., (purity 99 %, Penta, Czech Republic), zinc acetate dihydrate, p.a., (purity 99 %, Penta, Czech Republic), diethylene glycol, p.a., (purity 99 %, Penta, Czech Republic), polyethylene glycol 400, p.a., (Fluka, Germany), poly(vinyl alcohol) Mowiol 8-88, (Mw~67 000, Sigma Aldrich) were used as starting chemicals. Precursor (sample denoted as S0) was prepared by grinding of 11 g $Zn(CH_3COO)_2{\cdot}2H_2O$ with 20 ml of 10 wt % solution of poly(vinyl alcohol) (PVA) in diethylene glycol (DEG) for 5 min in a vibration mill (VM 4, Czech Republic), followed by addition of 5.3 g of Na_2CO_3 and grinding continued for about 20 minutes. Obtained pasty mixture was washed by demineralised water and ethanol to remove possible by-product or rests of original soluble chemicals. The white powder dispersion was collected by a suction filtration and obtained filtration cake was left to dry freely. Synthesis of final products started by a mixing of 1.5 g of precursor with 80 ml of DEG and 10 ml of polyethylene glycol (PEG) in a boiling flask. The mixture was stirred vigorously with a magnetic stirrer and then sonicated in ultrasound bath (Elma S 80, Ultrasonic) for 15 min to achieve better dispersion of the precursor in the liquid medium. Possible metal chips originating from milling drum and bodies were removed by a magnet. Six individual mixtures were prepared and then exposed to microwave (MW) irradiation in open vessel system for different reaction times from 1.5 to 5 minutes. Microwave reaction was performed in a modified domestic microwave oven (CRW-TECH, frequency 2.45 GHz, maximum power 1150 W, unknown land of origin) equipped with an external condenser. All mixtures were heated at maximum heating power. The suspensions were left to cool to the laboratory temperature after MW exposure. Precipitates were collected by suction filtration, washed with demineralised water followed by ethanol and finally dried in air up to the constant weight. In this way, six different final products were obtained numbered according to their order from shortest to longest reaction time, i.e. from S1 to S6 (S1-1.5 min; S2-2 min; S3-2.5 min; S4-3min; S5-4 min; S6-5min).

2.2 Measurements and analysis

Microscopic images of samples were taken by the use of scanning electron microscope Tescan Vega LMU (Tescan, Czech Republic).

The phase structure of powders was characterized by powder X-ray diffraction (XRD) using X´Pert PRO X-ray diffractometer (PANalytical, The Netherlands) with Cu Kα radiation of λ = 0.1540598 nm. The size of ZnO crystallites was considered to be nearly identical with the size of diffracting area d_{diffr} which is easily accessible via Scherrer's formula using $\Delta(2\theta)$ which is full-width at half-maximum (FWHM) of XRD patterns. The particle shape and other factors were neglected to simplify the procedure and the calculation followed the well-known formula [35]:

$$d_{diffr} = \frac{0.9\,\lambda}{\beta \cos\theta} \qquad (\textit{Error! Reference source not found.})$$

Where the constant 0.9 is the shape factor, λ is the wavelength of the X-ray source, β is the FWMH in radians. The actual value of β was obtained by deconvolution of instrumental broadening effects using Warren correction method. The θ is the Bragg angle, i.e. the half of the 2θ position of the selected diffraction line.

The TA Q 500 apparatus (TA Instruments, US) was used for thermogravimetric analysis (TGA). This analysis was performed at the constant heating rate of 10 °C/min under stable air flow. The amount of each sample was approximately 15 mg.

The study of UV-vis absorption of the powder samples was performed with the aid of the UV-vis spectrometer AvaSpec 2048-2 (Avantes, The Netherlands) with the light source type AvaLight-DHS-DUV. Integrating sphere ($BaSO_4$ coated) and white tile $BaSO_4$ reflectance standard were used for relative diffuse reflectance (DRUV-vis) spectrometry. The relative reflectance was recorded for wavelengths in the range 265-800 nm due to relatively small sensitivity of the detector in NIR on one side and reflectance limit of the sphere coating material in UV on other side of spectral range.

FTIR spectrometer Nicolet 6700 (Thermo Scientific, US) was used for collection of infrared DRIFT spectra, utilizing 32 scans and resolution 4 cm^{-1} setup. The spectra are presented in Kubelka-Munk units.

The specific surface area was obtained via the multipoint Brunauer-Emmet-Teller analysis of nitrogen adsorption/desorption isotherms at 77 K recorded by Belsorp-mini II (BEL Japan, Inc.) apparatus. Samples were outgassed for 3 h at 115 °C prior to the measurements.

The lipophilic degree (LD) of nanoparticles is usually characterized by examination of dispersibility of defined amount of nanoparticles in water with the addition of organic solvent (methanol). Hence, the LD is expressed actually in vol % units. The original method [19,36] is relatively material demanding as each test of single liquid concentration consumes 0.5 g of sample. Therefore, we adopted the LD concept but modified the procedure in accordance with the framework of theoretical and practical analysis of wetting and dewetting of powders [37]. A series of stock water-methanol mixtures was prepared ranging from pure distilled water up to pure methanol graded in 5 vol % steps. The lipophilic degree was estimated as the concentration of the water-methanol mixture which readily wetted the tested powder. In more detail, the procedure was as follows: A small amount of powder (approx. 0.5 g) was spread into a uniformly thick layer on a glass substrate and tested by droplets of 5 μL of testing liquids. The measurement was several times repeated for each sample in ascending as well as in descending order of used concentrations to find precisely the transition between wetting and dewetting behaviour.

3. Results and Discussion

The morphology of prepared precursor is shown in SEM images in Fig.1. From the higher magnification image, it can be clearly seen that the mechano-chemically prepared particles possess lenticular shape with submicron size. The lower magnification image is displayed for comparison with SEM images of microwave-synthesized products at the same magnification. The morphology of final products is strongly changing with increasing synthesis time. Sample S1 still hold particulate-like character. On contrary to that, the morphology of sample S2 has more condensed appearance possibly due to agglomeration of smaller particles. This trend continues from S3 to S6. The agglomerated habit is affected by preparation method of the sample for SEM. A simple drying of a drop of redispersed (e.g. sample S2) nanoparticle suspension on the SEM substrate holder or just powder from crushed dried filter cake (e.g. sample S6) was used. More sophisticated sample preparation methods were omitted due to low resolution of used SEM apparatus.

HERE FIG. 1

The conversion of submicron inorganic precursor to the final zinc oxide nanoparticles can be followed according to the results from XRD analysis in Fig. 2. Compared with the ICDD PDF-2 entry 00-003-0787, diffraction peaks of precursor S0 fit well with those of $Zn_4CO_3(OH)_6 \cdot H_2O$ (Zinc Carbonate Hydroxide Hydrate) and diffraction peaks of sample S6 fit well with those of hexagonal ZnO wurtzite structure given in the ICDD PDF-2 entry 01-074-0534.

The steepest change is observed between samples S2 and S4 when the phase transformation occurs as diffraction pattern changes from precursor to ZnO. Moreover, the width of diffraction peaks implies the presence of nanocrystaline ZnO. The line broadening was evaluated by the application of Sherrer's equation for the calculation of crystallite size for samples S3 to S6. The diffraction line from (101) planes in ZnO that can be found in the diffractograms at 2θ angle 36.25° was used for diffracting area size estimation. The results displayed in Table 1 confirmed that nanocrystalline ZnO powders with average crystallite sizes below 10 nm were obtained. As the Zinc Carbonate Hydroxide Hydrate is a layered compound, a high aspect ratio between the diameter and thickness of the crystalline slabs can be expected for samples S0, S1 and S2 and, thus, the information obtained from wide angle diffraction lines would be of problematic interpretation value with respect to the geometry of the whole particles. Also, a pronounced layered structure would compromise the assumptions which were framed for applicability of Sherrer's equation in the experimental section.

HERE FIG. 2

HERE TABLE 1

Normalised intensities of selected diffraction lines from the diffractograms are shown in the Fig. 3. The intensity of the ZnO diffraction peak at 2θ angle 56.5° is plotted with full triangles. It can be clearly seen that ZnO phase appears in the material after 2.5 minutes of MW heating. Than it increases and reaches nearly maximum in samples S5 and S6. The conversion of the precursor can be followed by the evolution of diffraction line intensity at 2θ angle 28.07° marked by full squares. The sample S1consist from the precursor only, however a steep decrease of its content can be seen for samples S2,S3 and S4 when no intensity of signal at that 2θ angle is observable which means that the conversion of the precursor was finished. However, at the same time, the ZnO is only at a half way. Therefore, we focused on other diffraction line at 2θ angle 59.6°, which certainly does not belong to the ZnO diffraction pattern but can be found in the precursor's diffractogram. Due to significant line broadening, it cannot be better separated from that precursors set of lines. The evolution of intensity of this line is plotted in Fig. 3 (marked by stars). It is evident that this line belongs to an intermediate product. The residual intensity of this line in the sample S6 testifies for incomplete yet nearly full conversion of the intermediate to the ZnO product. We did not succeed in the separation of the intermediate diffraction lines from the lines of the precursor due to nanosize effect line broadening. Nevertheless, we were even not able to obtain identifiable diffraction pattern of the intermediate by subtraction of known ZnO patterns from S4 or S5 patterns, although the ZnO diffraction patterns are much simpler than those ones of the precursor.

HERE FIG. 3

The development of ZnO structure as well as organic film coating was studied by DR-UV-vis spectrometry. Results are shown in Fig. 4. Generally, it can be noted that the spectra of samples are ordered according to the position and intensity of their UV absorption maxima which correlates perfectly with the order according to the time of MW reaction. It may be easily followed in the graph starting in the left upper corner and continuing down and slightly to higher wavelengths.

HERE FIG. 4

As can be seen in Fig. 4, the spectra of precursor S0 and sample S1 do not possess almost any absorption between 350 and 400 nm which confirms absence of ZnO. These results are in correspondence with the observed brilliant white colour for samples S0 as well as S1. Although there is not manifested ZnO in XRD, there is observable a peak with the maximum at wavelength about 340 nm tailing into the spectral region of UV-A and even to the visible range up to 550 nm. Thus it is not ZnO which contributes to the cream-like colour of the sample S2 but it must be due to its organic coating component. Development of ZnO structure is clearly observable for samples S3, S4, S5 and S6 by the presence of strong absorption maxima below 380 nm. This value is blue-shifted from typical bulk ZnO maximum [38] confirming thus the nano-dimensionality of prepared materials. Evolution of organic film coating can be observed by broad tails of absorption curves ranging far to the red region. The main change can be seen between samples S3, S4 and S5. The sample S4 represents evidently the transition step for the reaction. Observed trends are in agreement with the naked eye observation of colour of prepared powders that changed from white (S0, S1) via cream (S2), beige (S3), light brown (S4), brown (S5) to dark brown (S6), respectively. The spectral and colour change can be associated with the microwave heating assisted thermal degradation of used polymers present in the reaction mixture. The observed changes correspond to development of conjugated double bond structures, so called oligo or polyenes. The MW assisted degradation of PVA was thoroughly investigated and interpreted in detail in our previous work [39].

The composition of both, inorganic and organic phases can be studied with advantage by the suitable Infrared absorption technique. Fig.6 shows the DRIFT spectra of all samples. By virtue of the simpler description of obtained spectra, main absorption bands are discussed in separate regions denoted by capital letters from A to E. In the region A, the main broad band centred at 3200 cm^{-1} observed for samples S0 to S2 can be attributed to the O-H stretching vibration of hydrozincite, which corresponds to hydroxyl groups co-ordinated to the metal ions referring to the absence of free bonded water molecules [40]. The structural formula $Zn_4CO_3(OH)_6 \cdot H_2O$ used in ICDD database of X-Ray diffraction data force a most-likely improper notion that the compound is a hydrate. More probably, the water molecule is co-ordinated to Zinc ion in positively charged hydroxide slabs and is strongly bonded than it would be in the interlayer gallery space in hydrates (consult the TGA section too) and the interlayer space is occupied by carbonate counterions only. On the other hand, this hydroxyl absorption band has no finer resolved structure and it can be concluded that the layered mineral structure is not perfectly developed and the particles of precursor suffer from some irregularity as one might expect due to used mechano-chemical preparation route. In next, the slight blue shift to 3360 cm^{-1} can be observed for samples S3 to S6 as well as the appearance of additional shoulder band centred at 3590 cm^{-1} that can be assigned to OH free hydroxyl group. This structural feature may be associated with the intermediate product deduced from XRD patterns. The increase in resolution of the hydroxyl absorption band may be ascribed to the increased perfection of the crystal structure. No mechanical agitation that could interfere the crystal growth is used during MW synthesis.

HERE FIG. 5

Fewer intense absorption bands in the region B match well with vibrations of asymmetrical 2940 $cm^{-1}$and symmetrical 2880 cm^{-1} stretches of C-H bond [41]. It is clearly visible, that intensities of C-H vibrations first gradually increased along with the synthesis time up to 2.5 minutes (sample S3) which can be explained by the continuous surface absorption of polymer capping agents. Later on, the intensities of C-H vibrations decreased at the expense of thermal degradation that was unambiguously visible by the change of powders colour from beige to dark brown. The two strong bands at 1520 cm^{-1} and 1390 cm^{-1} located in region C can be assigned to v_3 asymmetric stretching mode of carbonate. These two original bands splits into more complicated structures with increasing reaction time. This can be explained as the manifestation of partial changes of the coordination mode of carbonate anions. Theoretically, they can be unidentate, bidentate or bridging ligands [41]. The change of shape of these bands testifies for a transformation reaction consuming the precursor with relatively simple coordination situation of carbonate ions. On the other hand, there are no carbonate associated peaks in the bulk ZnO spectrum. Hence, it can be concluded that this material is either on the surface of ZnO nanoparticles or aside the ZnO nanoparticles in a separated phase. The presence of various carbonate-like surface contaminations on ZnO nanoparticles surface is reported frequently for similar reaction systems [19,28,42,43]. The weaker bands in region D at 1050 cm^{-1}, 949 cm^{-1} and 739 cm^{-1}, 709 cm^{-1} can be attributed to the v_1 symmetric stretching and v_4 in-plane bending mode of carbonate respectively, while the middle intensity band at 833 cm^{-1} corresponds to the v_2 out-of-plane bending motion of carbonate [44,45]. As can be seen from the Fig. 6, all of afore mentioned carbonate vibration intensities decreased with the extension of synthesis time.

The last region E is associated with the typical strong absorption band of ZnO [41]. Indeed, the intensity increase of the band with maximum at 460 cm^{-1} corresponding to the vibration of Zn-O bond is evidently in good agreement with results obtained by powder XRD as well as DR-UV-vis spectroscopy. The ZnO absorption band starts to developed from the sample S3 and steeply increases up to sample S5 where it becomes the strongest band in the whole measured spectral range.

HERE FIG. 6

To analyse the composition and contribute to structure clarification, the TGA was performed in non-isothermal mode under air atmosphere. Obtained thermoanalytical curves are plotted in Fig. 6. The total weight loss for the precursor was 28.6 % which is slightly more than the theoretical mass loss (26.3%) calculated for $Zn_4CO_3(OH)_6 \cdot H_2O$. The difference can be ascribed to adsorbed polymers used as stabilising additives. In contrast to the literature [44], the release of hydrate water was not observed in a separate step but as a slow gradual mass decrease from the beginning of the thermogravimetric curve followed by a well-defined decomposition step with the maximum rate at 216 °C. Hence we inclined to the observation of Chen et al. [46] and their interpretation of the decomposition as a single step process. This result is in agreement with FTIR analysis discussed above too. Two small steps above 250 °C with maximum mass loss rate at 300 °C and 380 °C, respectively are manifested on the curve most likely due to the contribution of the capping polymer degradation. The thermogravimetric curves of S1, S2 and S3 samples form a group of similar decomposition profiles resembling the S0 material but the main step is shifted by 40-50 °C towards higher temperatures. It can be assumed that the precursor losses its layered structure and planar aggregate forms quickly during the first 2.5 minutes of MW irradiation as can be seen in SEM figures and most likely it is manifested by the afore mentioned shift of decomposition temperature. The total weight loss varies about the value obtained for the precursor which also points towards the phase structural changes in the material during this first stage of MW reaction, rather than towards precursor transformation to ZnO product and the release of CO_2 and H_2O. The content of polymer seems to be comparable with its content the precursor in all these samples. The thermogravimetric curve obtained for sample S4 shows evidently a transient position between the first and the second group of curves recorded for S5 and S6. The total mass loss observed for S4 is a moderate value of 24 %. The last group of curves (S5 and S6) has the total mass loss about 16 %. The trend observed for thermogravimetric curves is in accordance with the trends observed by other techniques discussed in above sections. However, the total mass loss is quite large even for the samplesS5 or S6. This suggests that the material contains non-negligible amount of the organic component besides the residual amount of the decomposable intermediate, while ZnO is virtually invisible in TG curves.

The Specific Surface Area ($A_{s,BET}$) of prepared powder materials was expected to be quite high according to our other analyses. Therefore, it was characterised by the BET analysis. Table 2 summarises the results. It can be seen, that the precursor and sample S1and S2 have lower specific surface area. The sample S3 which has similar thermogravimetric characteristic as previous samples has significantly different structure due to formation of reasonable amount of ZnO nanoparticles, while the organic component is only weakly manifested in DR-UV-vis spectrum and still very similar to that of previous samples according to FTIR. The sudden increase in $A_{s,BET}$ can be ascribed to this nanostructure transformation. The sample S4 shows transitive behaviour with respect to the presence and structure of organic components and moieties volatile under high temperature. It might be hypothesised that the reduction of specific surface area is due to the polymeric content although the mechanism remains unclear. The samples S5 and S6 have again large specific surface, which might be correlated with the progress of organic component degradation that is well documented by DR-UV-vis spectra. Another possible explanation might be searched in the intermediate phase occurrence.

HERE TABLE 2

As the final property, the lipopilicity of prepared nano-particulate material was tested. The graph in Fig. 7 shows obtained results. The precursor behaves hydrophilically while the S1 sample has LD of 20 vol %. The material S2 is again hydrophilic and then the LD increases nearly linearly with synthesis time progress up to 25 vol % for sample S6. It seems that the initial role of added polymers is rather complicated. It might be expected that the out-lying lipophilicity of S1 sample is due to adsorbed diethylene glycol or poly(ethylene glycol) because the sample is otherwise similar to S0 in all other investigated properties. The sample S2 shows remarkable signs of structural changes and becomes hydrophilic with LD = 0 vol %. The lipophilicity increase of following samples corresponds to the development of conjugated double bond systems caused by the polymer thermal degradation [39]. Once the progressive polymer degradation in DR-UV-vis spectra was observed it was possible to expect increase in lipophilicity of prepared particles. This property is straightforwardly linked to to oligo- and polyene structural units in polymers. There are well known natural analogues to the double bond conjugated system on a linear carbon chain, namely lycopene and other carotenoids. Members of this class of fat-soluble isoprenoid compounds have up to fifteen conjugated double-bonds in a line. This structural feature of polyene backbone chain imparts them not only light-absorbing but also excellent lipophilicity [47]. The formation of ZnO which is normally (in dark) of hydrophobic nature [48,49] may contribute to the LD increase too.

HERE FIG. 7

4. Conclusion

Zinc oxide based nanoparticulate materials with various surface degree of lipophilicity were prepared successfully by a fast and simple two stage method. Firstly, the zinc carbonate hydroxide hydrate was prepared mechanochemically and its structure was confirmed as containing the water molecule coordinated into the hydroxide slabs of the layered material. In next, although the precursor consists of submicron lenticular shaped particles, it gives rise to nanoparticulate materials with nanocrystallite size bellow 10 nm in the second reaction step. This second process is microwave enhanced synthesis and allows achieving nearly complete conversion of the precursor to ZnO within 5 minutes. It was shown that an intermediate phase is involved in this transformation, however its phase structure was not identified. The optical properties of the material are governed first by ZnO nanoparticles development and then by the development of conjugated oligo- to polyene coating. The specific surface area of prepared powders varied between 35 and 86 $m^2\ g^{-1}$. Its value depends most likely on the competition between the nanoparticle formation and coating development. The lipophilic degree of the products varied from 0 to 25 vol % and its dependence on synthesis time is simple enough to allow targeted synthesis.

Acknowledgments

This article was written with support of Operational Program Research and Development for Innovations co-funded by the European Regional Development Fund (ERDF) and national budget of Czech Republic, within the project Centre of Polymer Systems (reg. number: CZ.1.05/2.1.00/03.0111).

The authors also acknowledge the support of Operational Program Education for Competitiveness co-funded by the European Social Fund (ESF) and national budget of Czech Republic, within the framework of project Advanced Theoretical and Experimental Studies of Polymer Systems (reg. number: CZ.1.07/2.3.00/20.0104).

The work of J. S. was supported by the Internal Grant Agency of Tomas Bata University in Zlin; contract grant number: IGA/FT/2014/008.

References

[1] H. Morkoç, Ü. Özgür, Zinc Oxide, Fundamentals, Materials and Device Technology, John Wiley and Sons Ltd., Weinheim, 2009.

[2] M.F Melendrez, K. Hanks, F. Leonard-deepak, F. Solis-pomar, E. Martinez-guerra, E. Perez-tijerina, M. Jose-yacaman, Growth of aligned ZnO nanorods on transparent electrodes by hybrid methods, Journal of Material Science, 47 (2012) 2025 - 2032.

[3] Q.F Zhang, C.S. Dandemeau, X.Y. Zhou, G.Z. CAO, ZnO Nanostructures for Dye-Sensitized Solar Cells, Advanced Materials, 21 (2009) 4087 - 4108.

[4] H.G. Guo, J.Z. Zhou, Z.G. Lin, ZnO nanorod light-emitting diodes fabricated by electrochemical approaches, Electrochemistry Communications, 10 (2008) 146 - 150.

[5] A.K. Singh, Synthesis, characterization, electrical and sensing properties of ZnO nanoparticles, Advanced Powder Technology, 21 (2010) 609 - 613.

[6] N. Kiomarsipour, R.S. Razavi, K. M. Kioumarsipour, Evaluation of shape and size effects on optical properties of ZnO pigment, Applied Surface Science 270 (2013) 33 - 38.

[7] T.T. Wong, K.T. Lau, W.Y. Tam, J.S. Leng, J.A. Etches, UV resistibility of a nano-ZnO/glass fibre reinforced epoxy composite, Materials & Design, 56 (2014) 254 - 257.

[8] J.H. Li, R.Y. Hong, M.Y. Li, H.Z. Li, Y. Zheng, J. Ding, Effects of ZnO nanoparticles on the mechanical and antibacterial properties of polyurethane coatings, Progress in Organics Coatings, 64 (2009) 504 - 509.

[9] X.Z. Ma, W.D. Zhang, Effects of flower-like ZnO nanowhiskers on the mechanical, thermal and antibacterial properties of waterborne polyurethane, Polymer Degradation and Stability, 94 (2009) 1103 - 1109.

[10] Z.A. Lewicka, W.W. Yu, B.L. Oliva, E.Q. Contreras, V.L. Colvin, Photochemical behavior of nanoscale TiO_2 and ZnO sunscreen ingredients, Journal of Photochemistry and Photobiology A: Chemistry, 263 (2013) 24 - 33.

[11] S. Baldwin, M.R. Odio, S.L. Haines, R.J. O'Connor, J.S. Englehart, A.T. Lane, Skin benefits from continuous topical administration of a zinc oxide/petrolatum formulation by a novel disposable diaper, Journal of the European Academy of Dermatology and Venereology, 15 (2001) 5 - 11.

[12] A. Moezzi, A.M. McDonagh, M.B. Cortie, Zinc oxide particles: Synthesis, properties and applications, Chemical Engineering Journal, (185- 186) 2012 1 - 22.

[13] Z. Xiaohua, Li. Meng, L. Xiangdong Sol-gel assisted hydrothermal synthesis of ZnO microstructures: Morphology control and photocatalytic activity, Advanced Powder Technology, 25 (2014) 372 - 378.

[14] H.M. Xiong, ZnO Nanoparticles Applied to Bioimaging and Drug Delivery. Advanced Materials, 25 (2013) 5329 - 5335.

[15] M. Machovsky, I. Kuritka, P. Bazant, D. Vesela, P. Saha, Antibacterial performance of ZnO-based fillers with mesoscale structured morphology in model medical PVC composites, Materials science & engineering. C, Materials for biological applications, 41 (2014) 70 - 77.

[16] R.Y. Hong, J.H. Li, L.L. Chen, D.Q. Liu, H.Z. Li, Y. Zheng, J. Ding, Synthesis, surface modification and photocatalytic property of ZnO nanoparticles, Powder Technology 189 (2009) 426 - 432.

[17] W. Hongqiang, C.H. Li, H.G. Zhao, J.R. Liu, Preparation of nano-sized flower-like ZnO bunches by a direct precipitation method, Advanced Powder Technology, 24 (2013) 599 - 604.

[18] CH. Jagadish, S.J. Pearton Eds., Zinc Oxide Bulk, Thin Films and Nanostructures, Processing, Properties and Applications, 1st ed., Elsevier, Amsterdam, 2006.

[19] R.Y. Hong, T.T. Pan, J.Z. Qian and H.Z. Li, Synthesis and surface modification of ZnO nanoparticles, Chemical Engineering Journal 119 (2006) 71 - 81.

[20] B. Ozkal, W. Jiang, S. Kato, O. Yamamoto, Z.E. Nakagawa, Characterization of carbon-coated ZnO composite powders produced by polymer pyrolysis method, Journal of the Ceramic Society of Japan,113 (2005) 116 - 119.

[21] Z.G. Wang, X.T. Zu, S.Z. Yang, L.M. Wang, Blue luminescence from carbon modified ZnO nanoparticles, Journal of Material Science 41 (2006) 3729 - 3733.

[22] B. Ozkal, W. Jiang, O. Yamamoto, K. Fuda, Z.E. Nakagawa, Preparation and characterization of carbon-coated ZnO and CaO powders by pyrolysis of PVA, Journal of Material Science, 42 (2007) 983 - 988.

[23] S.Q. Tian, D.W. Zeng, X.L. Peng, S.P. Zhang, C.S. Xie, Processing-microstructure-property correlations of gas sensors based on ZnO nanotetrapods, Sensors and Actuators B-Chemical, 181 (2013) 509 - 517.

[24] Enhanced photocatalytic activity of zinc oxide synthesized by calcination of zinc sulfide precursor, X. Zhao, M. Li, X.D. Lou, Materials Science in Semiconductor Processing, 16 (2013) 489 - 494.

[25] M. Inagaki, S. Kobayashi, F. Kojin, N. Tanaka, T. Morishita, B. Tryba, Pore structure of carbons coated on ceramic particles, Carbon, 42 (2004) 3153 - 3158.

[26] X.Q. Wei, H.C. Li, C. Yuan, Q.H. Li, S.X. Chen, Preparation of nano-ZnO supported on porous carbon and the growth mechanism, 118 (2009) 307 - 313.

[27] M. Ramasamya, Y.J. Kim, H. Gao, D.K. Yi, J.H. An, Synthesis of silica coated zinc oxide–poly(ethylene-co-acrylic acid) matrix and its UV shielding evaluation, Materials Research Bulletin, 51 (2014) 85 - 91.

[28] I.A. Siddiquey, T. Furusawa, M. Sato, N. Suzuki, Microwave-assisted silica coating and photocatalytic activities of ZnO nanoparticles, Materials Research Bulletin, 43 (2008) 3416 - 3424.

[29] B. Faure, G. Salazar-Alvarez, A. Ahniyaz, I. Villaluenga, G. Berriozabal, Y.R. De Miguel, L. Bergstrom, Dispersion and surface functionalization of oxide nanoparticles for transparent photocatalytic and UV-protecting coatings and sunscreens, Science and Technology of Advanced Materials, 14 (2013) 1 - 23.

[30] M. Machovsky, Z. Kozakova, I. Kuritka, Microwave assisted synthesis of nanostructured Fe_3O_4/ZnO microparticles, Materials Letters, 86 (2012) 136 - 138.

[31] M. Machovsky, I. Kuritka, J. Sedlak, M. Pastorek, Hexagonal ZnO porous plates prepared from microwave synthesized layered zinc hydroxide sulphate via thermal decomposition, Materials Research Bulletin, 48 (2013) 4002 - 4007.

[32] P. Bazant, I. Kuritka, O. Hudecek, M. Machovsky, M. Mrlik, T. Sedlacek, Microwave-Assisted Synthesis of Ag/ZnO Hybrid Filler, Preparation, and Characterization of Antibacterial Poly(vinyl chloride) Composites Made From the Same, Polymer Composites, 35 (2014) 19 - 26.

[33] M. Machovsky, M. Mrlik, I. Kuritka, V. Pavlinek, V. Babayan, Novel synthesis of core-shell urchin-like ZnO coated carbonyl iron microparticles and their magnetorheological activity, RSC advances, 4 (2014) 996 - 1003.

[34] J.S. Liu, J.M. Cao, Z.Q. Li, G.B. Ji, M.B. Zheng, A simple microwave-assisted decomposing route for synthesis of ZnO nanorods in the presence of PEG400, Materials Letters, 61 (2007) 4409 - 4411.

[35] B.E. Warren, X-ray Diffraction, 2nd ed., Dover Publications Inc., New York, 1990.

[36] R. Hong, H.H. Li, H. Wang, H.Z. Li, Comparison of schemes for preparing magnetic Fe_3O_4 nanoparticles, China Particuology, 5 (2007) 186 - 191.

[37] S. Chander, R. Hogg, D.W. Fuerstenau, Characterization of the wetting and dewetting behavior of powders, Kona 28 (2007) 56 - 75.

[38] Z.S. Hu, G. Oskam, R.L. Penn, N. Pesika, P.C. Searson, The influence of anion on the coarsening kinetics of ZnO nanoparticles, Journal of Physical Chemistry B, 107 (2003) 3124 - 3130.

[39] A. Bernal, I. Kuritka, V. Kasparkova, P. Saha, The Effect of Microwave Irradiation on Poly(vinyl alcohol) Dissolved in Ethylene Glycol, Journal of Applied Polymer Science, 128 (2013) 175 - 180.

[40] N. Kanari, D. Mishra, I. Gaballah, B. Dupre, Thermal decomposition of zinc carbonate hydroxide, Termochimica Acta, 410 (2004) 93 - 100.

[41] G. Socrates, Infrared and Raman Characteristic Group Frequencies: Tables and Charts, 3rd ed., Wiley, Chichester, 2001.

[42] S. Liufu, H. Xiao, Z.P. Li, Investigation of PEG adsorption on the surface of zinc oxide nanoparticles, Powder Technology 145 (2004) 20 - 24.

[43] M.S. Mohajerani, M. Mazloumi, A. Lak, A. Kajbafvala, S. Zanganeh, S.K. Sadrnezhaad, Self-assembled zinc oxide nanostructures via a rapid microwave-assisted route, Journal of Crystal growth, 310 (2008) 3621 - 3625.

[44] Z.J. Li, XQ. Shen, X. Feng, P.Y. Wang, Z.S. Wu, Non-isothermal kinetics studies on the thermal decomposition of zinc hydroxide carbonate, Termochimica Acta, 438 (2005) 102 - 106.

[45] D. Stoilova, V. Koleva, V. Vassileva, Infrared study of some synthetic phases of malachite ($Cu_2(OH)_2CO_3$) – hydrozincite ($Zn_5(OH)_6(CO_3)_2$) series, Spectrochimica Acta Part A, 58 (2002) 2051 - 2059.

[46] J. Chen, R. Zhao, H. Jiang, Y. Li, G. Bao, Thermal decomposition of zinc carbonate hydroxide hydrate powders of different particle size and sample mass, Transactions-Nonferrous Metals Society of China-English Edition, 8 (1998) 149 - 153.

[47] M.H. Walter, D. Strack, Natural Product Reports, 28 (2011) 663 - 692.

[48] J. Wu, J. Xia, W. Lei, B.P. Wang, Superhydrophobic surface based on a coral-like hierarchical structure of ZnO, Plos One 5 (2010) e14475

[49] X.J. Feng, L. Feng, M.H. Jin, J. Zhai, L. Jiang, D.B. Zhu, Reversible super-hydrophobicity to super-hydrophilicity transition of aligned ZnO nanorod films, Journal of The American Chemical Society, 126 (2004) 62 - 63.

Table 1 ZnO nanocrystalite size calculated according to Scherer's equation for prepared materials. Samples S0, S1 and S2 do not contain ZnO phase.

Sample code	S0	S1	S2	S3	S4	S5	S6
d_{diffr} [nm]	-	-	-	8.0	9.1	7.4	7.0

Table 2 SSA of precursor S0 and products S1 to S6 obtained by the application of BET method.

Sample code	S0	S1	S2	S3	S4	S5	S6
$A_{s,BET}$ [m^2g^{-1}]	58.6	34.5	44.6	86.3	42.7	76.9	74.5

Figure Captions

Fig. 1 SEM images of the precursor S0 and products S1-S6.

Fig. 2 X-Ray diffractograms recorded for samples S0-S6. The diffraction lines assigned to ZnO are marked by stars, the diffraction lines associated with the precursor are marked by hollow circles. The symbols are placed for S0 and S6 samples as they represent the most pure phases.

Fig. 3 Normalised intensities of selected diffraction lines plotted versus reaction time. The sample codes are indicated at the bottom of the graph window. Used symbols are associated with diffractogram peaks at 2θ angles as follows: full squares for 28.07°, full triangles for 56.5° and stars for 59.6°.

Fig. 4 DR-UV-vis spectra of the precursor S0 and products S1-S6.

Fig. 5 DRIFT spectra of the precursor S0 and products S1-S6.

Fig. 6 TGA curves recorded for the precursor S0 and products S1-S6.

Fig. 7 The dependence of LD on the synthesis time for the precursor S0 and products S1-S6.

*Highlights (for review)

Highlights:

- Mechanochemical preparation of precursor from simple chemicals
- Extremely fast microwave assisted solvothermal synthesis of ZnO nanoparticles
- Particles covered by organic shell from adsorbed degraded capping polymers
- Prepared nano-ZnO with variable surface lipophilicity and specific surface area

*Graphical Abstract (for review)

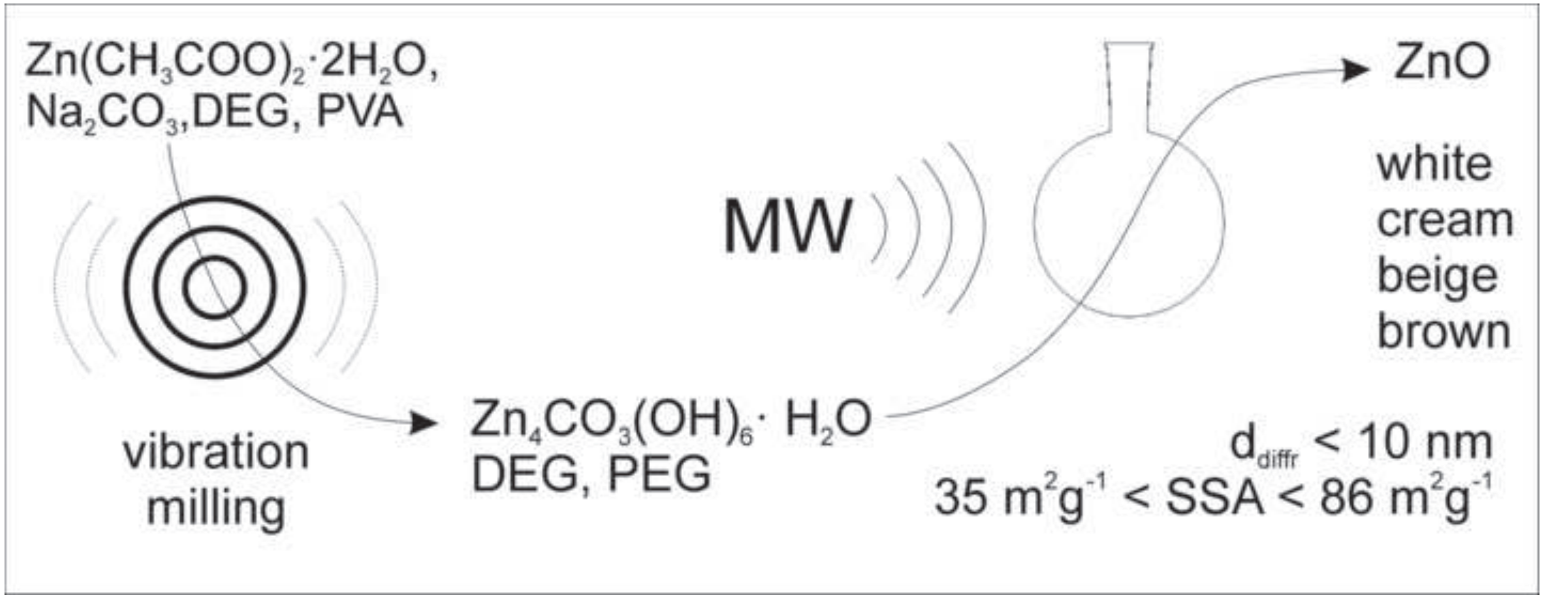

Figure 1
Click here to download high resolution image

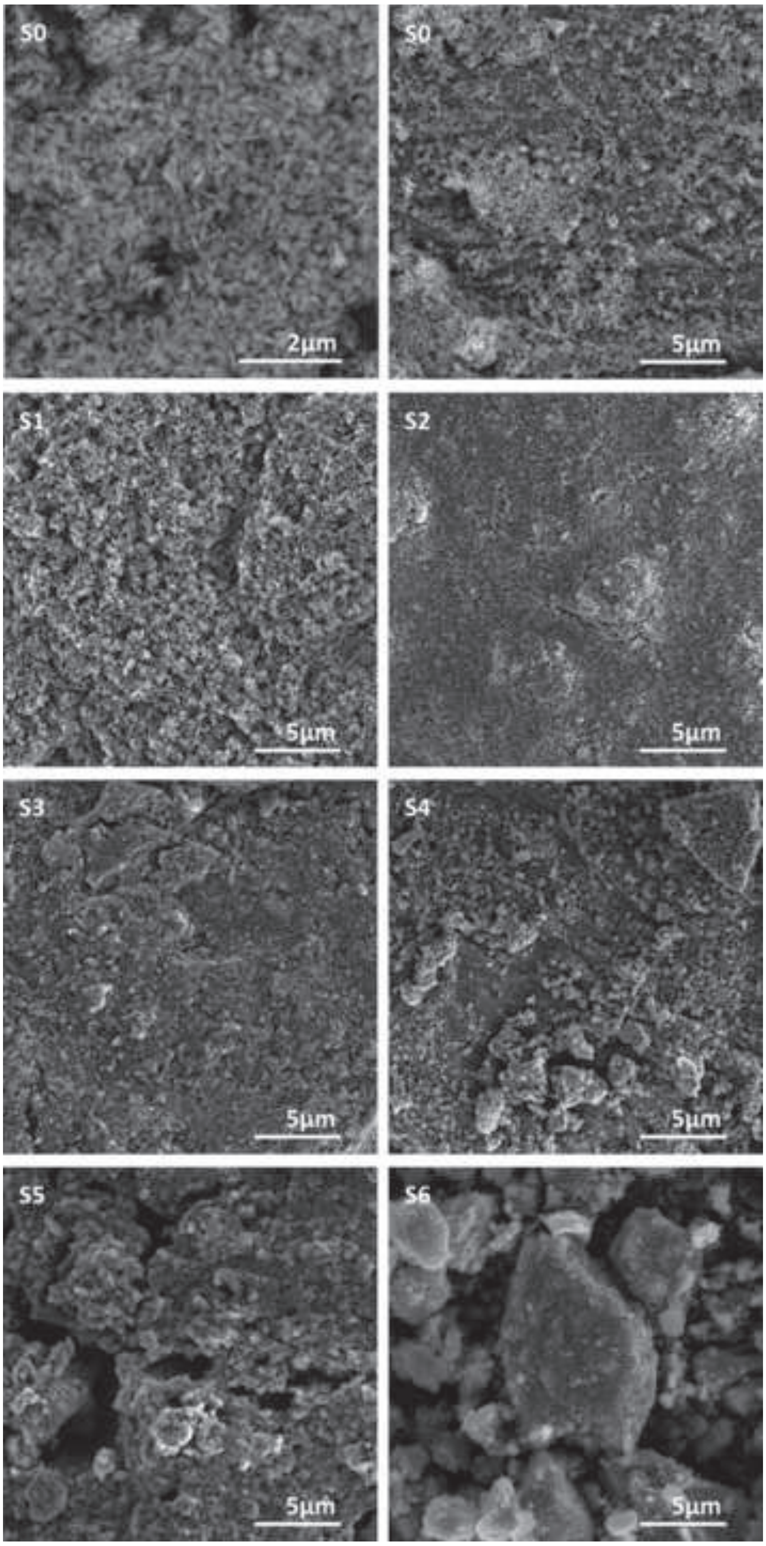

Figure 2
Click here to download high resolution image

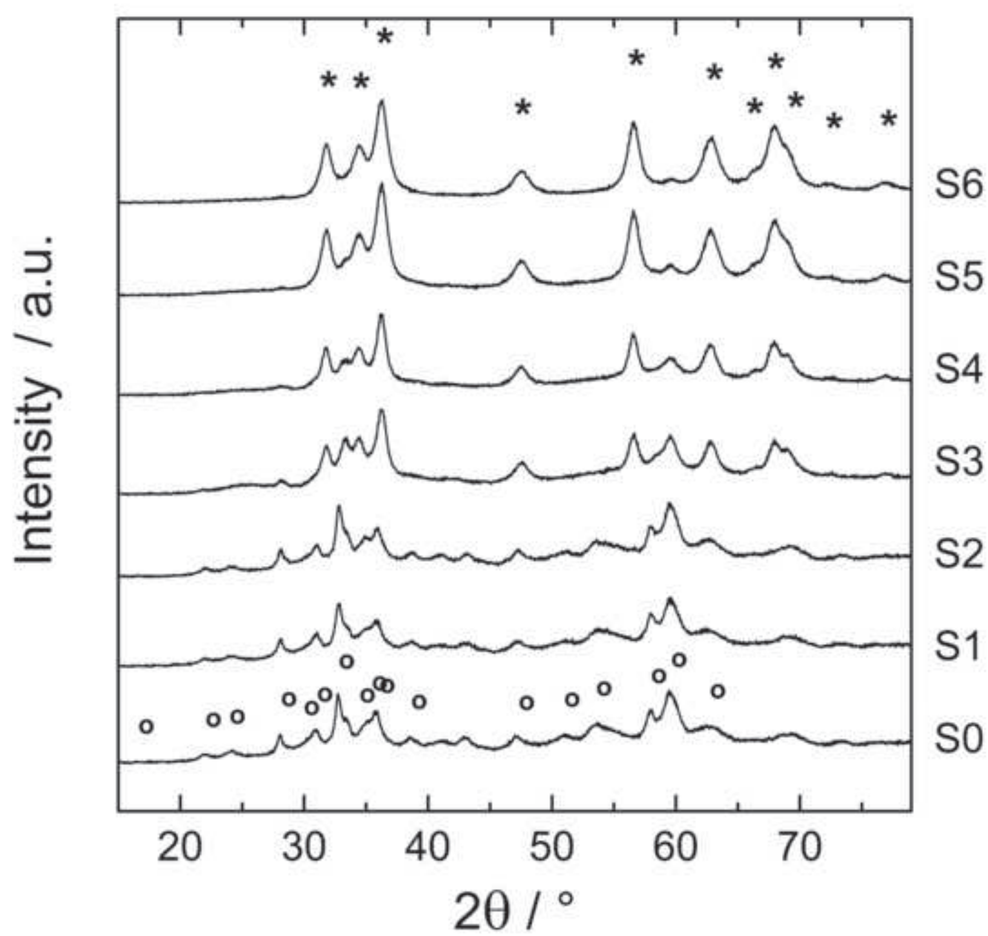

Figure 3
Click here to download high resolution image

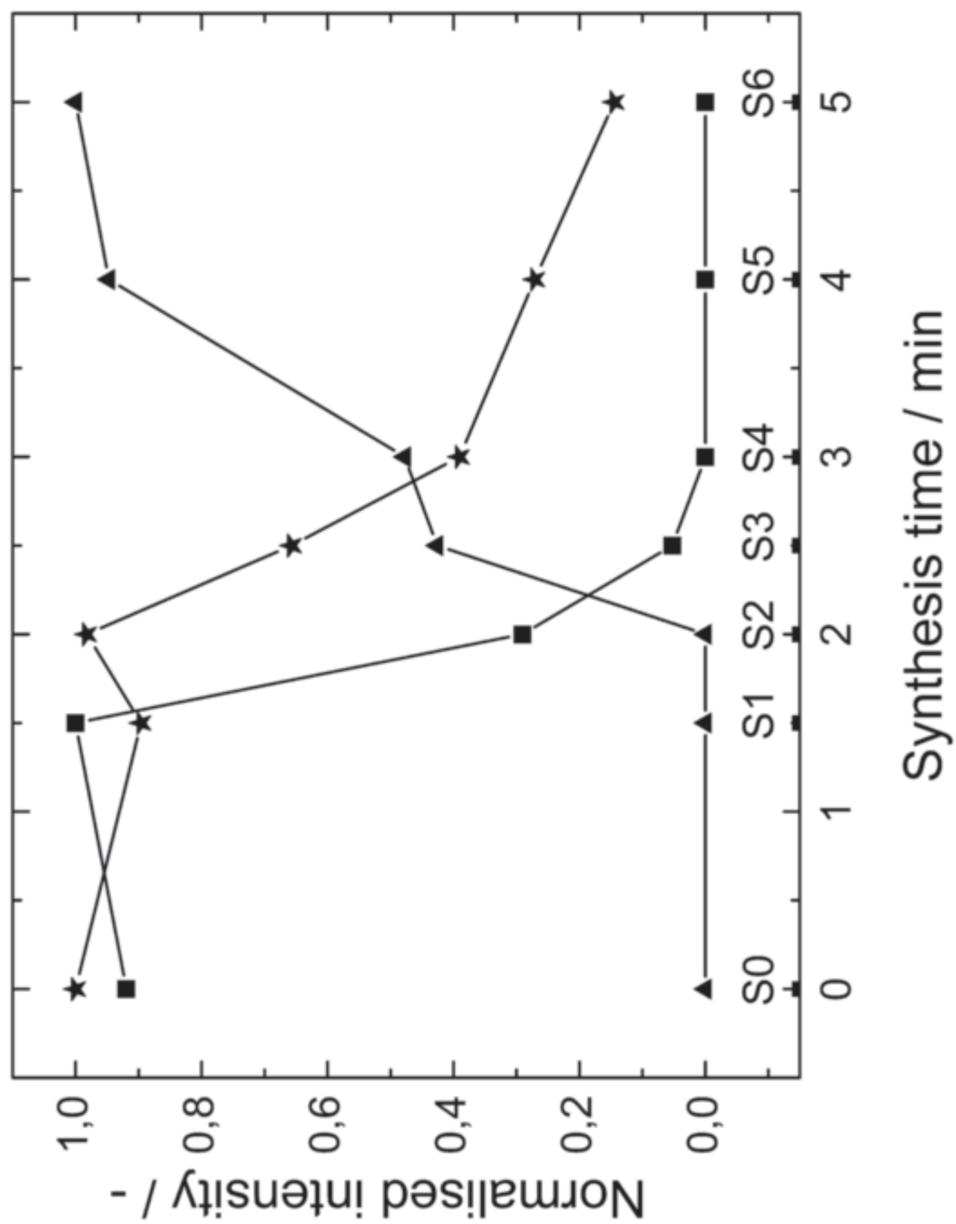

Figure 4
Click here to download high resolution image

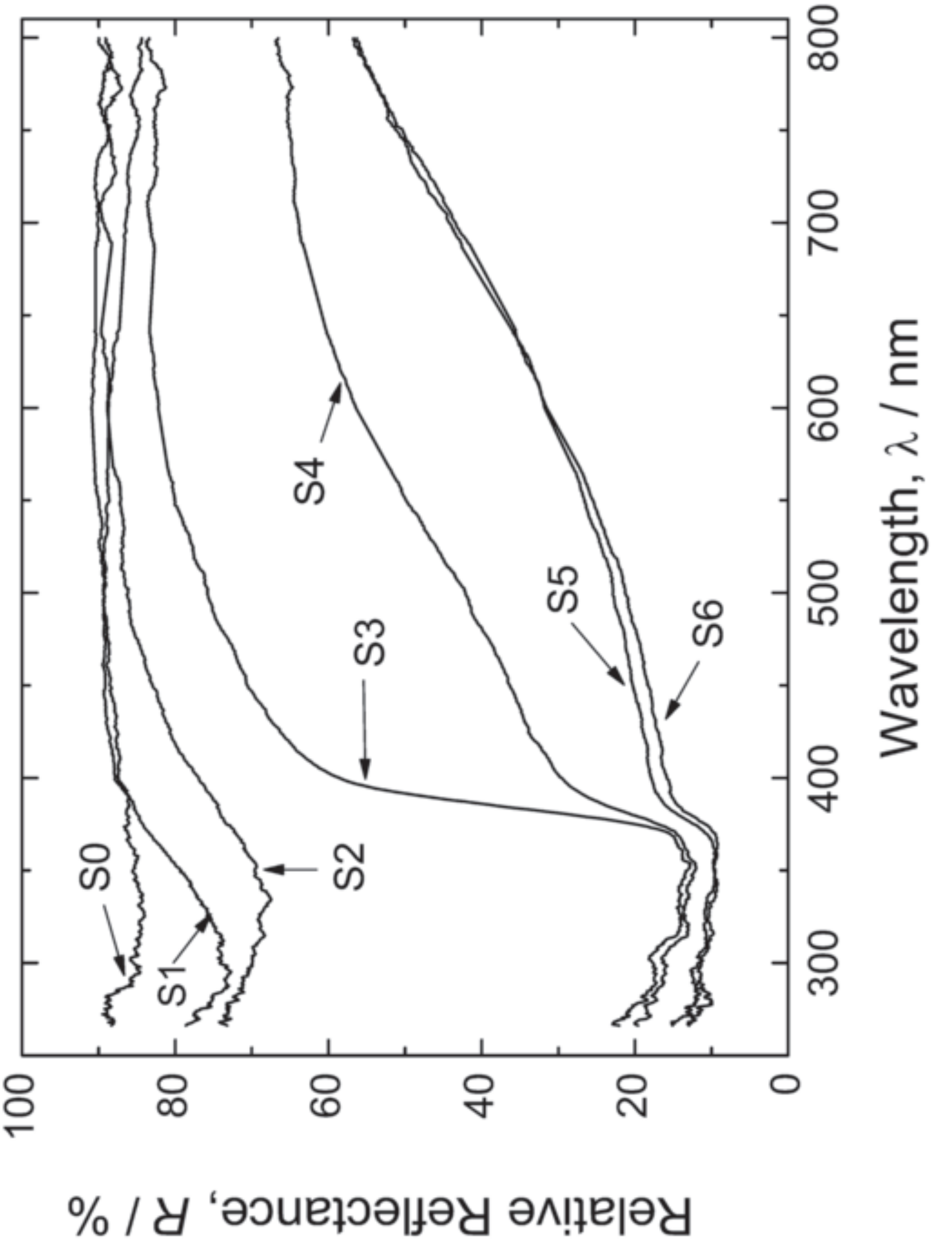

Figure 5
Click here to download high resolution image

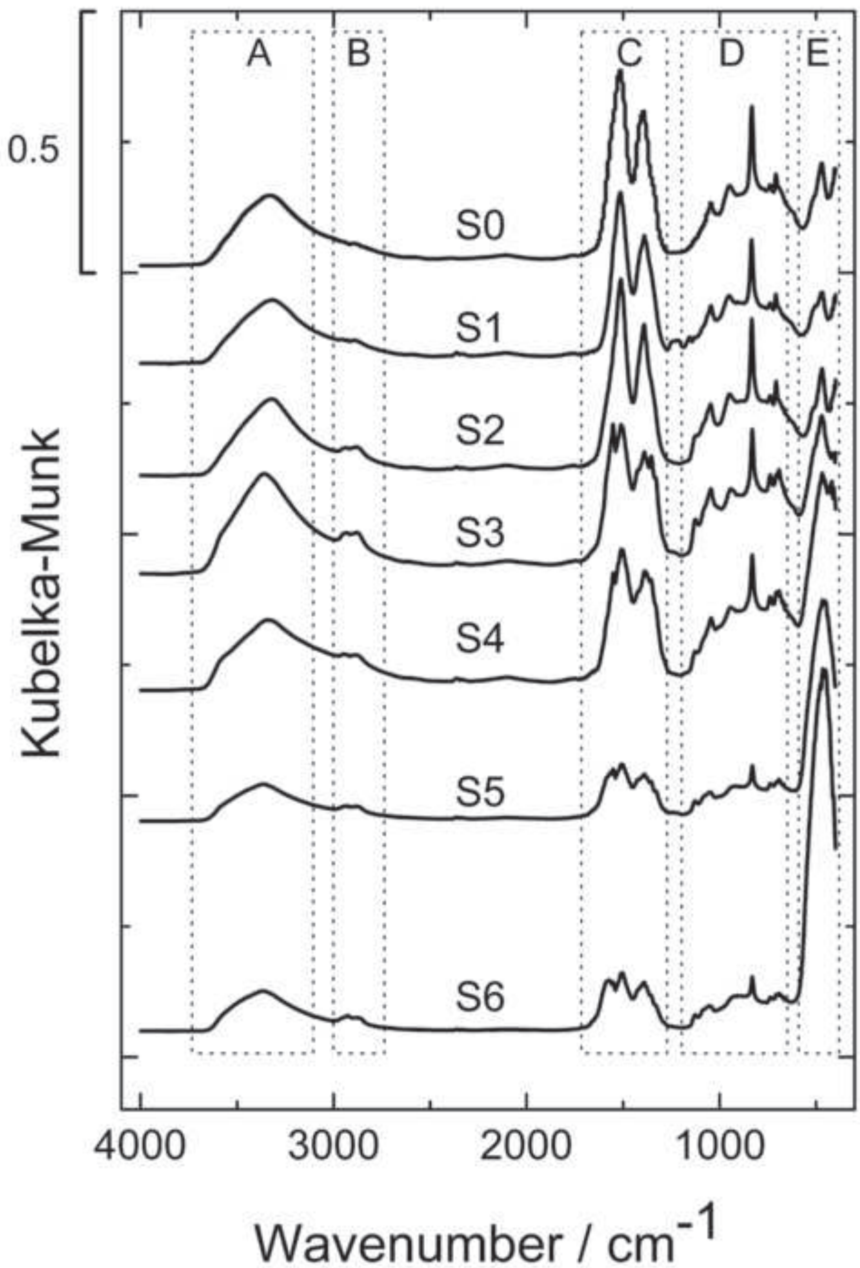

Figure 6
Click here to download high resolution image

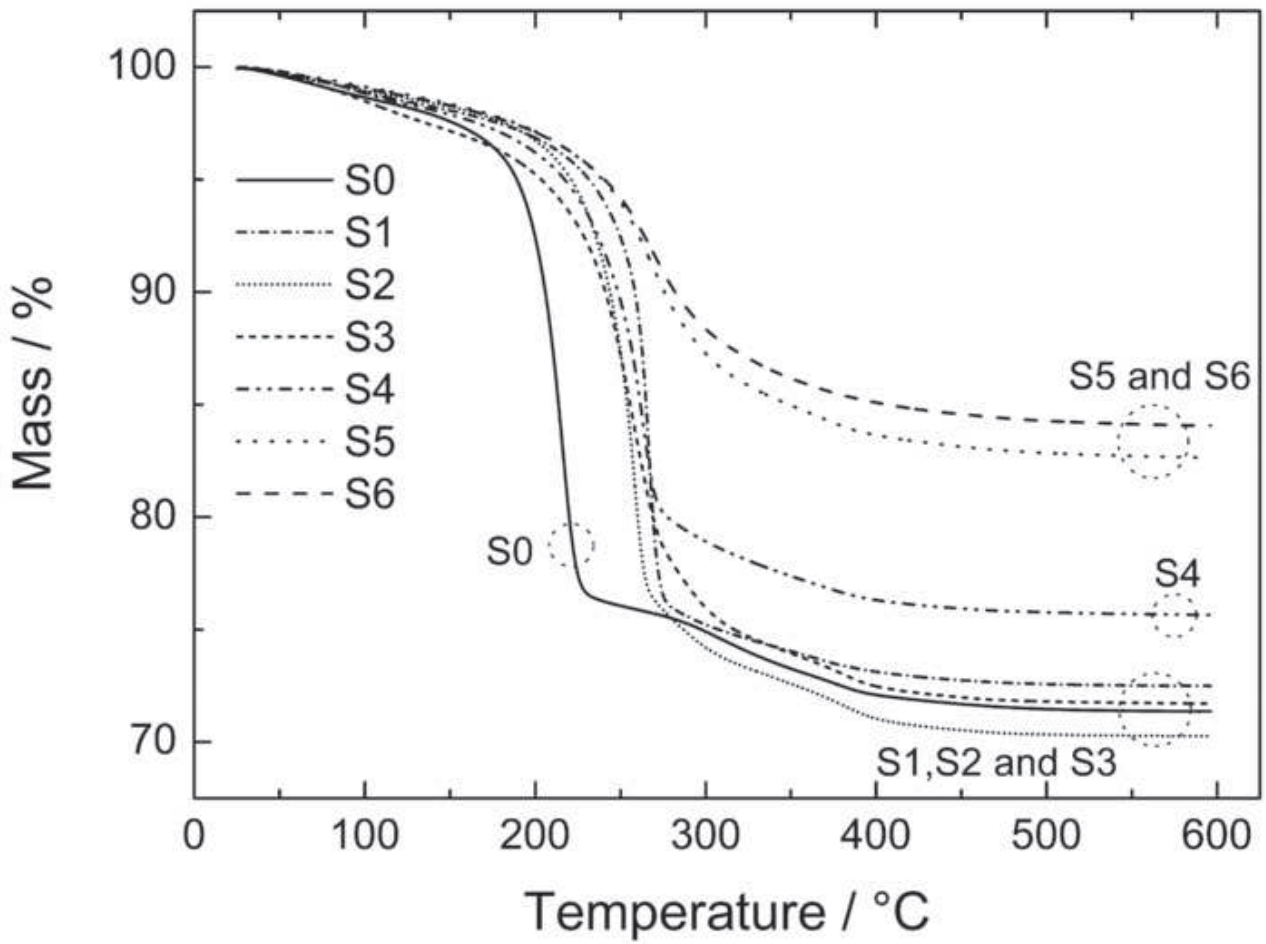

Figure 7
Click here to download high resolution image

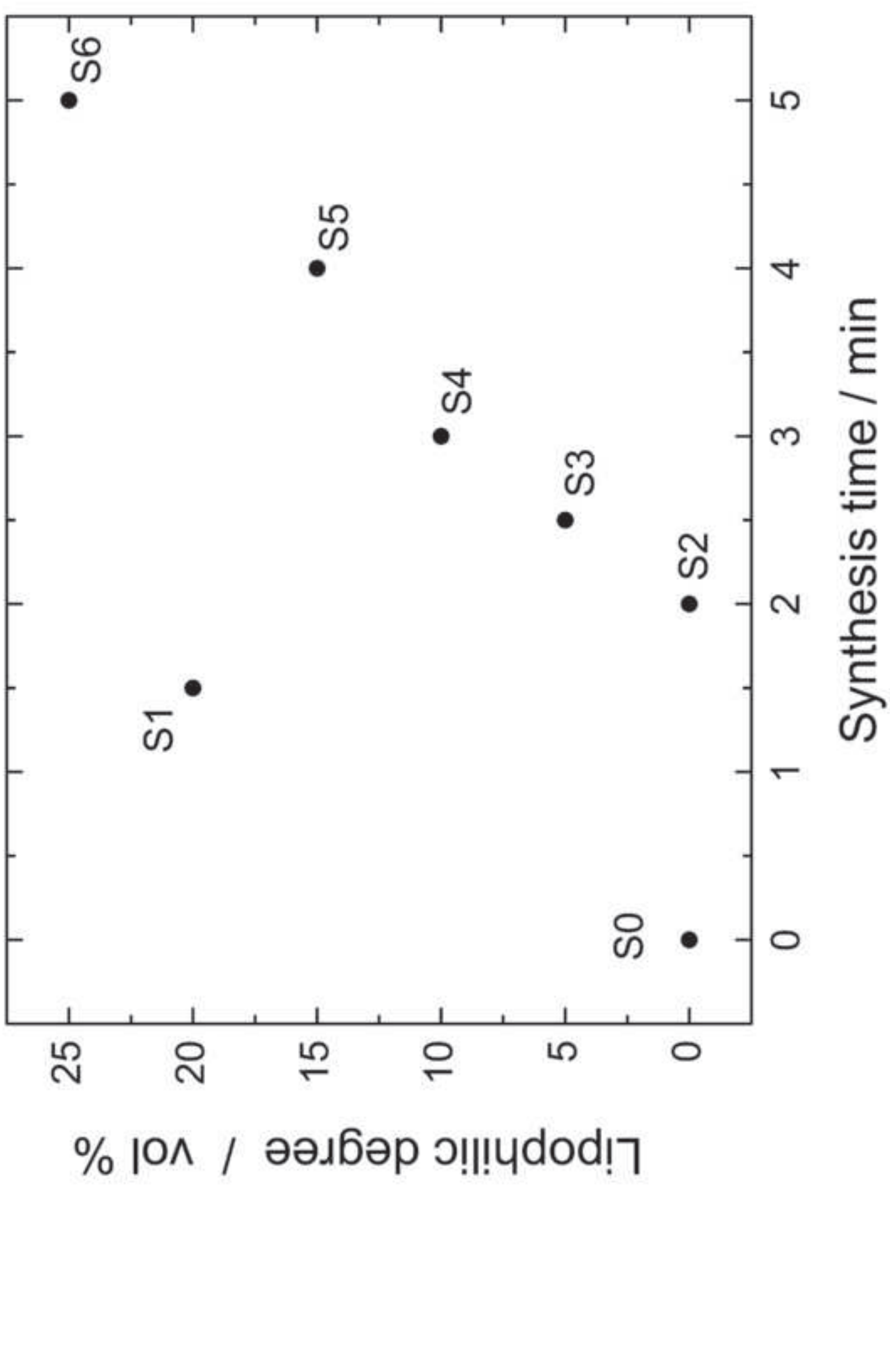

Paper IV.

SEDLAK, J. (50 %); KURITKA, I; MACHOVSKY, M.; BAZANT, P.; JANOTA, P.; DVORACKOVA, M. ZnO micro-beads with mesoporous architecture prepared by annealing at different temperatures and their photocatalytic activity. *Submitted to Materials Characterization.*

*Title Page

ZnO micro-beads with mesoporous architecture prepared by annealing at different temperatures and their photocatalytic activity

Jakub Sedlak[a], Ivo Kuritka*[,a], Michal Machovsky[a], Pavel Bazant[a], Pavel Janota[a,c], Marie Dvorackova[b,c]

[a]Centre of Polymer Systems, University Institute, Tomas Bata University in Zlin,
Nad Ovcirnou 3685, 760 01 Zlin, Czech Republic

[b]University Institute, Tomas Bata University in Zlin,
Nad Ovcirnou 3685, 760 01 Zlin, Czech Republic

[c]Department of Environmental Protection Engineering, Faculty of Technology, Tomas Bata University in Zlin,
Nam. T. G. Masaryka 275, 762 72 Zlin, Czech Republic

*Corresponding author

Name: Ivo Kuritka

Adress: Centre of Polymer Systems, University Institute, Tomas Bata University in Zlin, Nad Ovcirnou 3685, 760 01 Zlin, Czech Republic

Phone: +420 576 038 049

Fax: +420 576 031 444

E-mail: kuritka@cps.utb.cz

e-mails of co-authors:

Jakub Sedlak: j1sedlak@ft.utb.cz; Michal Machovsky: machovsky@ft.utb.cz; Pavel Bazant: bazant@uni.utb.cz; Pavel Janota: p_janota@ft.utb.cz; Marie Dvorackova: dvorackova@ft.utb.cz

Graphical Abstract (for review)

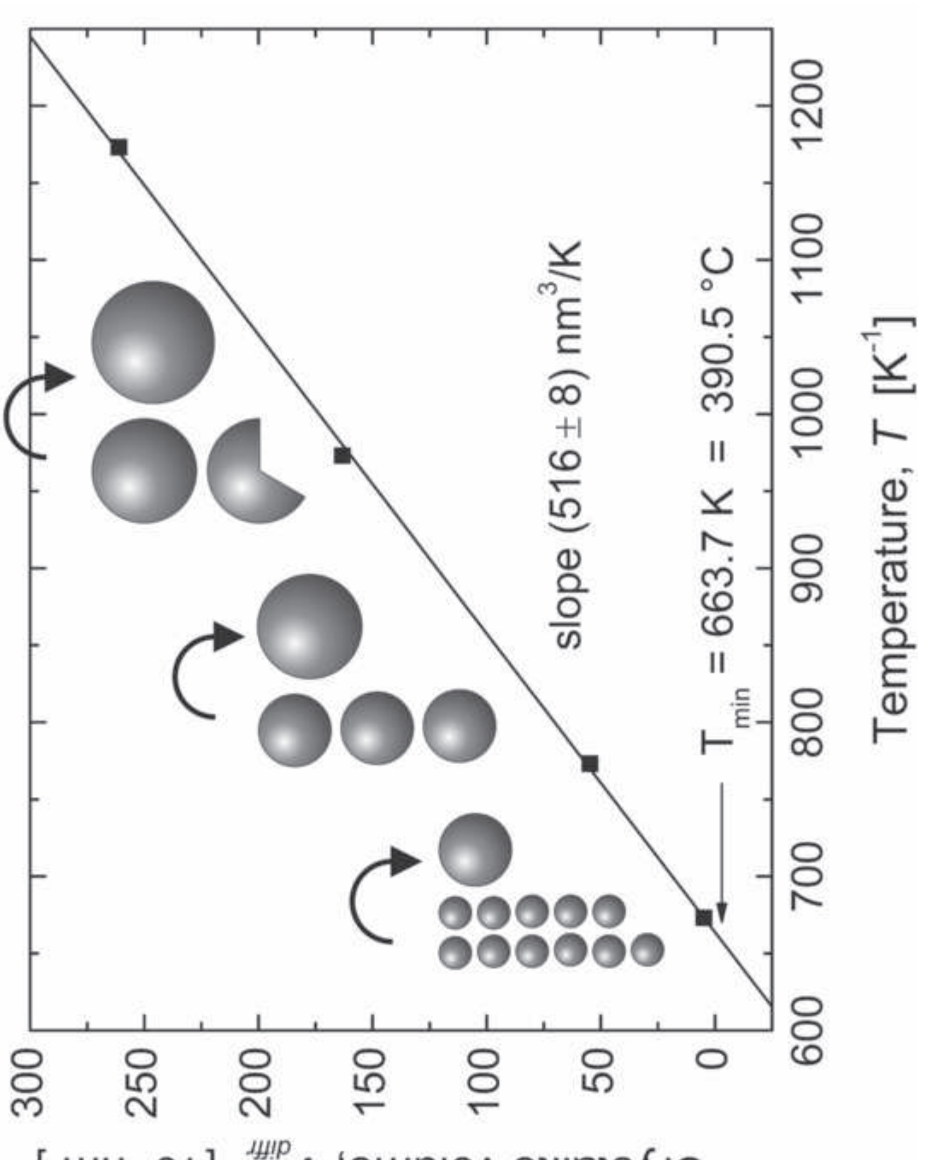

Highlights:

- Mesoporous nanostructured ZnO microbeads prepared by thermal annealing
- Estimation of self-diffusion coefficient and its activation energy
- Identification of the nanocrystallite growth mechanism
- Estimation of the activation energy of sintering
- Correlation of the morphology and structure with photocatalytic activity

ABSTRACT

Nano-crystalline mesoporous zinc oxide (ZnO) polyhedral microbeads were prepared by annealing of zinc oxalate dihydrate ($ZnC_2O_4{\cdot}2H_2O$) precursor at various temperatures. The development of the mesoporous nanoarchitecture of the ZnO microbeads was studied by powder X-ray diffraction analysis (XRD) corroborated with the analysis of their specific surface area by means of nitrogen sorption via Brunauer-Emmet-Teller (BET) method. The morphology was investigated by scanning electron microscopy (SEM). A description of the crystallite growth and sintering process is given together with analysis of the activation energy of the grain and crystallite growth. Self-diffusion coefficient, its activation energy and diffusion mechanisms involved in the growth of crystallites were identified. An agreement between our experiment and theory from literature was observed. Crystallite size and specific surface area can be simply tuned by the variation of annealing temperature. The set of dependences of morphological and structural parameters on the annealing temperature is correlated with photocatalytic activity of prepared ZnO powders which was evaluated by the UV degradation of Methyl violet 2B. The best photocatalytic performance was observed for the sample annealed at 500 °C.

KEYWORDS:

ZnO; mesoporous; self-diffusion coefficient; sintering; grain growth; photocatalysis

1. Introduction

In recent years, zinc oxide (ZnO) has drawn serious attention of scientific community as a versatile semiconductive material with direct wide band gap of about 3.4 eV and large exciton binding energy of 60 meV at room temperature. Moreover, it can be easily doped by both p and n type dopants and its band gap can be engineered to desired value by simple substitution of Zn by other divalent ions [1,2]. These characteristics make ZnO promising material in the field of electronics, solar cells, light emitting devices, gas sensors and photocatalysis [3-8].

Zinc oxide is one of the most variable inorganic material, which can be obtained by various wet and dry chemical or physical methods in different shapes and therefore the plethora of morphology dependent properties can be obtained. Up to now, thin films, quantum dots, nanorods, nanowires, nanosheets, as well and complex shape structures assembled from low-dimensional crystal components have been prepared [9-12].

Many useful properties of ZnO are related with high surface area to volume ratio. Among them, catalysis, namely photocatalysis, critically depends on the specific surface area, besides other factors. Preparation of nanoparticulate materials generally offers this important feature therefore the use of nano-ZnO is the first choice for photocatalysis [13]. However, the issues of safety and risk management open when dealing with nanos even if their microsized analogues are considered as green and non-toxic. The eventual toxicity of nano-sized ZnO and the inconvenience in removal of the catalyst from the reaction system hamper the wider use of such materials [14]. Therefore, it seems to be reasonable to prepare materials with multiscale hierarchical organization that combines the nano-scale imparted properties of nanostructured building blocks packed safely into a micro-scale sized body. This concept of nanostructured microparticulate materials was successfully introduced in medical plastics in our previous work

[15]. Classical bottom-up strategies may be used; however, they are usually quite demanding on chemicals and processing complexity. Their counterparts, i.e. top-to-bottom techniques like milling etc. are extremely simple but they give very simple forms of product suffering for non-uniformity and defects [16]. A very subtle method is combination of these two approaches taking the advantages from both. From this point of view, a simple synthesis of inorganic or organic crystalline ZnO precursor followed by its thermal decomposition seems to be a suitable method. First, a microsized crystalline powder precursor with desired particle shape is prepared from simple chemicals by conventional method and obtained without any complicated handling with nanoparticles. In the second stage, the powder material is annealed over its decomposition temperature which results ideally into a topotactic transformation of the precursor to porous nanostructured material. The pores are developed at the expenses of decomposed percursors component. Two-dimensional as well as three dimensional porous nanostructured materials have been successfully demonstrated [17,18].

With the aim to prepare nanostructured high specific surface area microsized ZnO beads for photocatalysis, the zinc oxalate dihydrate was chosen as the best possible candidate [19]. At given precursors particle shape, the annealing temperature during the thermal decomposition of precursor is the important parameter, which influences the structure and morphology of prepared zinc oxide powders. The low annealing temperature limit is given by the thermal decomposition temperature of the precursor. It can be reasonably expected that particles prepared at such temperature will have the smallest grain size and the lowest resistance against mechanical disintegration into its nano-building blocks. On the other side of the temperature scale, the maximum annealing temperature is limited by the melting point of the material. During the thermal treatment at sufficiently high temperatures, sintering takes place which can be observed by the increase of grains size as well as the decrease of specific surface area and influence the average pore size [20].

Once obtained, the photocatalytic function of prepared ZnO nanostructured beads has to be evaluated. However, the efficiency of the photocatalyst depends not only on the catalyst morphology and structure itself, but also on the reactive system setup, solvent choice, reactant concentration, as well as on impurities. The physical parameters, like reactor geometry, temperature, pressure and radiation intensity are important too. To summarize, the performance is a complex function of chemical, transport and physical processes with respect to given morphological and structural properties of the tested form of photocatalyst [21]. Therefore, within one experiment, only the photocatalyst morphology may be varied ceteris paribus.

Here we present a study, which describes the influence of annealing temperature on structural and morphological properties of nanostructured ZnO microbeads and correlation with their photocatalytic performance in a standard methyl violet UV fading test. The material was prepared by thermal decomposition of zinc oxalate dihydrate as the precursor. The precursor was previously synthesised by a fast and simple precipitation method from solutions of oxalic acid and zinc acetate in our laboratory.

2. Experimental section

2.1 Preparation of the precursor

Zinc acetate dihydrate, p.a., (Penta, Czech Republic) and oxalic acid dihydrate, p.a., (Penta, Czech Republic), were used as starting chemicals. Precursor was prepared by simple precipitation of 400 ml 0.05 M solution of solution of zinc acetate by the addition of 200 ml of

0.5 M solution of oxalic acid at room temperature under the strong agitation of magnetic stirrer for 5 minutes. Resulting precipitates were separated by suction filtration, washed several times by distilled water to remove possible by-product or rests of original soluble chemicals. Filtration cake was left to dry at 42 °C for 24 hours.

2.2 Annealing of the precursor

Obtained white precursor powder was subjected to the thermal heating in the muffle furnace (LMH 07/12, LAC, Czech Republic) up to different temperatures (400 °C; 500 °C; 700 °C and 900 °C). All these samples were annealed by constant heating rate of 10 °C/min and held at maximum temperature for one hour. Then, the oven was left to cool naturally without controlling the rate of cooling and annealed precursors were removed from the furnace at room temperature.

2.3 Testing of photocatalytic activity

The photocatalytic activity of ZnO porous powders was evaluated by measuring photocatalytic degradation of Methyl Violet 2B (MV) in distilled water under the constant illumination of 100W focused UV-lamp (Super-Light C 10 A-SH, Helling Gmbh., Germany) with the strongest emission at 365 nm. The temperature of the reaction was maintained at aprox. 25 °C by thermostatic circulation through the double-wall glass baker. In a typical experiment, 50 mg of the ZnO porous powder sample was added into the double-wall glass baker containing 50 ml of MV solution having concentration of 3.7 mg/l. Before the degradation starts, the suspension was stirred in the dark for 10 minutes to assure an adsorption/desorption equilibrium of used dye at the surface of ZnO particles. During the degradation, 12 solutions of about 1mL were withdrawn from the reaction suspension within the time range from 0 to 120 minutes and filtered through a syringe filter to completely remove the ZnO catalyst from the solution. Time dependent degradation was monitored by measurement of absorption of MV solutions at 580 nm by UV-vis spectroscopy [18].

2.4 Characterization techniques

The TA Q 500 apparatus (TA Instruments, US) was used for thermogravimetric analysis (TGA). This analysis was performed at the constant heating rate of 10 °C/min under stable air flow. The amount of each sample was approximately 15 mg.

Microscopic images of samples were taken by the use of scanning electron microscope Tescan Vega LMU (Tescan, Czech Republic) at accelerating voltage of 10 kV. The detail SEM image was taken by JEOL JSM6700 F (Jeol, Japan).

The crystalline phase structure of prepared powders was characterized by powder X-ray diffraction (XRD) using X´Pert PRO X-ray diffractometer (PANalytical, The Netherlands) with Cu Kα radiation of $\lambda = 0.1540598$ nm. The size of ZnO nanocrystallites was considered to be nearly identical with the size of diffracting area d_{diffr} which is easily accessible via Scherrer's formula using $\Delta(2\theta)$ which is full-width at half-maximum (FWHM) of XRD patterns. The particle shape and other factors were neglected to simplify the procedure and the calculation followed the well-known formula [22]:

$$\boldsymbol{d_{diffr}} = \frac{\mathbf{0.9}\,\boldsymbol{\lambda}}{\boldsymbol{\beta}\ \boldsymbol{cos}\,\boldsymbol{\theta}} \qquad (1)$$

Where the constant 0.9 is the shape factor, λ is the wavelength of the X-ray source, β is the FWMH in radians. The actual value of β was obtained by deconvolution of instrumental broadening effects using Warren correction method. The θ is the Bragg angle, i.e. the half of the 2θ position of the selected diffraction line.

The specific surface area A_{BET} was obtained via the multipoint Brunauer-Emmet-Teller analysis of nitrogen adsorption/desorption isotherms at 77 K recorded by Belsorp-mini II (BEL Japan, Inc.) apparatus. The grain size is expressed as the mean diameter d_{BET} according to [23]:

$$\boldsymbol{d_{BET}} = \frac{6}{\rho_S \cdot A_{BET}} \tag{2}$$

Where the ρ_s is a density of adsorbent material.

The study of UV-vis absorption of solutions was performed with the aid of the UV-vis spectrometer (UV-Vis Varian Cary 300, Varian Inc., United States). The absorbance was recorded for wavelengths in the range 300-800 nm.

3. Results and Discussions

The composition of prepared zinc oxalate dihydrate was analysed by thermogravimetric analysis (TGA) in air atmosphere. The thermogravimetric curve as well the mass loss rate obtained as its derivative is shown in the Figure 1. The decomposition occurs in two steps. First mass loss of about 18 % corresponds to the loss of crystal water. The second step connected with the loss of 39 % of the sample mass is attributed to oxidative decomposition of anhydrous zinc oxalate into the ZnO, carbon dioxide and water. The mass loss rate reaches its maximum at 390 °C as evident from the –dTG curve. The decomposition reactions can be summarised as follows:

$$ZnC_2O_4 \cdot 2H_2O \rightarrow ZnC_2O_4 + 2H_2O \tag{3}$$

$$ZnC_2O_4 + 1/2O_2 \rightarrow ZnO + 2CO_2 \tag{4}$$

These results are in good agreement with previous studies and composition derived from structural formula. [24,25] The second step finishes approximately at 400 °C if the heating rate is

10 °C/min. Therefore, the first temperature for the series of annealing experiment was set to 400 °C.

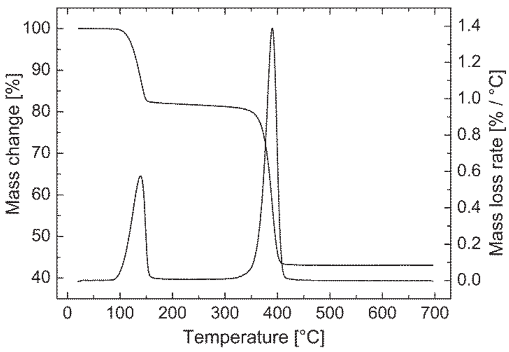

Figure 1. The TGA analysis of precursor under air atmosphere.

The precursor and samples obtained by annealing at selected temperatures were analysed by electron microscopy. The morphology of samples is exemplified in SEM images in Figure 2. The precursor was obtained in form of polyhedral crystals in size ranging mainly from 1 to 3 μm with only a small portion of less developed particles. No particles smaller than several hundreds of nanometres were observed. The product of annealing keeps evidently the size and the envelope polyhedral shape of the precursor on the micrometric scale. It is evident, that its surface is dissected into a very dense network of cracks and the whole particle became porous yet undisrupted assembly of nanoparticles by the annealing procedure. With increasing temperature, coarsening of the particle structure can be observed. The samples obtained at 400 and 500 °C have very fine structure. The image D magnifies the nanostructured material obtained at 500 °C. The size of grains is in order of several ten of nanometres. Sintering and further coalescence of grains can be followed from the images E and F for higher temperatures.

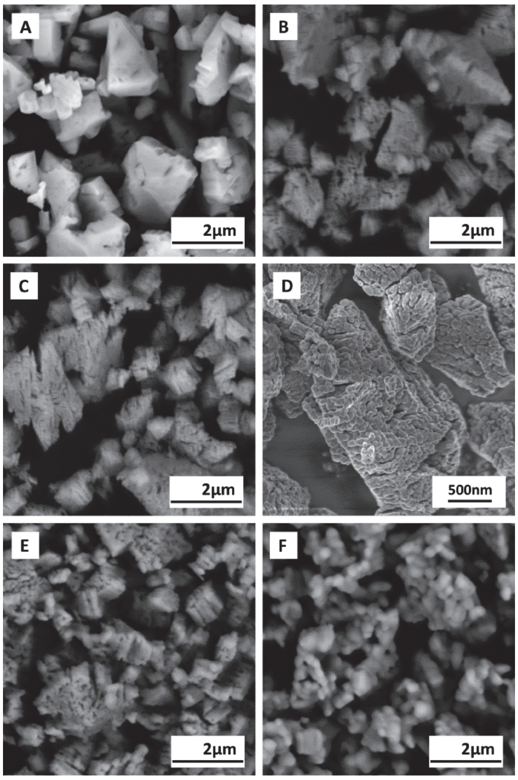

Figure 2. SEM images of precursor and products prepared by annealing of the precursor at different temperatures, A: precursor; B: 400 °C; C,D: 500 °C; E: 700 °C; F: 900 °C.

The conversion of microsized organic precursor to the final zinc oxide nanostructured beads can be followed according to the results of XRD analysis in Figure 3. Compared with the ICDD PDF-2 entry 25-1029, diffraction peaks of the precursor fit well with those of monoclinic $ZnC_2O_4{\cdot}2H_2O$ (Zinc oxalate dihydrate) and diffraction peaks of all annealed products fit well with those of hexagonal ZnO wurtzite structure given in the ICDD PDF-2 entry 01-074-0534. The shape of the diffractogram background testifies for well-developed crystalline phase and no or negligible presence of amorphous phase.

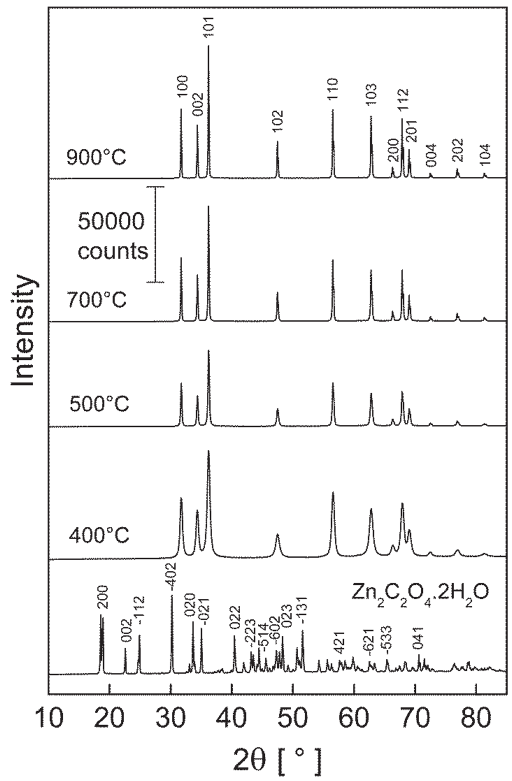

Figure 3. Diffractograms with indexed diffraction lines of the precursor and ZnO samples obtained by annealing at temperatures indicated in the graph.

Table 1. Summary of XRD and BET analyses of annealed samples. The last row contains rate constant obtained for the photocatalysis reaction.

	Annealing temperature	400 °C	500 °C	700 °C	900 °C
XRD met.	Crystallite size, d_{diffr} [nm]	21.0	47.1	67.8	79.3
	Crystallite surface area, A_{diffr} [m^2g^{-1}]	51.0	22.7	15.8	13.5
BET method	BET surface area, A_{BET} [m^2g^{-1}]	29.9	10.2	3.4	1.7
	BET total pore volume, $V_{p\ BET}$ [$10^{-2}cm^3g^{-1}$]	3.55	1.12	0.36	0.17
	BET mean pore diameter, $d_{p\ BET}$ [nm]	4.7	4.4	4.2	4.0
	Grain size, d_{BET} [nm]	35.8	105.0	315.1	630.3
UV cat.	Rate constant, k [s^{-1}]	0.0438 ± 0.0018	0.066 ± 0.002	0.0412 ± 0.0015	0.0391 ± 0.0019

The diffraction line from (101) planes in ZnO that can be found in diffractograms at 2θ angle 36.2° was used for diffracting area size calculation. The results are listed in Table 1 alongside with the results of other analyses. It is evident, that the diameter of nanocrystallites (d_{diffr}) grows with increasing temperature of annealing. The specific Crystallite surface area (A_{diffr}) can be easily calculated from the size of crystallites and the material density of ZnO (5.6 g/cm^3). Volume of crystallites (V_{diffr}) can be calculated with the same easiness and obtained values are shown in Figure 4. The dependence of V_{diffr} on temperature is perfectly linear. This result is not that surprising as it looks if a simple fact taken into account that the growth of one crystallite proceeds at the expense of other crystallites and the total volume change is zero. The ball diagram insert into the graph shows, how many crystallites of each size are needed to create one nearest bigger crystallite. The intercept of the linear dependence with the abscissa is the minimum possible temperature at which the crystallite size would be theoretically zero. This initial minimum temperature is 663.7 K (390.5 °C) which is identical with the temperature of the maximum decomposition rate of the precursor.

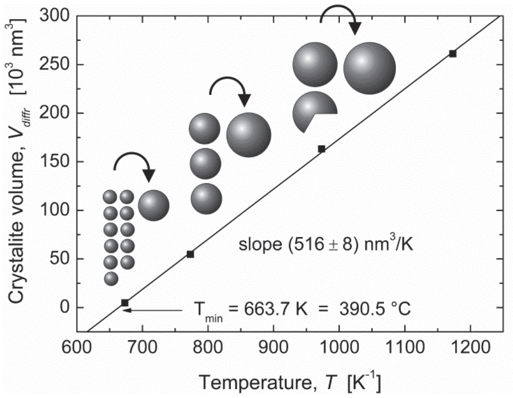

Figure 4. Calculated crystallite volume of ZnO samples annealed at different temperature.

The results obtained from X-ray diffraction line broadening analysis can be compared with the results obtained from gas sorption BET analysis. The first and usually the most sought after information from BET is the Specific surface area (A_{BET}). Obtained values are relatively high and in agreement with other literature values available for similar systems. The values ranging from 30 m^2/g for nanodisperse system up to only several m^2/g for submicrometric systems (consult the commercial ZnO materials for rubber vulcanisation) can be considered as typically achievable for ZnO nanostructured systems [26,27]. On the first sight, the A_{BET} is smaller than the specific crystallite surface area. The X-ray diffraction characteristics are correctly obtained for coherently diffracting areas, i.e. to the size of nanocrystallites (nanocrytalline domains) while gas sorption analysis examines the actual surface of the porous body accessible to N_2 molecules, which means, that it characterises the surface of grains. Thus, the A_{BET} is related to the surface of grains which consist from one or more crystallites and from amorphous phase if the amorphous phase is present at all. The ratio between these two specific areas is called packing factor ($1/F$) which gives information about particle agglomeration and availability of the nanocrystallite surface to adsorption of molecules [28]. Figure 5 shows the dependence of $1/F$ on the annealing temperature for prepared materials. The packing factor decreases with increasing temperature significantly.

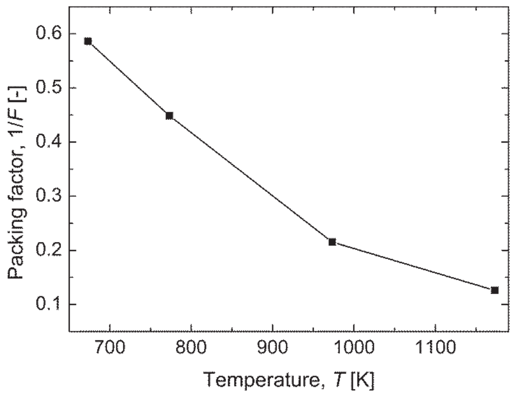

Figure 5. Plot of the Packing factor ($1/F$) versus thermodynamic temperature for annealed ZnO samples.

The total pore volume estimated by BET analysis V_{pBET} decreases with the annealing temperature approximately with the same slope as the A_{BET} while the BET mean pore (diameter) d_{pBET} decreases very slowly from 4.7 to 4.0 nm which classifies these materials as mesoporous. Assuming that the grains have spherical shape and uniform size, the average particle size can be estimated according to equation 2 as the Grain size (d_{BET}). Obtained values confirm reasonable coarsening of particles due to sintering with increasing annealing temperature and are evidently in agreement with SEM observations even without image analysis. Under the same assumptions concerning mean values obtained from XRD and BET, the ratio between grain and crystallite volumes can be calculated which characterises how many crystallites are agglomerated into one grain. The value increases from cca 5 for 400 °C up to cca 500 for 900 °C. The observed linear logarithmic dependence on thermodynamic temperature can be extrapolated to the initial temperature and compared with the crystallite volume dependence. It seems that the first crystallites appear already in a grain assembly with the mean number of crystallites about 4.5 per grain. On the other hand, the hypothetical 1:1 ratio is expectable at 232 °C which is deep below the decomposition temperature of the precursor and evidently cannot be correct and thus support the hypothesis of initial agglomeration.

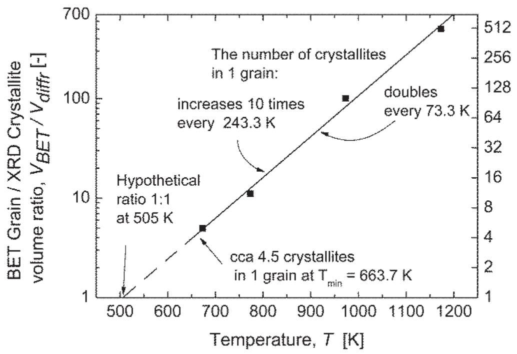

Figure 6. A semi-log plot of BET Grain / XRD Crystallite volume ratio versus thermodynamic temperature for annealed ZnO samples.

The annealing of precursor results evidently in sintering of the ZnO particles. As shown in Figure 6, the number of crystallites sintered into one grain doubles every 73.3 K with the increase of temperature. This process can be characterised by activation energy. Although various approaches can be used, the simplicity favours the basic models. A linear relationship between the rate of grain growth and the inverse grain size is assumed, which in turn is proportional to the radius of curvature of the grain [29,30]

$$\frac{\mathrm{d}X}{\mathrm{d}t} = \frac{k}{X} \tag{5}$$

where X is the length scale, i.e. the diameter of the grain, t is time and k is the rate constant depending on temperature (T). This equation can be integrated with X_0 being the integration constant as the grain size at $t = 0$.

$$X^2 - X_0^2 = k \cdot t \tag{6}$$

Although this equation describes ideal state and many corrections and improved models have been introduced, it still works well in many cases and as a very good first choice.

The constant k depends exponentially on temperature.

$$k(T) \propto e^{\frac{-E_a}{RT}} \tag{7}$$

Where R is the gas constant (8.314 J mol^{-1} K^{-1}) and the activation energy (E_a) for the sintering process can be estimated easily from the Arrhenius plot for values obtained at the same annealing time. The heating rate 10 °C/min in our case is considered as high enough with respect to the isothermal annealing holding time of 1 hour. The integration constant is often relatively small and does not influence the result much in case of steep dependences. Actually it is a grain diameter at the time zero. Nevertheless, the zero time estimation is an "old pain" in thermal analysis – see our initial assumptions concerning the heating rate in comparison with the holding time. Hence it may be neglected for practical reasons and the equation (6) transforms for d_{BET} into:

$$\ln d_{BET}^2 = -\frac{E_{as}}{R} \cdot \frac{1}{T} + const \tag{8}$$

Under the real experimental conditions, it is difficult to estimate properly the X_0 constant. Another approach how to handle this issue is to use the value of grain diameter obtained for the lowest annealing temperature as the initial guess.

$$\ln(d_{BET}^2 - d_{BET\,0}^2) = \ln\left(d_{BET}^2 - d_{BET}^2(400\ °C)\right) = -\frac{E_{as}}{R} \cdot \frac{1}{T} + const \qquad (9)$$

It can be expected that the correct value lies in the interval between these two values. The data for both approaches are plotted in graphs in Figure 7 and 8. Indeed, the activation energy for corrected data is slightly lower and the actual value can be found between 74 and 70 kJ/mol.

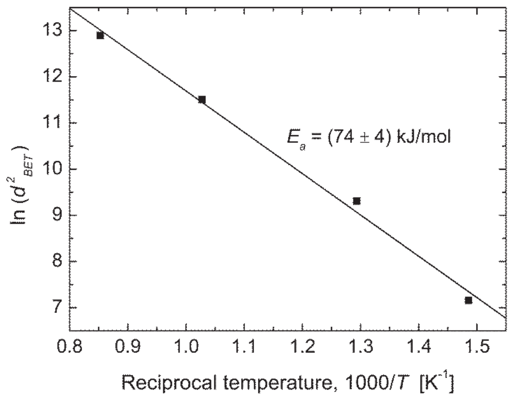

Figure 7. Activation energy of sintering of annealed ZnO obtained from linear plot of data according to the equation (8).

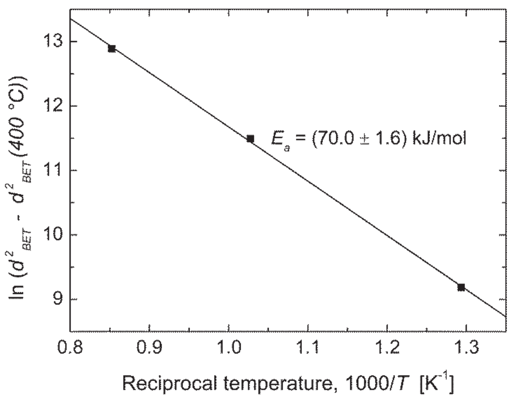

Figure 8. Activation energy of sintering of annealed ZnO obtained from linear plot of data according to the equation (9).

Similar approach can be adopted for data obtained from XRD analysis, however, a linear dependence of $(d_{diffr})^2$ on reciprocal value of thermodynamic temperature was found.

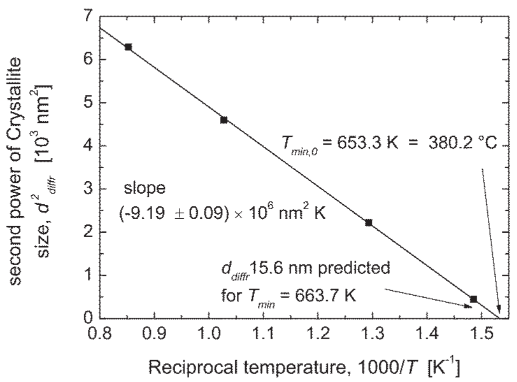

Figure 9. Rate constant estimation for crystallite growth according to equation (15)

Such dependence points towards the crystallite growth rate (u) derived as a product of Gibbs energy change (ΔG) and crystallite boundary mobility (M).

$$u = \Delta G \cdot M \tag{10}$$

In accordance with our notation, the change of Gibbs energy is proportional to the specific surface energy (γ) and molar volume (V_{mol}). The term in brackets represent change in size of the crystallites between integration limits [31].

$$\Delta G = -4\gamma V_{mol}\left(\frac{1}{d_{diffr\,1}} - \frac{1}{d_{diffr\,2}}\right) \tag{11}$$

The crystallite boundary mobility *(M)* is dependent on the self-diffusion coefficient D_s:

$$M = \frac{D_S}{k_B\, T\, \lambda} \tag{12}$$

Where k_B is the Boltzman constant, T is thermodynamic temperature and λ is the thickness of the boundary, usually in order of the size of atoms. In general form i.e. without λ, the equation (12) is known as the Einstein relation.

Thus, we can obtain the rate constant k' from the equations (10, 11 ,12) and substitute k_B by R due to the use V_{mol}:

$$k' = -\frac{4\,\gamma\,D_s\,V_{mol}}{R\,T\,\lambda} \tag{13}$$

And adopt the equation (6):

$$d_{diffr}^2 - d_{diffr\,0}^2 = -k' \cdot t \tag{14}$$

However, we obtained V_{diffr} = 0 nm^3 => d_{difr} = 0 nm for the lower integration limit (see Figure 4, the minimum temperature 390.3 °C), thus the equation may be formulated as:

$$d_{diffr}^2 = -k' \cdot t \tag{15}$$

It must be noted, that this approach considers the surface energy as a constant together with the assumption of temperature independence of the molar volume. Therefore, the slope of the linear plot in Figure 9 according to the equation (15) contains contributions from at least two other yet minor terms and did not meet perfectly the minimum temperature. The value 380.2 °C is predicted instead of 390.3 °C as for the V_{diffr} dependence on T. With respect to the whole experimental setup, we consider this difference as acceptably small keeping in mind the perfect linearity of the data. Moreover, the slope can be refined more, as the time integral can be roughly estimated as the annealing temperature holding time of 1 hour (t_{hold} = 3600 s), the specific surface energy can be estimated about 2 J/m^2 [32], molar volume can be estimated from the molar mass and density, λ can be estimated as 0.35 according to the unit cell parameters from the ICCD card, hence the self-diffusivity may be estimated:

$$D_s = \frac{-k' R\, \lambda}{4\, \gamma\, V_{mol}} \cdot \frac{1}{t_{hold}} = 6.4\ \times\ 10^{-16} cm^2 s^{-1} \tag{16}$$

The value of 6.4×10^{-16} cm^2s^{-1} can be considered as the mean D_s estimation for temperature range 670-1150 K and is in excellent agreement with the values from the comprehensive reference of Erhart and Albe [33].

Since the diffusivity (D_s) depends exponentially on temperature, it obeys Arrhenius law with the activation energy Q contributing thus to the deviation of the strict linearity and simplicity of the equation (13):

$$D_s(T) \propto e^{\frac{-Q}{RT}} \tag{17}$$

Hence, the first $1/T$ dependence may be removed by multiplying with T together with the problem of the initial crystallite size similarly as in the grain case:

$$\left(d_{diffr}^2 -\ d_{diffr\,0}^2\right) T = -Tk't \tag{18}$$

Obtaining:

$$|Tk'| \propto e^{\frac{-Q}{RT}} \tag{19}$$

Hence, Arrhenius plot for the additional $1/T$ dependence may be drawn:

$$\ln\left(\left(d_{diffr}^2 - d_{diffr}^2(400\ °C)\right)\ T\right) = \ -\frac{Q}{R} \cdot \frac{1}{T} + const \tag{20}$$

And the activation energy Q for the D_s in equation (16) of the crystallite growth in Figure 10 was obtained as 31 kJ/mol which is equivalent to 0.32 eV. This value is much smaller than values of migration barriers reported for oxygen or zinc vacancy diffusion mechanisms thus the zinc interstitials are considered to be responsible for the observed crystallite growth [34]. Our estimated value is somewhat smaller than 0.55 eV that was found by Thomas [35]. However, according to more elaborated analysis and theoretical calculation of Erhart and Albe [33], there are several different mechanisms of Zn interstitials diffusion possible and among them this energetic barrier of 0.32 eV can be associated with the *interstitial in plane* mechanism and with the *interstitialcy out of plane* mechanism of Zn diffusion in the ZnO lattice.

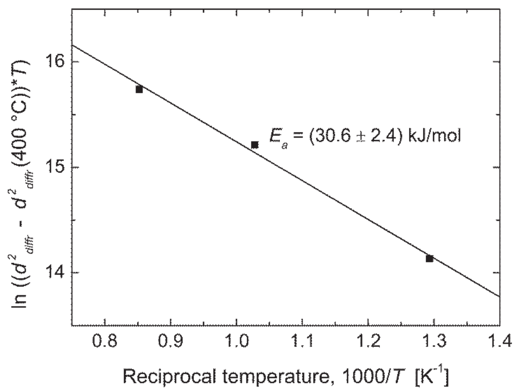

Figure 10. Activation energy of the self-diffusion coefficient of ZnO nanocrystallite growth obtained from linear plot of data according to the equation (20).

The photodegradation of methyl violet 2B (MV) in the presence of ZnO photocatalyst was monitored by UV-vis spectroscopy. [18, 21] Figure 11 exemplifies obtained UV-vis spectra for the system containing ZnO annealed at 500 °C. Here, the dye degradation is manifested by the decrease of the absorption maxima at 580 nm. Figure 12 shows the photodegradation curves of the dye for all ZnO samples prepared at various annealing temperatures. The ratio between actual and initial concentration is plotted against time of UV irradiation. As can be seen, complete degradation of the dye is accomplished within the 120 minutes and all curves obey first (or pseudofirst) order reaction kinetics. [25] The rate constant was obtained from fitting the first order model into the data. The highest degradation rate constant (consult Table 1) was found for sample annealed at 500 °C. Hence, the photocatalytic performance of our prepared materials has an optimum which can be correlated with the trends of morphological and structural parameters.

The correlation with analysis of chemical states of ZnO on its surface is beyond the scope of our article.

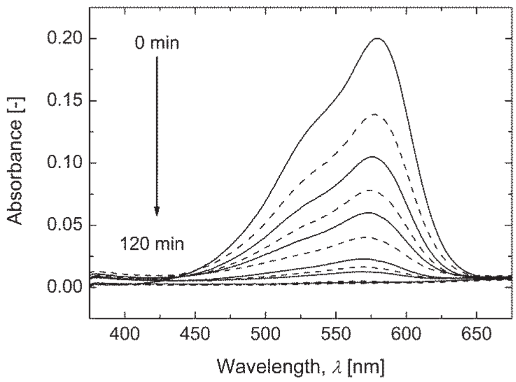

Figure 11. UV-vis spectra of of methyl violet in the presence of ZnO annealed at 500 °C.

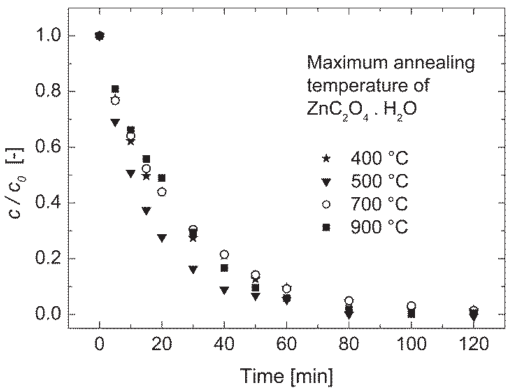

Figure 12. Photocatalytic degradation curves of methyl violet as a function of time for ZnO powders annealed at different temperatures, as illustrated in the graph.

The photocatalysis is a complex process with at least several parameters influencing the final performance of the system. In our case, mesoporous nanostructured beads floated due to mechanical agitation in the solution of substrate dye (MV) molecules. The system was irradiated from the top. The only variable in the experiment was the annealing temperature used for the preparation of the photocatalyst. All other conditions were kept constant.

It is generally known, that the catalytic activity of a heterogenous catalyst depends on its specific surface area. However, the catalytic activity may not be simply correlated with the size of surface area of the catalysts in our case at least from three reasons: (i) only that portion of surface is active which is attainable to the MV molecules by the mechanism of diffusion into the beads followed by the diffusion of degradation products out of the beads, (ii) only that portion of surface can contribute to the dye degradation which is so closer to the bead surface than the diffusion length of active species born on that surface like superoxide, hydroxyl radicals etc., if this is the mechanism and (iii) the availability of the ZnO material to be irradiated by the UV which has most likely only a limited penetration depth into the beads. According to our observations, the specific surface area of grains as well that of crystallites and other parameters depend monotonously on the annealing temperature which does not directly correspond to the observed dependence of the rate constant on the sample annealing temperature. However, in accordance with the considerations (i-iii) above, some of the observed parameters contribute positively and some of them negatively to the efficiency of the photocatalysis. All parameters are derived from the structure and morphology thus they are mutually strongly linked and therefore, they are even effective ambiguously with respect to the catalyst performance.

The specific surface area is expected to contribute positively; nevertheless, most likely the substantial part of the surface area is not accessible for the dye molecules. It must be noted, that the mean pore diameter is only cca three or four times bigger than is the size of a MV molecule and thus the total pore volume represents an impeding factor. In next, the dye molecule exists in the solution as the MV^+ ion and the pores can have surface charge strongly influenced by pH and ionic strength of the liquid medium. The porosity of the material (ϕ) can be estimated as quite small, however, the bigger it is the less it impedes diffusion in whichever direction. The length of pores is extremely increasing with the increase of the specific surface area while the pore diameter almost does not vary with the specific area. See Figure 13, the porosity was calculated from the total pore volume $V_{p\ BET}$ and the volume of 1 g of the material obtained from the material density. The BET mean pore size $d_{p\ BET}$ entered the calculation of the BET total length of pores $L_{p\ BET}$. These two parameters are shown together as a general pore flow geometric factor $(d_{p\ BET})^2 / L_{p\ BET}$. The bigger the value of this factor is, the less the flow through pores is impeded.

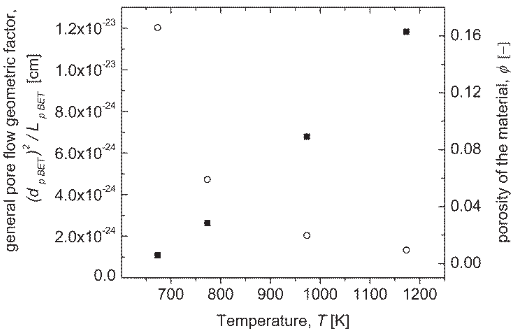

Figure 13. Dependence of general pore flow geometric factor (full squares) and porosity of the ZnO samples (hollow circles) on annealing temperature of the material.

There are neither sufficient morphological data in our results to evaluate tortuosity and constrictivity nor even reliable models in the literature for such low porosity regions of mesoporous systems available, however both criteria would work against the overall catalyst's performance. The packing factor ($1/F$) limits the efficiency of the electron/hole pair photogeneration process, as only those excitons that have not been captured on internal nanocrystallite boundaries during their travelling can be involved in the reaction. To summarize, observed morphological and structural parameters act both as promoting and impeding the photocatalytic activity of the prepared materials and the optimum was found for the material annealed at 500 °C.

Conclusion

A relatively small series of ZnO micro-beads with mesoporous architecture was prepared by annealing from zinc oxalate dihydrate precursor at four different temperatures on the air atmosphere. X-Ray diffraction data and BET analysis provided a set of structural and morphological parameters that were confirmed by SEM. Exemplary dependences of the specific surface area, grain and crystallite volume, their ratio, second power of their diameter and many other were obtained. The interpretation allowed to find initial (minimum) temperature about 390 °C at which the nano-crystallite volume is theoretically zero and the process starts. TGA showed that the maximum precursor decomposition rate is at the same temperature. Similarly, it was estimated that at the beginning of annealing at this temperature, grains start grow each from 4.5 crystallites in average. The data were further analysed with the help of the basic grain growth model. Agreement between theory and experiment was observed. Activation energy was estimated for the sintering process as well as for the ZnO nano-crystallite growth. The crystallite growth was found to be linearly dependent on the reciprocal value of the thermodynamic temperature which means that the growth was limited by the crystallite boundary mobility. The rate constant was analysed and the value of ZnO self-diffusion coefficient $D_s = 6.4 \times 10^{-16}$ cm^2s^{-1} was estimated which is in agreement with the literature reported values. According to the refined analysis of the data, the activation energy of the self-diffusion coefficient $Q = 0.32$ eV was found which allowed to identify the mechanism of crystallite growth in corroboration with the literature as *interstitial in plane* mechanism and the *interstitialcy out of plane* mechanism of Zn diffusion in the ZnO lattice.

The observed trends in morphological and structural parameters were compared with the score of the prepared ZnO mesoporous microbeads in a standard test of photocatalytic performance. It was found that they act both as promoting and impeding the photocatalytic activity and the optimum activity was found for the material annealed at 500 °C.

Acknowledgements

This article was written with support of Operational Program Research and Development for Innovations co-funded by the European Regional Development Fund (ERDF) and national budget of Czech Republic, within the project Centre of Polymer Systems (reg. number: CZ.1.05/2.1.00/03.0111).

The authors also acknowledge the support of Operational Program Education for Competitiveness co-funded by the European Social Fund (ESF) and national budget of Czech Republic, within the framework of project Advanced Theoretical and Experimental Studies of Polymer Systems (reg. number: CZ.1.07/2.3.00/20.0104).

The work of J. S. was supported by the Internal Grant Agency of Tomas Bata University in Zlin; contract grant number: IGA/FT/2014/008.

Dr. F. Mika from Institute of Scientific Instruments of the Academy of Sciences of the Czech Republic, p.r.i. (public research institution) is acknowledged for help with acquisition of the micrograph D in Figure 2.

References

(1) Morkoç, H.; Özgür, Ü., *Zinc oxide : fundamentals, materials and device technology*. ed.; Wiley-VCH: Weinheim, 2009; p xi, 477 p.

(2) (24) Vidyasagar, C. C.; Naik, Y. A.; Venkatesh, T. G.; Viswanatha, R., Solid-state synthesis and effect of temperature on optical properties of Cu-ZnO, Cu-CdO and CuO nanoparticles. *Powder Technology* **2011**, 214, (3), 337-343.

(3) Melendrez, M. F.; Hanks, K.; Leonard-Deepak, F.; Solis-Pomar, F.; Martinez-Guerra, E.; Perez-Tijerina, E.; Jose-Yacaman, M., Growth of aligned ZnO nanorods on transparent electrodes by hybrid methods. *Journal of Materials Science* **2012**, 47, (4), 2025-2032.

(4) Zhang, Q. F.; Dandeneau, C. S.; Zhou, X. Y.; Cao, G. Z., ZnO Nanostructures for Dye-Sensitized Solar Cells. *Advanced Materials* **2009**, 21, (41), 4087-4108.

(5) Shinagawa, T.; Watase, S.; Izaki, M., Size-Controllable Growth of Vertical ZnO Nanorod Arrays by a Pd-Catalyzed Chemical Solution Process. *Crystal Growth & Design* **2011**, 11, (12), 5533-5539.

(6) Zhang, J.; Wang, S.; Xu, M.; Wang, Y.; Zhu, B.; Zhang, S.; Huang, W.; Wu, S., Hierarchically Porous ZnO Architectures for Gas Sensor Application. *Crystal Growth & Design* **2009**, 9, (8), 3532-3537.

(7) Hong, R. Y.; Li, J. H.; Chen, L. L.; Liu, D. Q.; Li, H. Z.; Zheng, Y.; Ding, J., Synthesis, surface modification and photocatalytic property of ZnO nanoparticles. *Powder Technology* **2009**, 189, (3), 426-432.

(8) Akin, M. B.; Oner, M., Photodegradation of methylene blue with sphere-like ZnO particles prepared via aqueous solution. *Ceramics International* **2013**, 39, (8), 9759-9762.

(9) Rajappan-Achary, S.; Agouram, S.; Reig, C.; Sanchez-Royo, J. F.; Carmen Martinez-Tomas, M.; Munoz-Sanjose, V., Self-Assembled Zinc Oxide Quantum Dots Using Spray Pyrolysis Methodology. *Crystal Growth & Design* **2011**, 11, (9), 3790-3801.

(10) Guillemin, S.; Rapenne, L.; Roussel, H.; Sarigiannidou, E.; Bremond, G.; Consonni, V., Formation Mechanisms of ZnO Nanowires: The Crucial Role of Crystal Orientation and Polarity. *Journal of Physical Chemistry C* **2013**, 117, (40), 20738-20745.

(11) Gu, P.; Wang, X.; Li, T.; Yu, H.; Meng, H., Solvothermal synthesis and growth mechanism of asymmetric ZnO hierarchical structures in diethylene glycol with ammonia solution. *Crystal Research and Technology* **2013**, 48, (11), 989-995.

(12) Yin, J.; Lu, Q.; Yu, Z.; Wang, J.; Pang, H.; Gao, F., Hierarchical ZnO Nanorod-Assembled Hollow Superstructures for Catalytic and Photoluminescence Applications. *Crystal Growth & Design* **2010**, 10, (1), 40-43.

(13) Li, X.; Wang, J.; Yang, J.; Lang, J.; Lu, S.; Wei, M.; Meng, X.; Kou, C.; Li, X., Comparison of photocatalytic activity of ZnO rod arrays with various diameter sizes and orientation. *Journal of Alloys and Compounds* **2013**, 580, 205-210.

(14) Bakand, S.; Hayes, A.; Dechsakulthorn, F., Nanoparticles: a review of particle toxicology following inhalation exposure. *Inhalation Toxicology* **2012**, 24, (2), 125-135.

(15) Machovsky, M.; Kuritka, I.; Bazant, P.; Vesela, D.; Saha, P., Antibacterial performance of ZnO-based fillers with mesoscale structured morphology in model medical PVC composites. *Materials science & engineering. C, Materials for biological applications* **2014**, 41, 70-7.

(16) Vollath, D., *Nanomaterials : an introduction to synthesis, properties and application*. ed.; Wiley-VCH: Weinheim, 2008; p ix, 352 p.

(17) Machovsky, M.; Kuritka, I.; Sedlak, J.; Pastorek, M., Hexagonal ZnO porous plates prepared from microwave synthesized layered zinc hydroxide sulphate via thermal decomposition. *Materials Research Bulletin* **2013**, 48, (10), 4002-4007.

(18) Zheng, J.; Jiang, Z.-Y.; Kuang, Q.; Xie, Z.-X.; Huang, R.-B.; Zheng, L.-S., Shape-controlled fabrication of porous ZnO architectures and their photocatalytic properties. *Journal of Solid State Chemistry* **2009**, 182, (1), 115-121.

(19) Audebrand, N.; Auffredic, J. P.; Louer, D., X-ray diffraction study of the early stages of the growth of nanoscale zinc oxide crystallites obtained from thermal decomposition of four precursors. General concepts on precursor-dependent microstructural properties. *Chemistry of Materials* **1998**, 10, (9), 2450-2461.

(20) German, R. M., *Sintering theory and practice*. ed.; Wiley: New York, 1996; p xv, 550 p.

(21) Kaneko, M.; Okura, I., *Photocatalysis : science and technology*. ed.; Kodansha; Springer: Tokyo; Berlin ; New York, 2002; p xvi, 356 p.

(22) Warren, B. E., *X-ray diffraction*. Dover ed.; Dover Publications: New York, 1990; p vii, 381 p.

(23) Rouquerol, F.; Rouquerol, J.; Sing, K. S. W., *Adsorption by powders and porous solids : principles, methodology, and applications*. ed.; Academic Press: San Diego, 1999; p xvi, 467 p.

(24) Hu, C.; Mi, J.; Shang, S.; Ju, S., The study of thermal decomposition kinetics of zinc oxide formation from zinc oxalate dihydrate. *Journal of Thermal Analysis and Calorimetry* **2014,** 115, (2), 1119-1125.

(25) Kaur, J.; Bansal, S.; Singhal, S., Photocatalytic degradation of methyl orange using ZnO nanopowders synthesized via thermal decomposition of oxalate precursor method. *Physica B-Condensed Matter* **2013**, 416, 33-38.

(26) Shang, C.; Barnabe, A., Structural study and phase transition investigation in a simple synthesis of porous architected-ZnO nanopowder. *Materials Characterization* **2013,** 86, 206-211.

(27) Kadlcak, J.; Kuritka, I.; Konecny, P.; Cermak, R. In *The effect of ZnO modification on rubber compound properties*, Recent Researches in Geography, Geology, Energy, Environment and Biomedicine - Proc. of the 4th WSEAS Int. Conf. on EMESEG'11, 2nd Int. Conf. on WORLD-GEO'11, 5th Int. Conf. on EDEB'11, 2011; 2011; pp 347-352.

(28) Allred, V. D.; Buxton, S. R.; McBride, J. P., Characteristic properties of thorium oxide particles. *Journal of Physical Chemistry* **1957**, 61, (1), 117-120.

(29) Beck, P. A.; Kremer, J. C.; Demer, L. J.; Holzworth, M. L., Grain growth in high-purity aluminum and in an aluminummagnesium alloy. *Transactions of the American Institute of Mining and Metallurgical Engineers* **1948**, 175, 372-400.

(30) Burke, J. E., Some factors affecting the rate of grain growth in metals. *Transactions of the American Institute of Mining and Metallurgical Engineers* **1949**, 180, 73-91.

(31) Yan, M. F.; Cannon, R. M.; Bowen, H. K., Grain-boundary migration .1. theory of impurity drag in ionic systems. *American Ceramic Society Bulletin* **1976**, 55, (4), 397-397.

(32) Na, S.-H.; Park, C.-H., First-Principles Study of the Surface Energy and the Atom Cohesion of Wurtzite ZnO and ZnS - Implications for Nanostructure Formation. *Journal of the Korean Physical Society* **2010**, 56, (1), 498-502.

(33) Erhart, P.; Albe, K., Diffusion of zinc vacancies and interstitials in zinc oxide. *Applied Physics Letters* **2006,** 88, (20), Article No. 201918.

(34) Janotti, A.; Van de Walle, C. G., Fundamentals of zinc oxide as a semiconductor. *Reports on Progress in Physics* **2009**, 72, (12), Article No. 126501.

(35) Thomas, D. G., Interstitial zinc in zinc oxide. *Journal of Physics and Chemistry of Solids* **1957**, 3, (3-4), 229-237.

(36) Matyka, M.; Khalili, A.; Koza, Z., Tortuosity-porosity relation in porous media flow. *Physical Review E* **2008**, 78, (2), Article No. 026306.

High-resolution Figure 1
Click here to download high resolution image

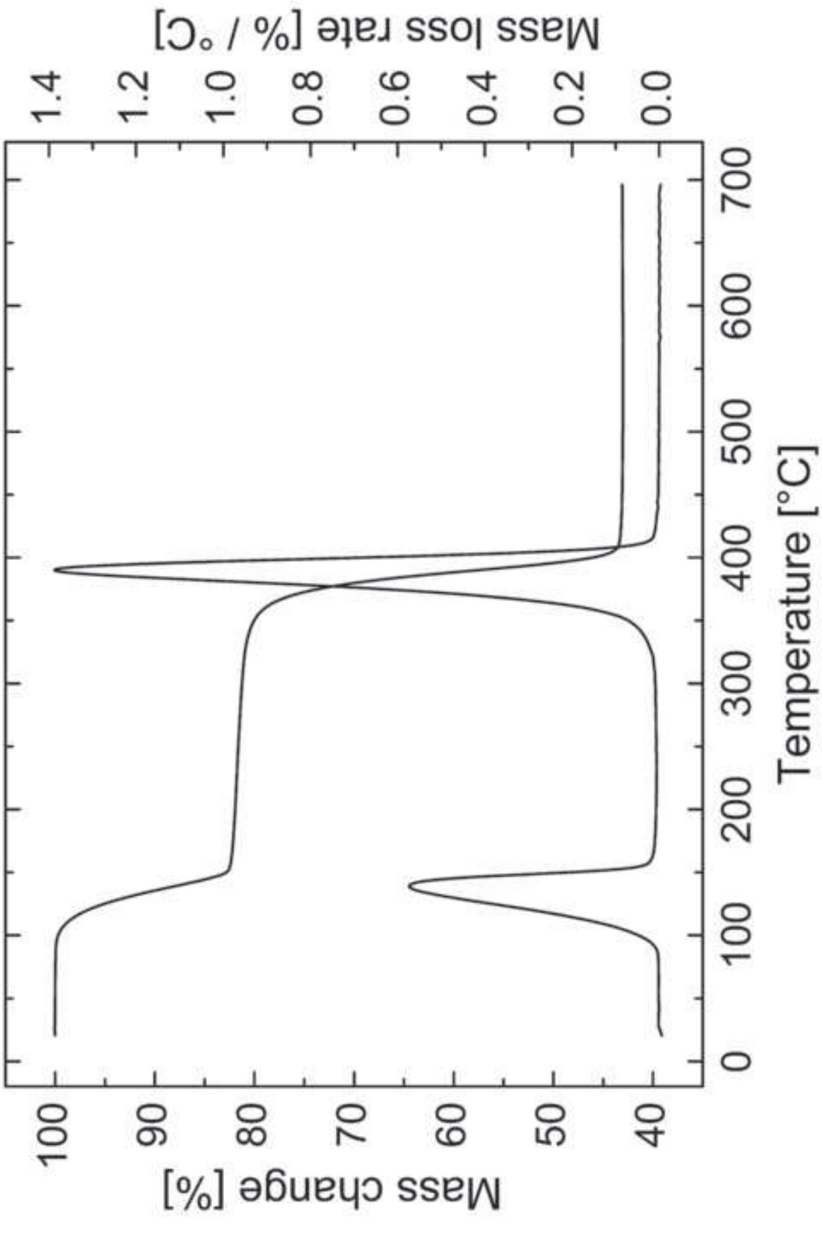

High-resolution Figure 2
Click here to download high resolution image

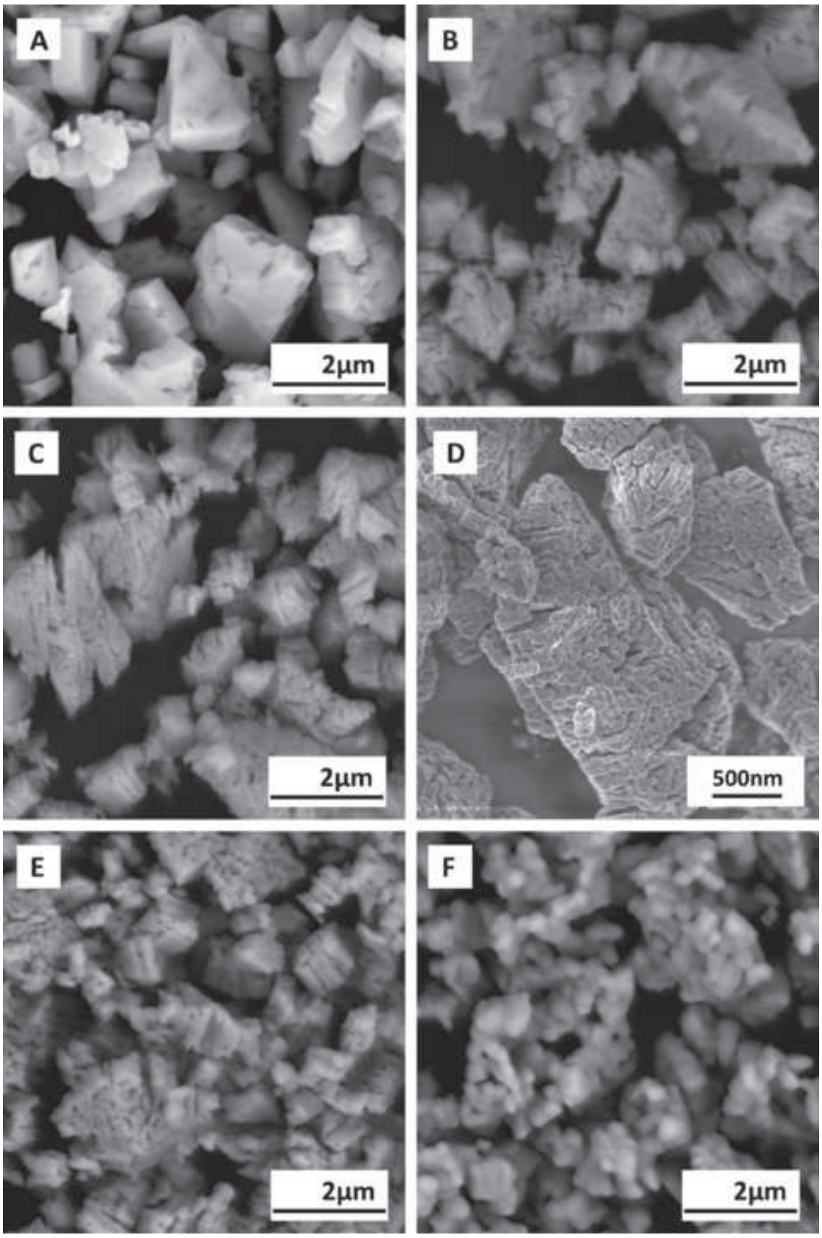

High-resolution Figure 3
Click here to download high resolution image

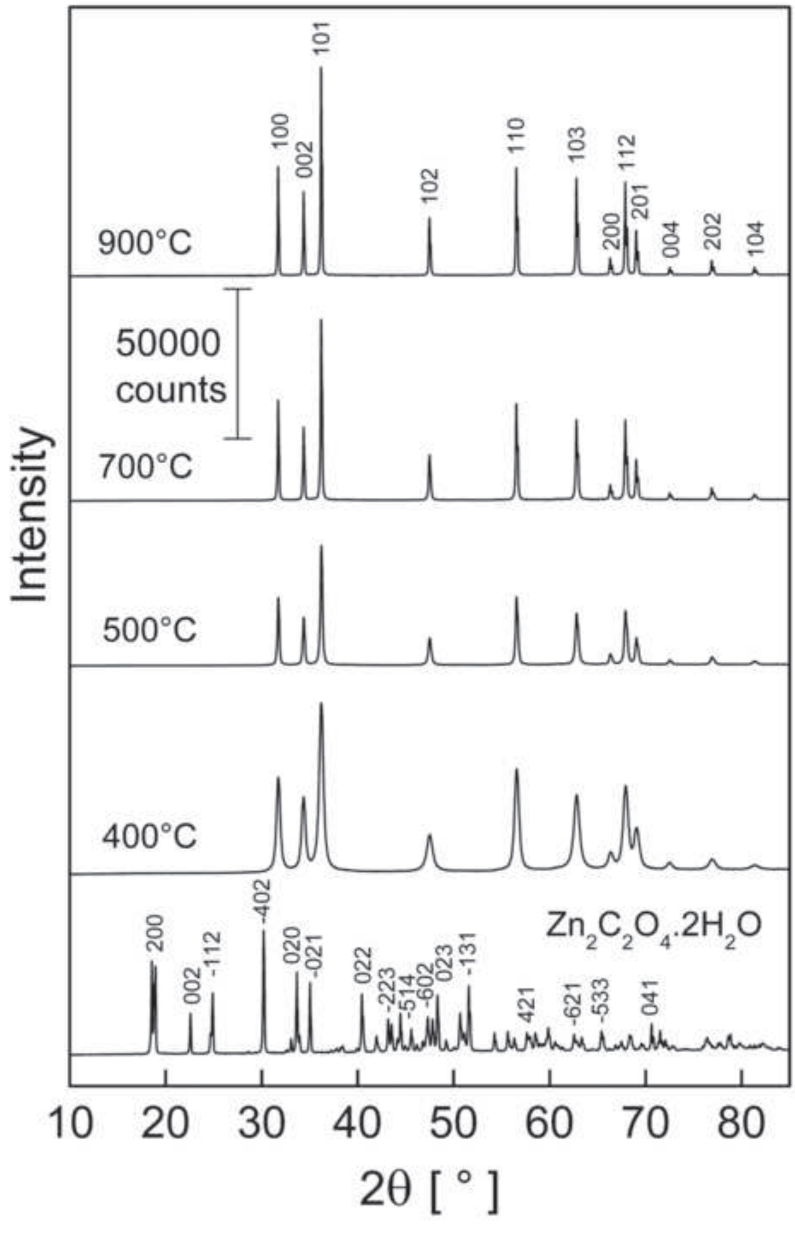

High-resolution Figure 4
Click here to download high resolution image

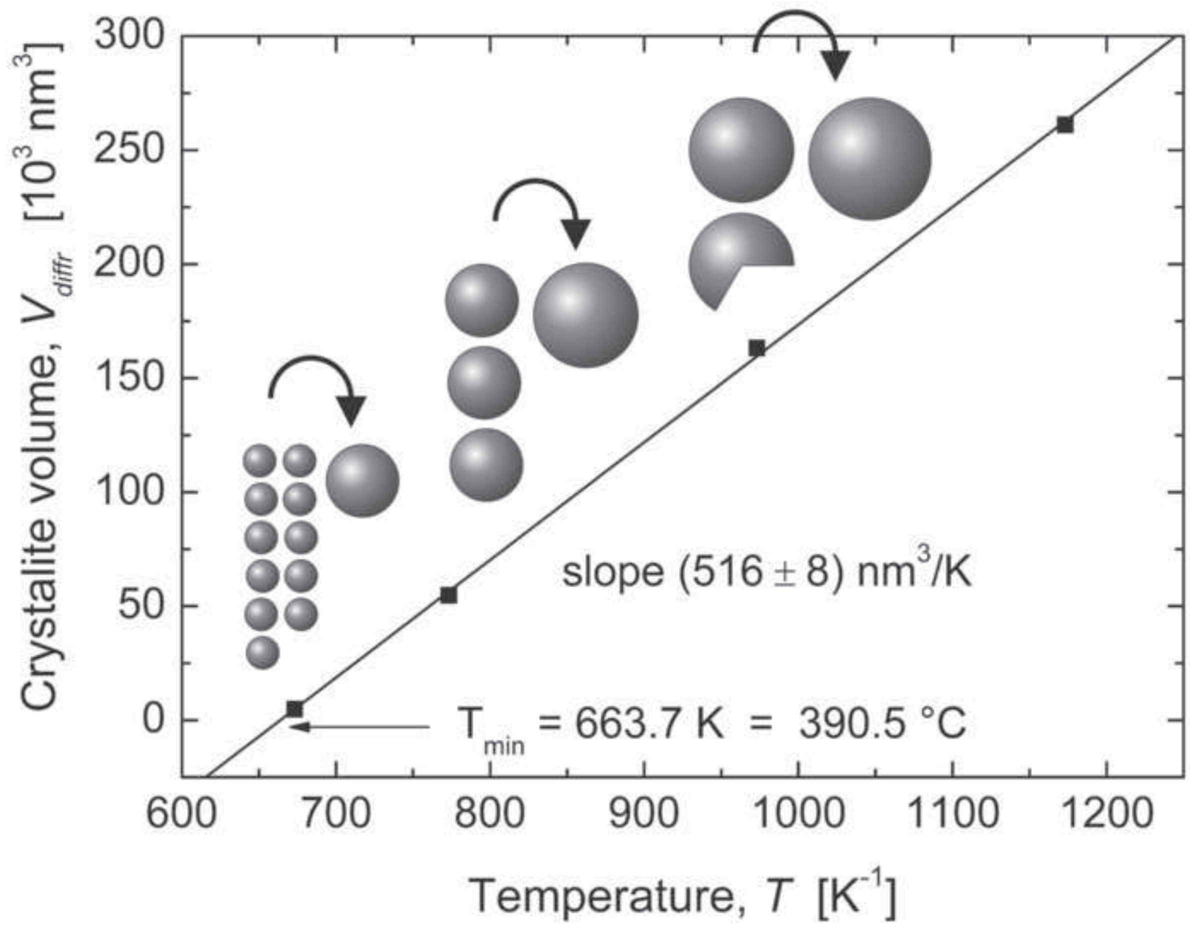

High-resolution Figure 5
Click here to download high resolution image

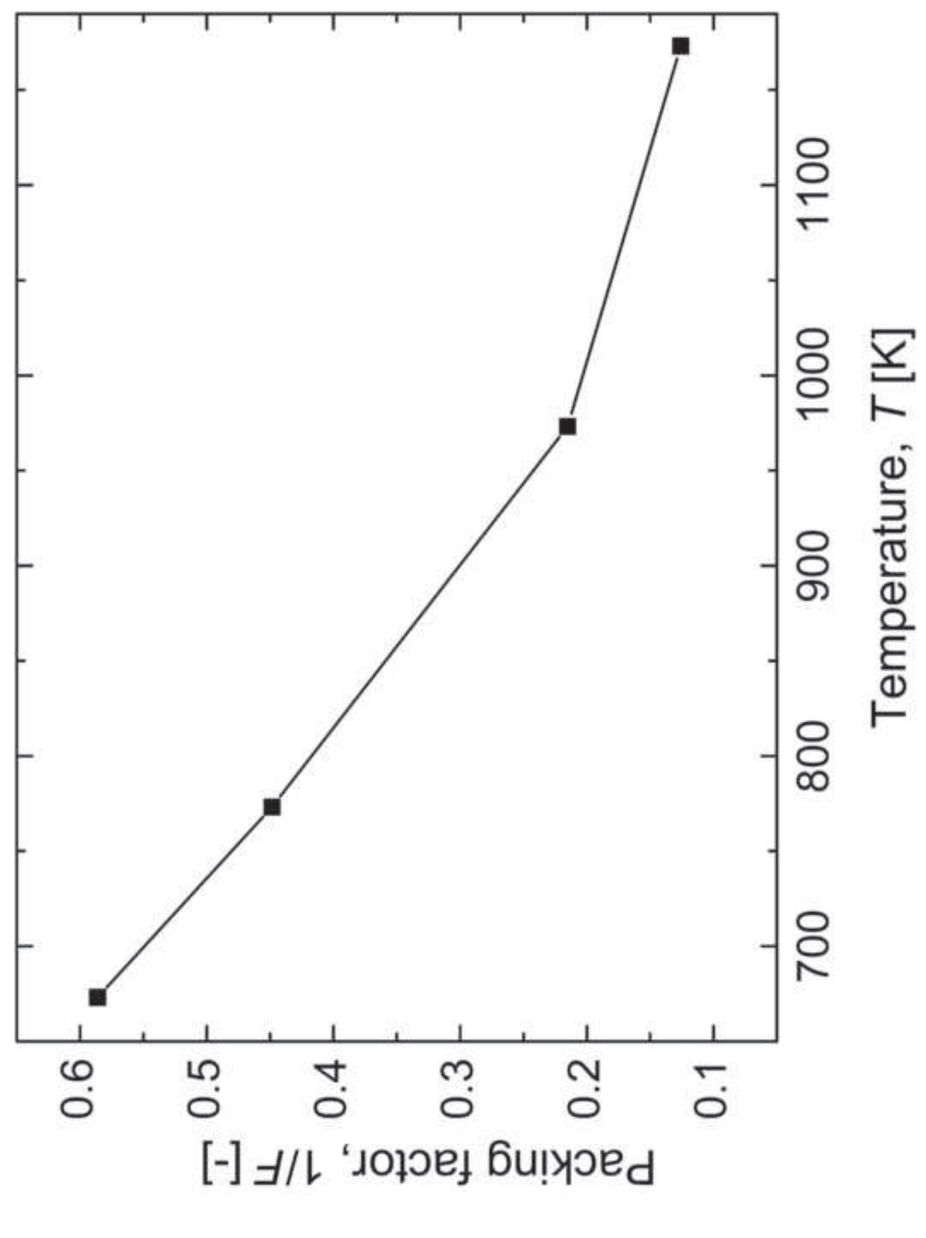

High-resolution Figure 6
Click here to download high resolution image

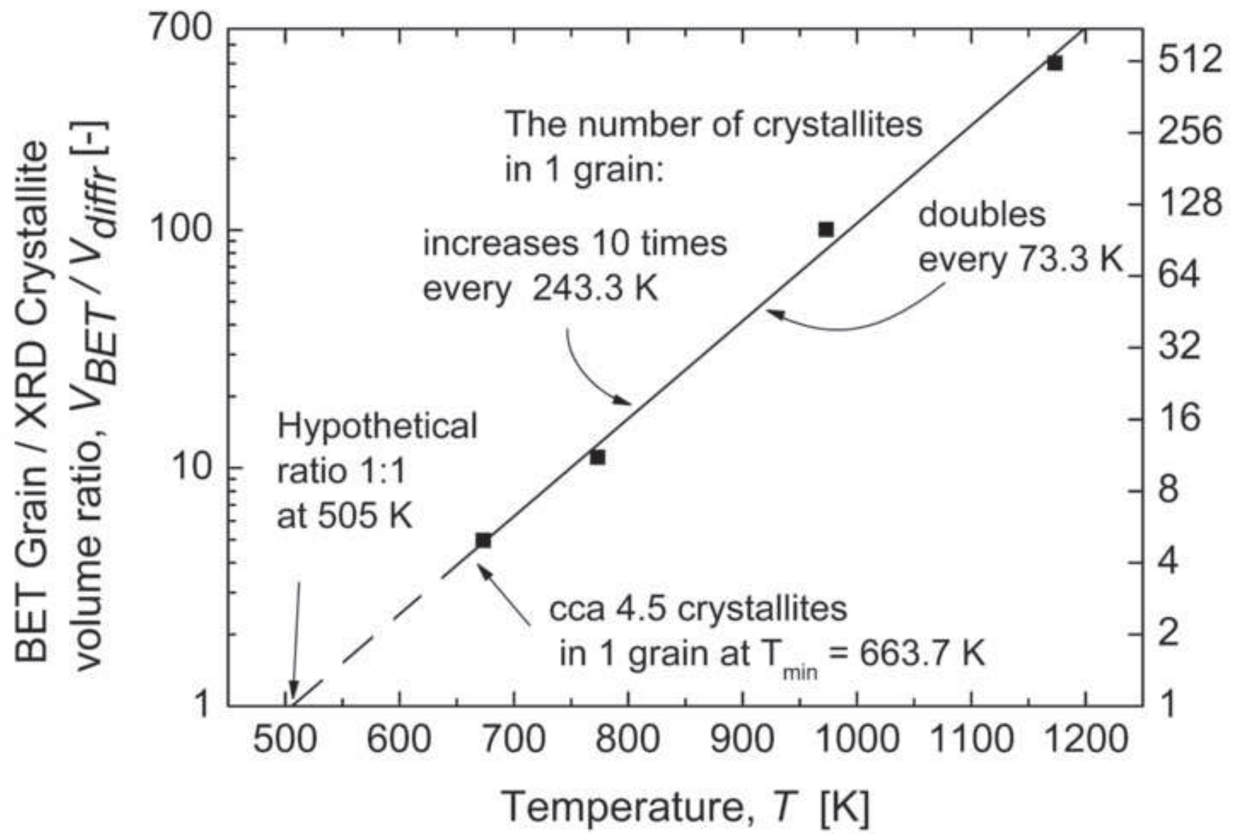

High-resolution Figure 7
Click here to download high resolution image

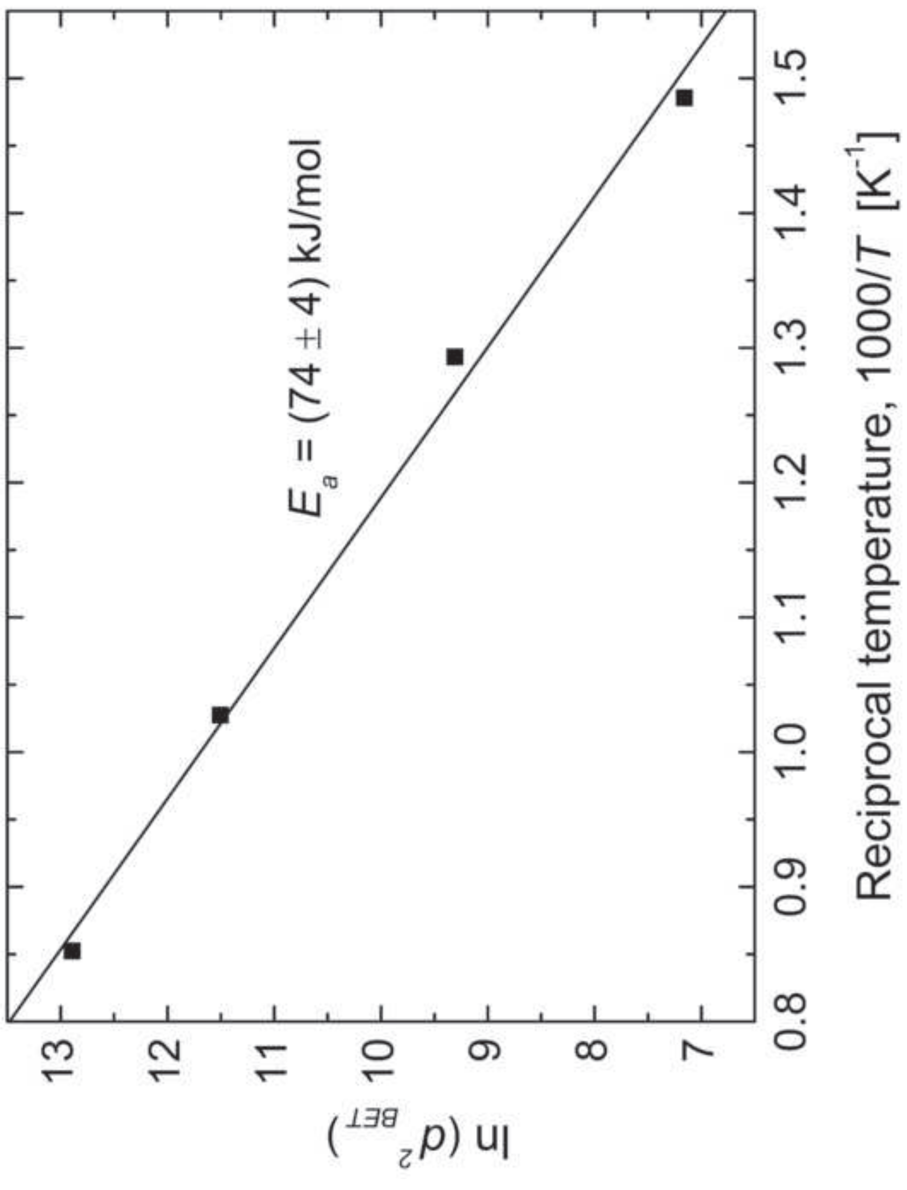

High-resolution Figure 8
Click here to download high resolution image

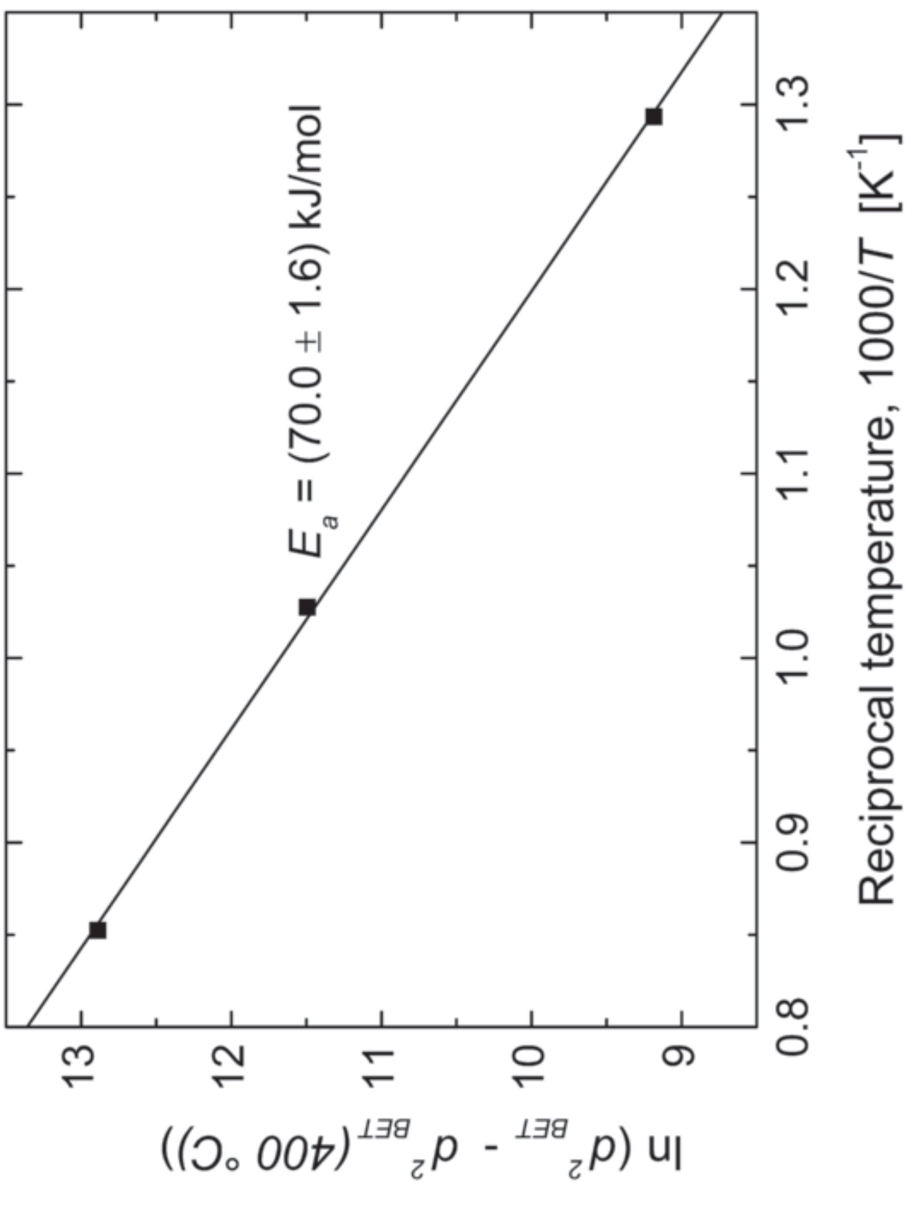

High-resolution Figure 9
Click here to download high resolution image

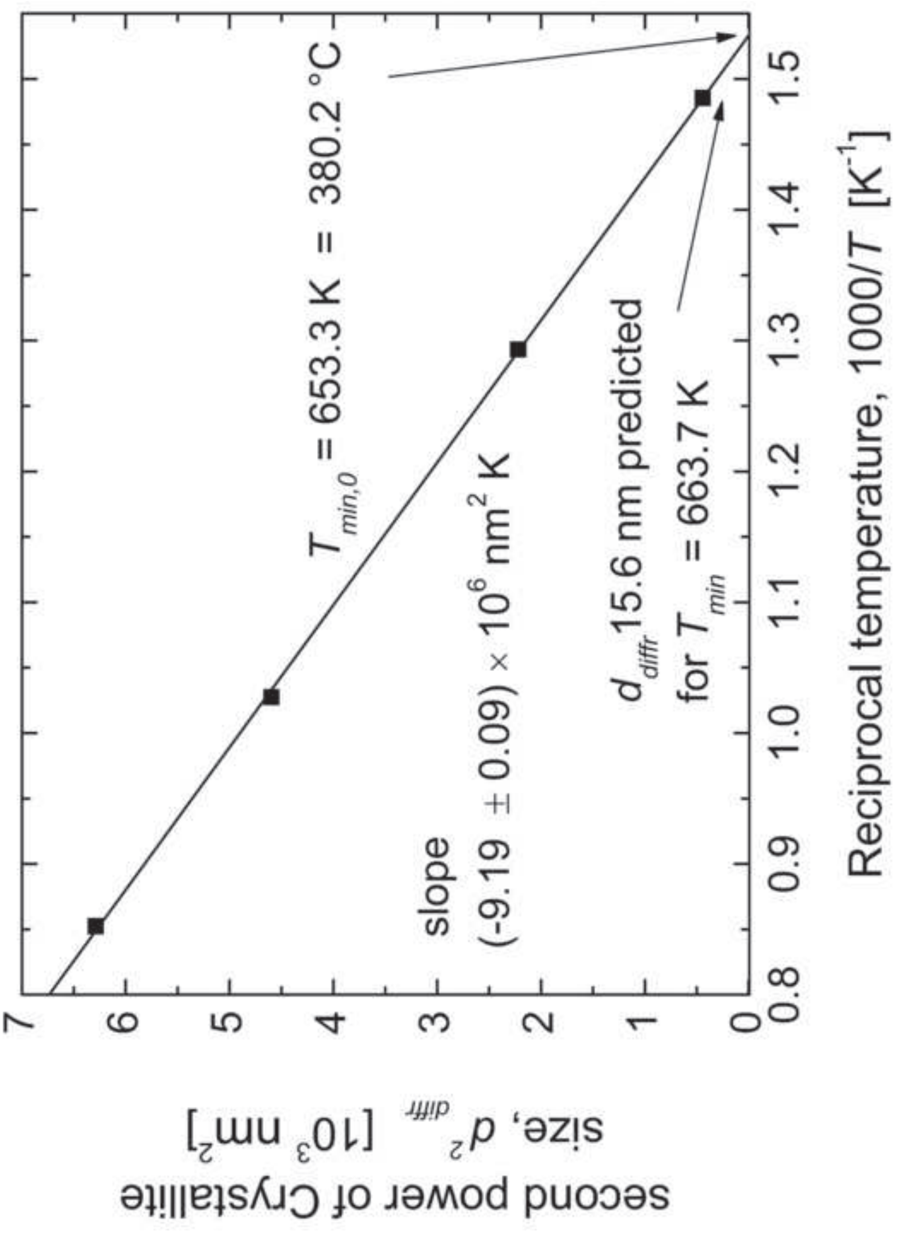

High-resolution Figure 10
Click here to download high resolution image

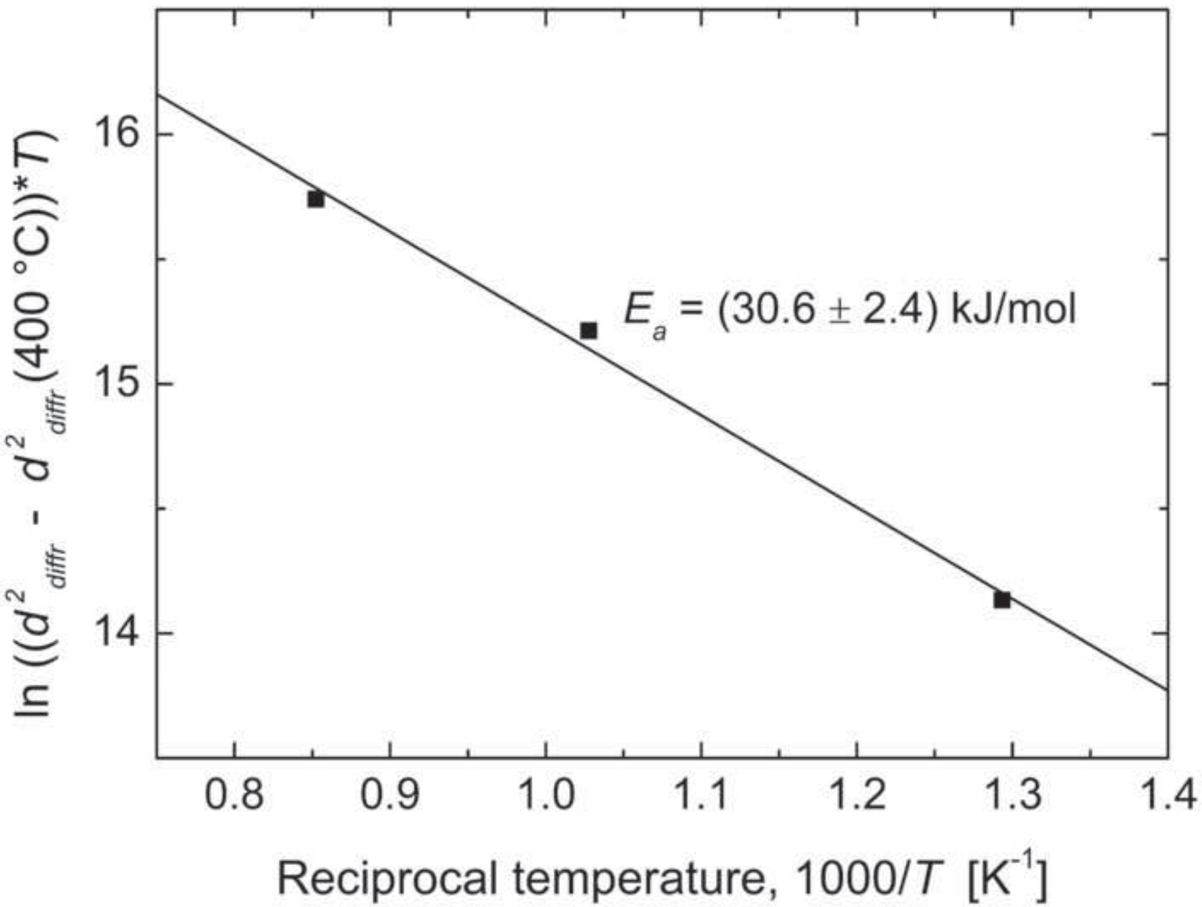

High-resolution Figure 11
Click here to download high resolution image

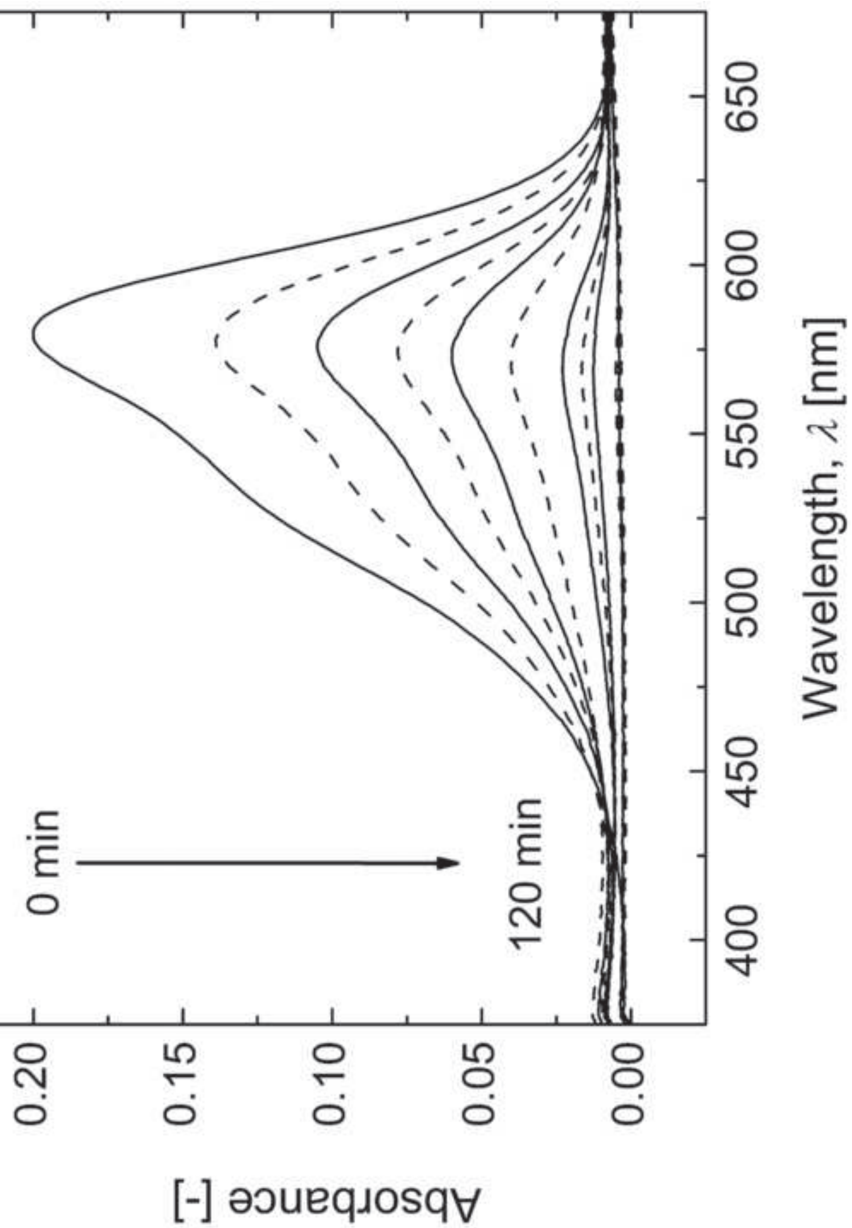

High-resolution Figure 12
Click here to download high resolution image

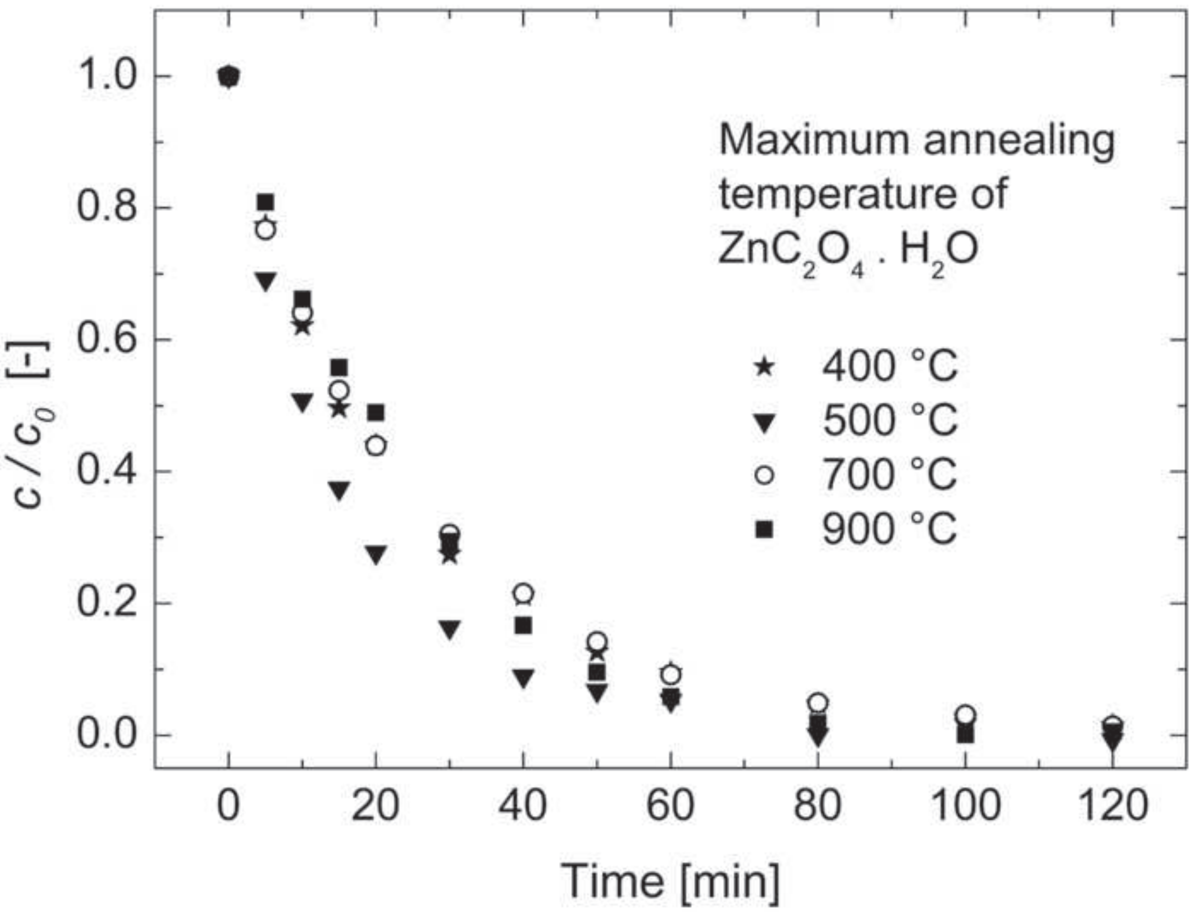

High-resolution Figure 13
Click here to download high resolution image

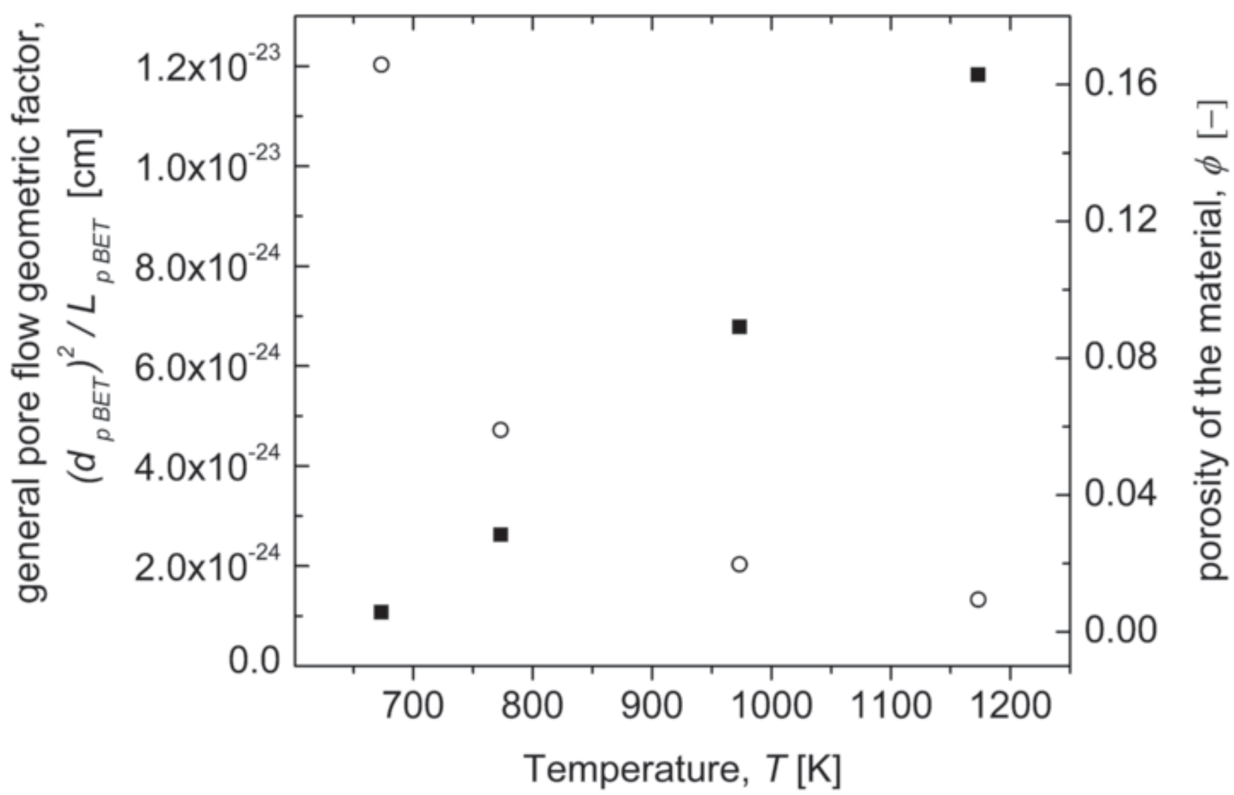

Paper V.

MACHOVSKY, M.; SEDLAK, J. (40 %); JANOTA, P.; URBANEK, P.; HAJEK, M.; DVORACKOVA, M.; KURITKA, I. Photocatalytic properties of nanocrystalline assembled ZnO spheres. Manuscript in preparation.

Photocatalytic properties of nanocrystalline assembled ZnO spheres

MACHOVSKY MICHAL [1,2], SEDLAK JAKUB [1,2], JANOTA PAVEL[3], URBANEK PAVEL[1,2], HAJEK MARTIN[3], DVORACKOVA MARIE[1, 3], KURITKA IVO*[1,2],

[1]Centre of Polymer Systems, University Institute, Tomas Bata University in Zlin, Nad Ovcirnou 3685, 760 01 Zlin, CZECH REPUBLIC
[2]Polymer Centre, Faculty of Technology, Tomas Bata University in Zlin, Nam. T. G. Masaryka 275, 762 72 Zlin, CZECH REPUBLIC
[3]Department of Environmental Engineering, Faculty of Technology, Tomas Bata University in Zlin, Nam. T. G. Masaryka 275, 762 72 Zlin, CZECH REPUBLIC

* Corresponding author: kuritka@ft.utb.cz, tel. +420 576 038 049, fax. +420 576 031 444

Abstract:
Nanocrystalline assembled zinc oxide (ZnO) spheres on mesoscale were prepared by thermal decomposition of zinc peroxide (ZnO_2) in air atmosphere. The phase transformation from ZnO_2 to ZnO was studied by thermogravimetric analysis, X-ray diffraction analysis (XRD), scanning electron microscopy (SEM), BET adsorption analysis and photoluminescence (PL). The photocatalytic activities of ZnO powders obtained by annealing at various temperatures were evaluated by the photodegradation of Methyl violet 2B. Moderate photocatalytic activity was observed for powders annealed to 200 °C and 300 °C, although possess high specific surface area. This can be attributed to the presence of intermediate amorphous like ZnO phase in the early stage of transformation from ZnO_2 cubic to ZnO hexagonal lattice and improperly developed crystalline phase. Excellent photocatalytic activity was achieved for samples annealed at 500 °C and more. The results suggest that photocatalytic activity is influenced by size of well developed crystalline array rather than by specific surface area. Photoluminescene study revealed green luminescence for sample annealed at the 700 °C and 900 °C, supporting data from XRD, TG, SEM analysis and photocatalytic activity testing.

Keywords: ZnO, photocatalysis, specific surface area, crystallite size, photoluminescence

1. Introduction

Zinc Oxide (ZnO) is a direct semiconducting material with numerous attractive characteristics for application in optoelectronics, blue/UV light emitting diodes, transparent electronics, spintronic devices and sensors [1-4]. Moreover, ZnO is a subject of scientific interest due to its significant antibacterial and photocatalytic activity [5-7]. In the field of photocatalysis, Titanium dioxide (TiO_2) is undoubtedly the material most extensively studied [8, 9] However, ZnO has been reported to exhibit photocatalytic activity comparable or sometimes even better to TiO_2 and is considered as a very promising alternative. Moreover, ZnO is cheap, low-toxic material that can be prepared by a large variety of methods [10, 11]. Due to intrinsic features of ZnO crystal structure, all possible morphologies of nano- and microstructures that one can imagine has been successfully prepared, making ZnO one of the richest family of structures among the entire family of inorganics. As the photocatalytic activity of semiconductors generally depends on crystal size, surface area, morphology and native defects, the abundancy in morphologies makes ZnO representative material in the research field of photocatalysis [12, 13]. It has been reported that photocatalytic activity of ZnO increases with increasing crystalline size up to the certain critical value, above which remains relatively constant and further increase resulted in its decrease [14]. Surface area is considered to be another important factor. It is reasonable to think, that higher surface area inevitably lead to an increase of photocatalytic activity due to greater maximum available active sites and surface for the adsorption of molecule to be degraded. However, many researchers reported on descending trend, ascribing this peculiarity to the reduced recombination losses with increased crystalline size. This suggests optimum balance between size of crystalline array and the surface area, (while) keeping other material parameters same. However, such relations are not predictable easily as the morphology has been shown to play also important role [15]. Significantly different photocatalytic rates for various crystal facets have been documentented in the literature [16, 17]. Although all these parameters greatly influence photocatalytic activity, can be optimized to reach highest performance for a given material.

Further enhancement of photocatalytic activity of the ZnO and other semiconductors remains an important issue for many research groups worldwide. Methods which may eventually result in improvement are principally based on either lowering of the semiconductor band gap, or in lowering recombination rate of separated charges. These include metal or non-metal doping, dye sensitization, or cocatalyst loading. [18-22] A lot of papers to each topic can be found in the literature, reflecting enormous effort devoted to improving semiconductors photocatalytic activity. The state of the art is well documented in many comprehensive reviews. [23-25]

Recently, oxygen vacancies as a kind of native defect have received much attention. It is well known that native defects in semiconductors strongly influenced the electrical and optical properties [3]. Therefore, the number of oxygen vacancies is rationally considered to affect photocatalytic performance as well. Indeed, lately published works refer on enhanced photocatalytic activity for ZnO samples containing higher concentration of oxygen vacancies compared to those with stoichiometric ratio, attributing this enhancement to the either oxygen vacancies induced band gap, or high separation efficiency of photogenerated electron–hole pairs [26-29]. Several methods have been proposed for preparation of oxygen vacancies rich ZnO [30, 31]. Among them, thermal decomposition of ZnO_2 precursor represents an easy and effective way of producing ZnO containing oxygen vacancy. The phase transition from cubic phase ZnO_2 and hexagonal wurtzite ZnO phase proceeds at relatively low temperature of about 200 °C, with the number of oxygen vacancies decreases with increasing annealing temperatures up to the thermodynamically stable stoichiometric state. [32] Moreover, ZnO/ZnO_2 composite as intermediate transformation product has been shown to possess excellent photocatalytic activity compared to its pure constituents [33].

In this paper, we propose large- scale method for producing nanocrystalline assembled ZnO sphere with dimension on mesoscale by thermal decomposition of ZnO_2. The precursor was obtained by simple recrystallization of commercial ZnO from ammonia solution in the presence of hydrogen peroxide. The phase transformation from ZnO_2 to ZnO was investigated by complementary instrumental techniques, including SEM, XRD, PL and specific surface area measurements. Preparation of such spherical nanocrystallites assemblies of ZnO are of great interest as a promising material for advanced applications due to its large surface area and ability of scattering incident light in sunlight spectrum [34]. Herein, we focus on the photocatalytic activity of ZnO powders obtained by annealing at various temperatures. The results of photocatalytic activity testing are discussed in context with specific surface area, crystalline grain size, and photoluminescence.

2. Experimental

2.2 Preparation of ZnO_2 precursor and ZnO

ZnO_2 powder was prepared by recrystallization of dissolved commercial ZnO powder. The synthesis process was optimized as follows; 4.2 g of ZnO powder was putted into beaker of volume 600 mL and 350 mL of 25-29 % aqueous solution of ammonia (Penta, Czech Republic) was added and stirred with revolution set up to 250 rpm. The solubility of ZnO in concentrated ammonia was enhanced by addition of 14 mL of hydrogen peroxide after 5 minutes and stirred for another 15 minutes until complete dissolution of ZnO take place. The obtained solution was filtered and after casted onto Petri dishes left dry at the hood. Ammonia evaporated completely in 8 hours under our experimental conditions and dried ZnO_2 powder was collected. ZnO was obtained by thermal decomposition of the ZnO_2 precursor by annealing at various temperatures ranging from 200 to 900 °C in a furnace with a static air atmosphere. The desired temperature was reached at the heating rate of 10 °C/min and held constant for 2 hours prior left to cool down slowly in a closed oven.

2.3 Characterization methods

Crystalline phases of prepared powders were characterized by the X-ray diffractometer X´Pert PRO X-ray (PANalytical, The Netherlands) with a Cu-Kα X-ray source (λ = 1.5418 Å) and the operation voltage and current maintained at 30 kV and 20 mA, respectively, in the diffraction angle range 5-85° 2θ. The morphology was investigated by scanning electron microscope Vega II/LMU (Tescan, Czech Republic) operated at accelerating voltage 10 kV. Thermogravimetric analysis (TGA) was carried out by the thermogravimeter Q500 (TA instruments, United States) in the temperature range from 25 to 800°C at a heating rate 10°C min-1 in flowing air (30 sccm). The specific surface area was calculated based upon the multipoint Brunauer-Emmet-Teller analysis of nitrogen adsorption/desorption isotherms at 77 K recorded by Belsorp-mini II (BEL Japan, Inc.). Samples were outgassed for 2 h at 70 °C prior to the measurements. The photoluminescence (PL) spectra were measured at the room temperature by using Fluorescence spectrometer FLS 920 (Edinburgh Instruments) with a monochromatized Xe lamp (150 W) as the excitation source. Samples for PL measurements were prepared by spin casting onto glass/ITO substrates using spin coater Laurell WS-650-MZ-23NPP without further treatment.

2.3 Photocatalytic activity testing

Photocatalytic activities of samples were assessed by monitoring degradation rate of Methyl Violet 2B (Sigma Aldrich) under the UV illumination. The dye solution was prepared by dissolving 3.5 mg of the dye in 1 L of deionized water. Prior to the experiment, suspension containing 20 mg of powder in 50 mL of dye solution was magnetically stirred under darkness for 1 hour to reach adsorption equilibrium. The solution was then illuminated by 100W focused UV-lamp (Super-Light C 10 A-SH, Helling Gmbh., Germany) with the strongest emission at 365 nm while further stirred. The temperature of suspension was regulated to be 20 °C by thermostat. A volume of 1 mL was sampled into disposable PS cuvette by using micropipette (Ependorf) at the beginning of photocatalytic reaction and than at fixed time intervals. Samples were diluted three times prior to the measurements of UV-VIS absorption (UV VIS spectrophotometer Cary 300, Varian Inc.).

3. Results and discussion

The powder XRD patterns of the ZnO_2 and ZnO obtained by its calcining at various temperatures are shown in Fig. 1. The diffractogram of powder obtained by recrystallization of the commercial ZnO powder dissolved in ammonia-peroxide solution at the room temperature is dominated by four broad diffraction peaks at 2θ = 31.8°, 36.9°, 53.2°, and 63.3° that can be correspondingly indexed as (111), (200), (220), and (311) of cubic ZnO_2 phase (JCDD PDF-2 entry 01-077-2414). The negligible peak at right shoulder of the last one can be identified at 2θ = 66.5°C and can be assigned to the (222) of the same phase. TG analysis was done prior to annealing of the precursor to get insight the kinetics of thermal decomposition of ZnO_2 powder and set-up annealing temperature reasonably. TG curve and its derivative recorded at the constant heating rate 10 °C/min in the air atmosphere are shown in Fig. 2. It can be clearly seen from derivative curve that the thermal decomposition involves two steps. The weight loss of nearly 5 % in the temperature up to cca 150 °C with the maximum mass change rate nearby 70 °C can be assumed as a moisture contribution. Above 150 °C, the decomposition reaction following Eq. 1 took place with a steepest mass change of about 13 % observed in the temperature region 200-250 °C with the maximum mass change rate at 221 °C. Then the decomposition reaction proceeds slowly reaching plateau at approximately 500 °C with simultaneous loss of 3 % total mass.

$$2ZnO_2 \rightarrow 2ZnO + O_2 \qquad \text{(Eq. 1)}$$

Based on the TG analysis, annealing temperatures were chosen as can be seen from labelling of diffractograms if Fig. 1. Although peaks that appeared for sample annealed at the 200 °C can be assigned to the hexagonal wurtzite ZnO (JCDD PDF-2 entry 01-079-0207), the crystalline phase is scarcely well developed. This temperature intercept the beginning of decomposition reaction and the phase transformation from cubic ZnO_2 phase to hexagonal ZnO phase can not be completed fully; the conversion is rather frozen in an intermediate like phase.

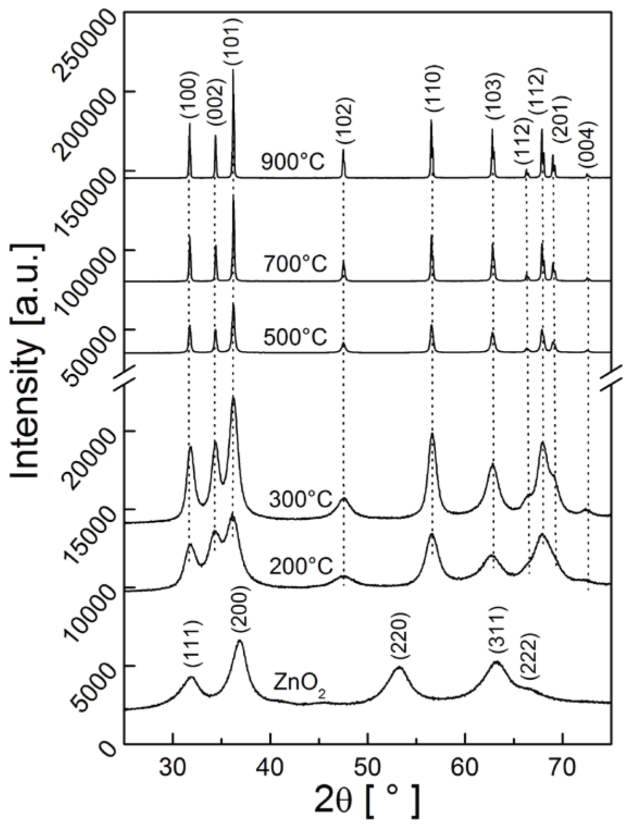

Figure 1 Diffractograms with indexed diffraction lines of the precursor and ZnO samples obtained by annealing at temperatures indicated in the graph.

With increasing of anneling temperature up to the 300 °C, the crystalline phase becomes more developed and the triad of peaks at higher angles can be resolved yet. Moreover, the crystalline size estimated according to the well known Debye-Scherrer formula [35, 36] increased to 10 nm from 6.5 nm calculated for sample annealed at 200 °C. Calculated values are included in Table. 1. along with the specific surface area and rate constants of dye degradation. On the other hand, fully developed crystalline ZnO hexagonal wurtzite phase was identified for sample annealed at 500 °C, which is in agreement with TG analysis. As indicated by diffraction peaks narrowing, the crystalline size increased abruptly up to 37.1 nm. Moreover, all planes characteristic for wurtzite hexagonal ZnO phase in a measured diffraction angle range can be identified unambiguously, suggesting well developed crystals (note on different scale of signal intensity). Further increase of annealing temperature to 700 °C and 900 °C resulted in next increase of crystalline size to 55.9 nm and 66.7 nm, respectively.

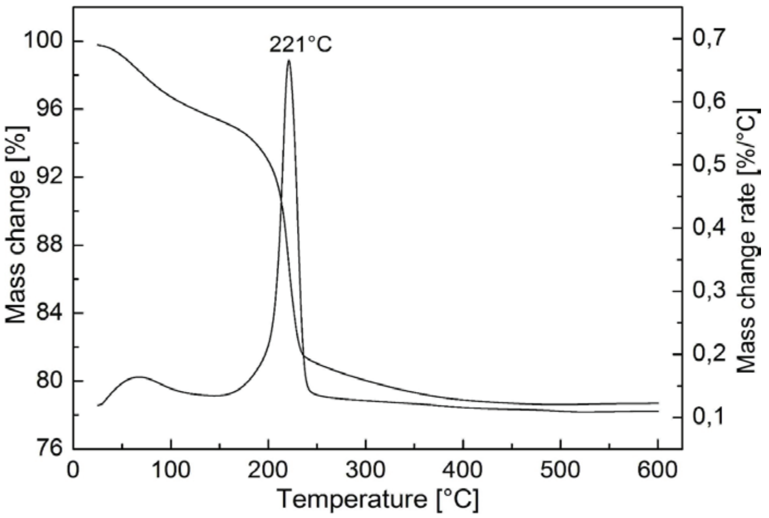

Figure 2 The TGA analysis of precursor under air atmosphere.

The increase of crystalline size with increasing annealing temperature is well documented in a series of scanning electron micrographs in the Fig. 3. Low resolution image of ZnO_2 in Fig. 2a shows that precursor powder consists of spherical particles with diameters ranging from several tens to several hundreds nananometers. High resolution image in Fig. 2b revealed that ZnO_2 spheres are covered by small randomly scattered crystals, resembled coconut balls. The morphology of particles has changed significantly by annealing of precursor at 200 °C as can be seen in Fig. 3c. The release of Oxygen resulted in development of nanocrystalline assembled ZnO while keeping the spherical shape of precursor. The size of crystals observed is in agreement with crystalline size values calculated according Debye-Scherrer equation.

Further increase of annealing temperature to 300 °C lead to slight increase in crystalline size, however, such small change is hardly detected by eye (Fig. 3d). While the morphologies of samples treated at 200 °C and 300 °C remained almost the same, dramatic change can be observed when annealing temperature increased to 500 °C as shown in Fig. 3e.

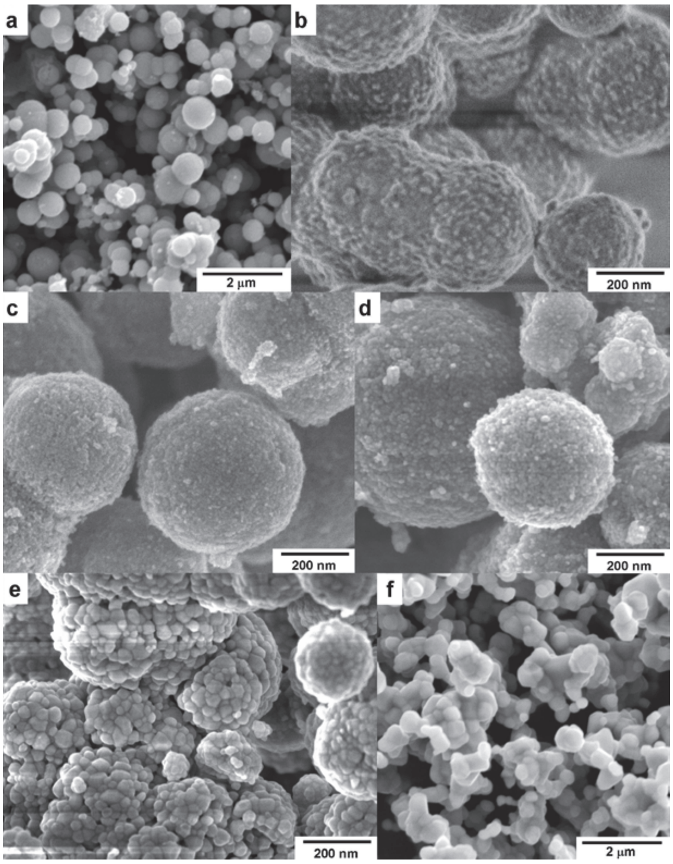

Figure 3. SEM images of precursor and products prepared by annealing of the precursor at different temperatures, A,B: precursor; C: 200 °C; D: 300 °C; E: 500 °C; F: 900 °C.

The size of crystals has increased abruptly due to the sintering of smaller crystals and the overall particles morphology resembled raspberries. Although particles still possess their spherical shape, there is also evidence of sintering of whole spheres. The observed crystals size is consistent with crystalline size values estimated to be 37.1 nm according to the Debye-Scherrer equation. Moreover, the phase transformation from ZnO2 to ZnO is expected to be

8

completed definitely as indicated by corresponding XRD pattern in which all planes characteristic for wurtzite ZnO hexagonal structure can be identified in contrast to the sample annealed at 200 °C and 300 °C. TG analysis supports this assumption as there is no mass loss above 500 °C observed. Samples annealed at 700 °C and 900 °C resembled raspberry like morphology similar to those observed for sample annealed at 500 °C. While the crystalline size further increased up to 66.7 nm for sample treated at 900 °C, sintering of individual spheres becomes has more pronounced effect on overall particles morphology as can be seen from Fig. 3f. The specific surface area calculated based upon the multipoint Brunauer-Emmet-Teller (BET) analysis was measured in order to gain information about maximum available surface area which may contribute to the process of photocatalytic degradation. The results of BET specific surface area measurements are summarized in Table. 1. It can be seen that specific surface area decreases with increasing annealing temperature from 41.2 m^2g^{-1} for powder annealed at 200 °C to 1.2 m^2g^{-1} for powder annealed at 900 °C. The decrease in specific surface area with increasing temperature is expected as the sintering of small crystals into large ones inevitably lead to decrease in specific surface area. On the other hand, closer inspection of data listed in Table 1. reveal that results of BET measurements match surprisingly well to the crystalline size calculated from XRD patterns and SEM observation. Similarly, there is steep decrease in specific surface area from 37 m^2g^{-1} to 6.3 m^2g^{-1} for samples annealed at 300 °C and 500 °C, respectively, followed by gradual decrease when annealed at higher temperatures.

Table 1. BETsurface area, crystallites size, rate constant of dye degradation for ZnO_2 precursor and ZnO obtained by annealing at various temperatures

	ZnO_2	ZnO_2 200C	ZnO_2 300C	ZnO_2 500C	ZnO_2 700C	ZnO_2 900C
BET surface area [m^2g^{-1}]	46.2	41.2	37.0	6.3	1.7	1.2
Crystallites size [nm]	4.67	6.5	10.0	37.1	55.9	66.7
rate constant [s^{-1}]	-	0,005 ±0.003	0,0210 ± 0,0017	0,0335 ±0,0015	0,0443 ±0,0011	0,040 ±0,0015

The photocatalytic activities of as prepared ZnO powders were evaluated by photodegradation of methyl violet 2B under UV illumination. The progress in degradation reaction was monitored by UV-VIS spectroscopy. The typical time dependent UV-VIS absorption spectra for sample annealed at 900 °C is shown in Fig. 4. The characteristic absorption peak maxima of methyl violet localized at 580 nm decreased gradually with the extension of illumination time and disappeared after 120 min.

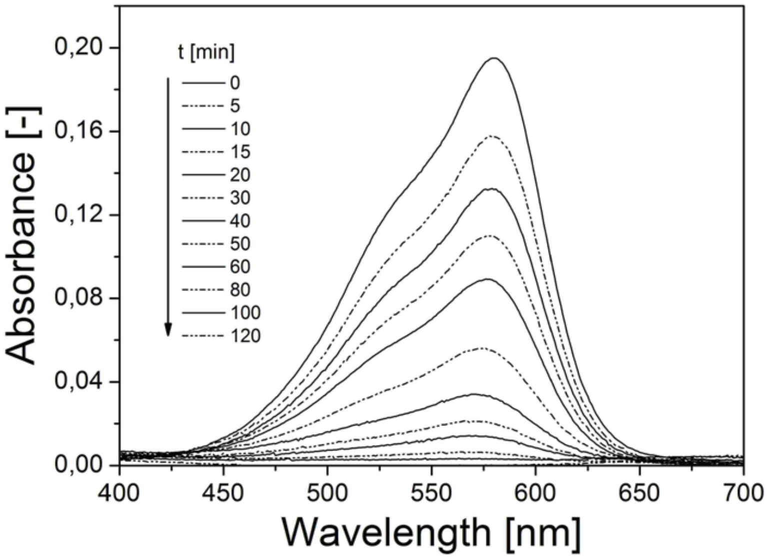

Figure 4 UV-vis spectra of of methyl violet in the presence of ZnO annealed at 700 °C.

The photodegradation curves of the dye for all ZnO samples prepared at various annealing temperatures are shown in Fig. 6. The ratio between actual and initial concentration is plotted against time of UV irradiation. As can be seen, sample annealed at 200 °C and 300 °C exhibit only moderate photocatalytic activity and entire photodegradation of the methyl violet is not achieved even after 2 hours of illumination. On the other hand, samples annealed at 500 °C and more show excellent photocatalytic activities with about 90 % of methyl violet degraded within first 80 minutes of photocatalytic driven reaction. Obviously, photodegradation curves obey first or pseudofirst order reaction kinetics. The rate constants obtained from fitting the first order model into the data are summarized in Table 1. The results of photocatalytic activity testing correlate with TG, XRD, and SEM analysis. All of these instrumental techniques registered steep change in properties when reached annealing temperature 500 °C.

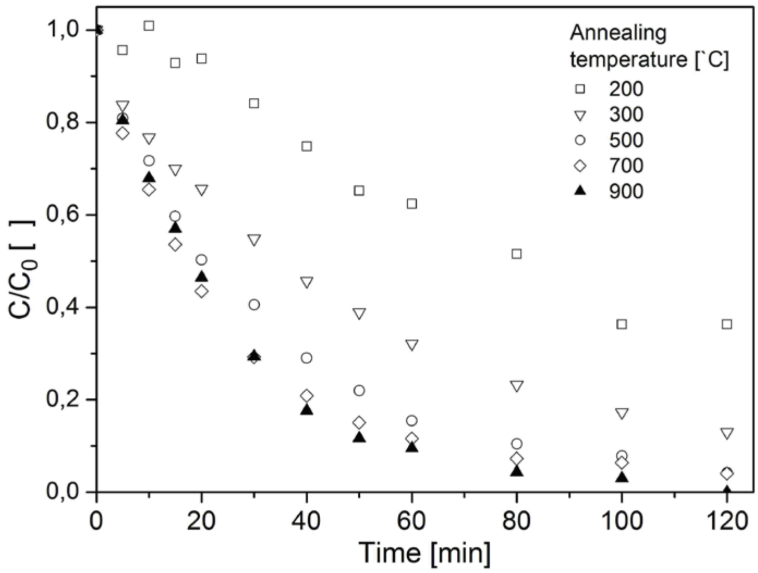

Figure 5 Photocatalytic degradation curves of methyl violet as a function of time for ZnO powders annealed at different temperatures, as illustrated in the graph.

Analysis of photoluminescence (PL) spectra should provide important information about crystals defects whose may directly affected photocatalytic activity. [38] The room temperature PL spectra of ZnO_2 precursors and ZnO obtained by its annealing at various temperatures are shown in Fig. 6. In materials annealed up to the 500 °C the PL was not observed. On the other hand, in materials heat-treated over the temperature 500 °C the PL was appeared. In case of 500 °C and 700 °C annealing temperatures, the blue emission was achieved. The origin of this emission can be explained as free excitons recombination bound to acceptors and donors and their two-electron satellites in the structural lattice, and donor-acceptor pairs. The luminescent centres are energetically positioned at about 3,2 eV, but small shifts can occur depending on the perfection of crystal structure and content of various defects in the crystal. Moreover, the green emission, located between 2,3 and 2,4 eV, is detected and rapidly increases if the material is heat treated at 900 °C. Any authors explain the green emission as a morphological variation of the particles [39]. But the major factor determining the PL properties for our nanostructured microparticles may be the number of oxygen vacancies. The idea of high number of oxygen vacancies seems to be suitable explanation because if oxygen vacancies predominate, they serve as luminescent centres of longwavelength band [40, 41]. Nevertheless, the explanation of green emission by developing of microstructure during heat treatment at 900 °C can play important role as well. Because we can observe sintering of individual crystals (Fig. 3f), and thus the energy lowering of luminescent recombination centres occurs.

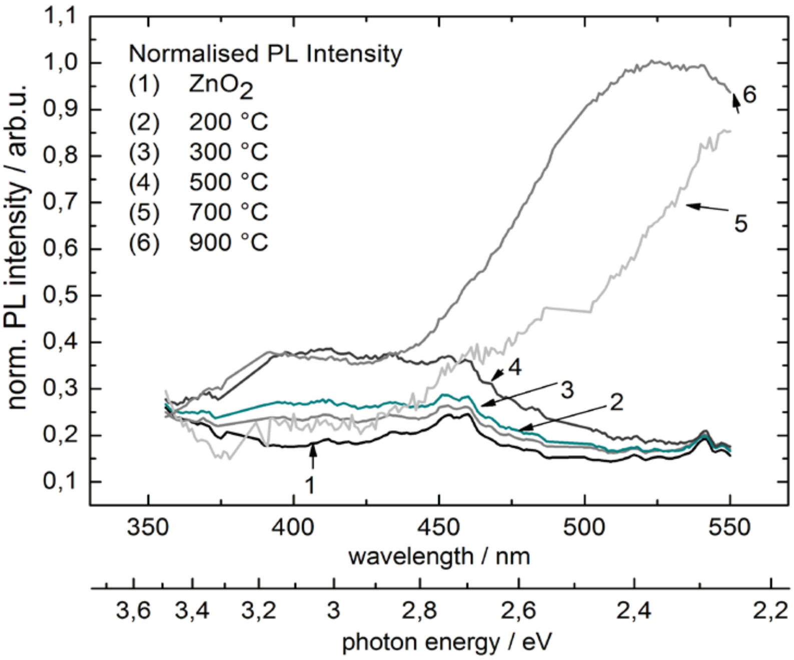

Figure 6 Photoluminiscence spectra of precursor and products prepared by annealing of the precursor at different temperatures as indicatd in the graph.

4. Conclusion

Simple and original method for preparation of nanocrystalline assembled ZnO spheres on mesoscale was proposed. It consists of thermal decomposition ZnO_2 precursor that can be obtained in large scale by recrystallization of commercial ZnO from ammonia solution in the presence of hydrogen peroxide. The phase transformation from ZnO_2 to ZnO was studied by complementary instrumental techniques including thermogravimetric analysis, X-ray diffraction analysis, scanning electron microscopy, BET adsorption analysis and photoluminescence spectroscopy. ZnO powders obtained by annealing at various temperatures in air atmosphere were tested on the photocatalytic activity by means of photodegradation of methyl violet. Although precursor decomposes at relatively low temperature of about 220 °C, only moderate photocatalytic activity was observed for powders annealed to the temperatures below 500 °C in spite of high specific surface area. This is attributed to the poorly developed crystalline phase in the early stage of transformation from ZnO_2 cubic to ZnO hexagonal lattice. Excellent photocatalytic activity was achieved for samples annealed at 500 °C and more. The results suggest that photocatalytic activity is for ZnO obtained from ZnO_2 precursor is influenced by size of well developed crystalline array rather than by specific surface area. Photoluminescene study revealed green luminescence for sample annealed at the 700 °C and 900 °C.

Acknowledgement

This article was written with the support of the Operational Programme 'Education for Competitiveness' co-funded by the European Social Fund (ESF) and the national budget of the Czech Republic, within the project 'Advanced Theoretical and Experimental Studies of Polymer Systems' (reg. number: CZ.1.07/2.3.00/20.0104).

This article was written with the support of Operational Programme 'Research and Development for Innovations' co-funded by the European Regional Development Fund (ERDF) and the national budget of the Czech Republic, within the 'Centre of Polymer Systems' project (reg. number: CZ.1.05/2.1.00/03.0111).

References

[1] U. Ozgur, Y.I. Alivov, C. Liu, A. Teke, M.A. Reshchikov, S. Dogan, V. Avrutin, S.J. Cho, H. Morkoc, A comprehensive review of ZnO materials and devices, Journal of Applied Physics, 98 (2005).

[2] S.J. Pearton, D.P. Norton, K. Ip, Y.W. Heo, T. Steiner, Recent progress in processing and properties of ZnO, Progress in Materials Science, 50 (2005) 293-340.

[3] A. Janotti, C.G. Van de Walle, Fundamentals of zinc oxide as a semiconductor, Reports on Progress in Physics, 72 (2009).

[4] A.B. Djurisic, X. Chen, Y.H. Leung, A.M.C. Ng, ZnO nanostructures: growth, properties and applications, Journal of Materials Chemistry, 22 (2012) 6526-6535.

[5] M. Machovsky, I. Kuritka, P. Bazant, D. Vesela, P. Saha, Antibacterial performance of ZnO-based fillers with mesoscale structured morphology in model medical PVC

composites, Materials science & engineering. C, Materials for biological applications, 41 (2014) 70-77.
[6] X.-G. Han, H.-Z. He, Q. Kuang, X. Zhou, X.-H. Zhang, T. Xu, Z.-X. Xie, L.-S. Zheng, Controlling Morphologies and Tuning the Related Properties of Nano/Microstructured ZnO Crystallites, Journal of Physical Chemistry C, 113 (2009) 584-589.
[7] P. Bazant, I. Kuritka, O. Hudecek, M. Machovsky, M. Mrlik, T. Sedlacek, Microwave-Assisted Synthesis of Ag/ZnO Hybrid Filler, Preparation, and Characterization of Antibacterial Poly(vinyl chloride) Composites Made From the Same, Polymer Composites, 35 19-26.
[8] K. Hashimoto, H. Irie, A. Fujishima, TiO2 photocatalysis: A historical overview and future prospects, Japanese Journal of Applied Physics Part 1-Regular Papers Brief Communications & Review Papers, 44 (2005) 8269-8285.
[9] A. Fujishima, X. Zhang, D.A. Tryk, TiO2 photocatalysis and related surface phenomena, Surface Science Reports, 63 (2008) 515-582.
[10] S. Baruah, J. Dutta, Hydrothermal growth of ZnO nanostructures, Science and Technology of Advanced Materials, 10 (2009).
[11] D. Ehrentraut, H. Sato, Y. Kagamitani, H. Sato, A. Yoshikawa, T. Fukuda, Solvothermal growth of ZnO, Progress in Crystal Growth and Characterization of Materials, 52 (2006) 280-335.
[12] S.M. Lam, J.C. Sin, A.Z. Abdullah, A.R. Mohamed, Degradation of wastewaters containing organic dyes photocatalysed by zinc oxide: a review, Desalin. Water Treat., 41 131-169.
[13] J. Xie, H. Wang, M. Duan, L. Zhang, Synthesis and photocatalysis properties of ZnO structures with different morphologies via hydrothermal method, Applied Surface Science, 257 6358-6363.
[14] O. Mekasuwandumrong, P. Pawinrat, P. Praserthdam, J. Panpranot, Effects of synthesis conditions and annealing post-treatment on the photocatalytic activities of ZnO nanoparticles in the degradation of methylene blue dye, Chemical Engineering Journal, 164 (2010) 77-84.
[15] J. Xie, H. Wang, M. Duan, L. Zhang, Synthesis and photocatalysis properties of ZnO structures with different morphologies via hydrothermal method, Applied Surface Science, 257 (2011) 6358-6363.
[16] D. Li, H. Haneda, Morphologies of zinc oxide particles and their effects on photocatalysis, Chemosphere, 51 (2003) 129-137.
[17] J. Yang, J. Wang, X. Li, J. Lang, F. Liu, L. Yang, H. Zhai, M. Gao, X. Zhao, Effect of polar and non-polar surfaces of ZnO nanostructures on photocatalytic properties, Journal of Alloys and Compounds, 528 (2012) 28-33.

[18] M.A. Mahmood, S. Baruah, J. Dutta, Enhanced visible light photocatalysis by manganese doping or rapid crystallization with ZnO nanoparticles, Materials Chemistry and Physics, 130 531-535.
[19] S. Cho, J.-W. Jang, J.S. Lee, K.-H. Lee, Carbon-doped ZnO nanostructures synthesized using vitamin C for visible light photocatalysis, Crystengcomm, 12 (2010) 3929-3935.
[20] Y. Zheng, L. Zheng, Y. Zhan, X. Lin, Q. Zheng, K. Wei, Ag/ZnO heterostructure nanocrystals: Synthesis, characterization, and photocatalysis, Inorganic Chemistry, 46 (2007) 6980-6986.
[21] H. Yu, H. Ming, J. Gong, H. Li, H. Huang, K. Pan, Y. Liu, Z. Kang, J. Wei, D. Wang, Facile synthesis of Au/ZnO nanoparticles and their enhanced photocatalytic activity for hydroxylation of benzene, Bulletin of Materials Science, 36 (2013) 367-372.
[22] J. Falgenhauer, C. Richter, H. Miura, D. Schlettwein, Stable Sensitization of ZnO by Improved Anchoring of Indoline Dyes, Chemphyschem, 13 (2012) 2893-2897.
[23] K. Takanabe, K. Domen, Preparation of Inorganic Photocatalytic Materials for Overall Water Splitting, Chemcatchem, 4 (2012) 1485-1497.
[24] S. Rehman, R. Ullah, A.M. Butt, N.D. Gohar, Strategies of making TiO2 and ZnO visible light active, Journal of Hazardous Materials, 170 (2009) 560-569.
[25] X. Chen, S. Shen, L. Guo, S.S. Mao, Semiconductor-based Photocatalytic Hydrogen Generation, Chemical Reviews, 110 (2010) 6503-6570.
[26] J. Wang, P. Liu, X. Fu, Z. Li, W. Han, X. Wang, Relationship between Oxygen Defects and the Photocatalytic Property of ZnO Nanocrystals in Nafion Membranes, Langmuir, 25 (2009) 1218-1223.
[27] J. Wang, Z. Wang, B. Huang, Y. Ma, Y. Liu, X. Qin, X. Zhang, Y. Dai, Oxygen Vacancy Induced Band-Gap Narrowing and Enhanced Visible Light Photocatalytic Activity of ZnO, Acs Applied Materials & Interfaces, 4 (2012) 4024-4030.
[28] B.M. Rajbongshi, S.K. Samdarshi, ZnO and Co-ZnO nanorods-Complementary role of oxygen vacancy in photocatalytic activity of under UV and visible radiation flux, Materials Science and Engineering B-Advanced Functional Solid-State Materials, 182 (2014) 21-28.
[29] F. Kayaci, S. Vempati, I. Donmez, N. Biyikli, T. Uyar, Role of zinc interstitials and oxygen vacancies of ZnO in photocatalysis: a bottom-up approach to control defect density, Nanoscale.
[30] J.N. Zeng, J.K. Low, Z.M. Ren, T. Liew, Y.F. Lu, Effect of deposition conditions on optical and electrical properties of ZnO films prepared by pulsed laser deposition, Applied Surface Science, 197â€"198 (2002) 362-367.
[31] Y. Lv, C. Pan, X. Ma, R. Zong, X. Bai, Y. Zhu, Production of visible activity and UV performance enhancement of ZnO photocatalyst via vacuum deoxidation, Applied Catalysis B: Environmental, 138â€"139 26-32.

[32] N. Uekawa, N. Mochizuki, J. Kajiwara, F. Mori, Y.J. Wu, K. Kakegawa, Nonstoichiometric properties of zinc oxide nanoparticles prepared by decomposition of zinc peroxide, Physical Chemistry Chemical Physics, 5 (2003) 929-934.

[33] C.-C. Hsu, N.L. Wu, Synthesis and photocatalytic activity of ZnO/ZnO2 composite, Journal of Photochemistry and Photobiology A: Chemistry, 172 (2005) 269-274.

[34] Q. Zhang, G. Cao, Hierarchically structured photoelectrodes for dye-sensitized solar cells, Journal of Materials Chemistry, 21 (2011) 6769-6774.

[35] V. Uvarov, I. Popov, Metrological characterization of X-ray diffraction methods for determination of crystallite size in nano-scale materials, Materials Characterization, 58 (2007) 883-891.

[36] P. Scherrer, Estimation of Size and Internal Structure of Colloidal Particles by Means of Röntgen Rays, Göttinger Nachrichten, 2 (1918) 98-100.

[37] T. Daley, E. Raj, S. Ramos, G. Cibin, A. Dent, T.I. Hyde, G. Sankar, Tracking the Formation of Nano-sized Zinc Oxide from Zinc Peroxide by In Situ XAS and XRD, 15th International Conference on X-Ray Absorption Fine Structure (Xafs15), 430 (2013).

[38] L.Q. Jing, Y.C. Qu, B.Q. Wang, S.D. Li, B.J. Jiang, L.B. Yang, W. Fu, H.G. Fu, J.Z. Sun, Review of photoluminescence performance of nano-sized semiconductor materials and its relationships with photocatalytic activity, Solar Energy Materials and Solar Cells, 90 (2006) 1773-1787.

[39] J. Zhang, L.D. Sun, J.L. Yin, H.L. Su, C.S. Liao, C.H. Yan, Control of ZnO morphology via a simple solution route, Chemistry of Materials, 14 (2002) 4172-4177.

[40] P.A. Rodnyi, I.V. Khodyuk, Optical and luminescence properties of zinc oxide (Review), Optics and Spectroscopy, 111 776-785.

[41] T. Hirai, Y. Asada, Preparation of ZnO nanoparticles in a reverse micellar system and their photoluminescence properties, Journal of Colloid and Interface Science, 284 (2005) 184-189.